UNIVERSITY OF SOUTHAMPTON
FACULTY OF ENGINEERING, SCIENCE AND MATHEMATICS
Optoelectronics Research Centre

Fabrication of novel geometry fibre lasers for high power applications

By
Laurence James Cooper

A thesis submitted for the degree of
Doctor of Philosophy

September 2005

University of Southampton

Abstract

Faculty of Engineering, Science and Mathematics
Optoelectronics Research Centre

Doctor of Philosophy

Fabrication of novel geometry fibre lasers for high power applications

By Laurence James Cooper

This thesis details my work on the development of fabrication techniques for high power doped fibre lasers, using novel fibre geometries, and their demonstration. The main methods for increasing output power were using helical cores, multiple cores and large cores.

A method for fabricating helical core fibres was proposed and implemented. Core and cladding pumped devices were successfully constructed, and were then tested in collaboration. A cladding pumped helical core fibre laser improved the beam from a $30\mu m$ core from an M^2 of 3.3 to < 1.4, with a maximum output power of $64W$ and slope efficiency of 84%.

A ribbon fibre with multiple laser emitting cores was fabricated. The difficulties in the fabrication of such a fibre required extensive research, and arise from the large aspect ratio of the preform and fibre, and the low size reduction during fibre drawing. Through many steps a ten core ribbon fibre was fabricated, which was used, in collaboration, to achieve an output laser power of $250W$, with a slope efficiency of 65%. Using a spectral beam combination technique, 5 cores were locked together.

The output from a number of cores within a circular fibre with no combination is a method for attaining stable high powers with moderate beam quality. A three core fibre was fabricated, and showed an M^2 of 5 and slope efficiency of 75%. This fibre was then tapered down from $150\mu m$ in order to improve the beam quality further, and for $125\mu m$ and $100\mu m$ tapers, the M^2 values measured were improved to 4.3 and 3.5, respectively.

An Yb-doped rod was fabricated, with a large core of $140\mu m$ diameter, and machined flats to break the cladding symmetry. The power attained was only $13.4W$ with a slope efficiency of 20%, due to surface imperfections. A fibre created with altered fabrication techniques showed no surface defects and showed over 90% transmission for $800nm$ light. Experiments performed by a colleague showed a slope efficiency of 69% and an M^2 of 11, indicating that the fabrication method could create an effective cladding pumped rod laser.

Contents

List of Figures

List of Tables

Acknowledgements

I would like to thank all the members of the Optoelectronics Research Centre, and in particular the members of the Fibre fabrication group for their help and support during this work. In particular I would like to thank Andrew Webb and Rob Standish for their ability to fix problems and keep machinery working through everything I could throw at them. Thanks also go to Richard Williams for help during the time he worked as the head of the fibre fabrication group, and Jae-sun Kim, for his help in the finer aspects of laser device measurements. My special thanks go to my supervisor, Jayanta Sahu, with out whose tutelage and support, this work would not have been possible, and also to Professor Payne.

I am deeply indebted to Andy Clarkson, Pu Wang and Vladimir Shcheslavskiy, from the Advanced Solid State Sources group, with whom many results were taken and without whose time, advice and use of laser setups, no lasers results would exist. My thanks also go to Eleanor Tarbox, for proof reading my thesis. Thanks are also extended to the EPSRC, for funding my PhD, and to QinetiQ for the funding of the helical fibre project.

Finally, and most importantly, I would like to thank my friends and family for being around me, and supporting me when my resolve was faltering! Special thanks go to Patrick Hole, Anna Peacock, Peter Wright, Andrew Weld, and Michael Roelans, who all decided to live with me. Finally I would like to thank my girlfriend Jenni, for her unwavering tolerance of me whilst attempting to write up.

Declaration of Authorship

I, Laurence James Cooper, declare that the thesis entitled 'Fabrication of novel geometry fibre lasers for high power applications' and the work presented in it are my own. I confirm that:

- this work was done wholly while in candidature for a research degree at this University;
- where any part of this thesis has previously been submitted for a degree or any other qualification at this University or any other institution, this has been clearly stated;
- where I have consulted the published work of others, this is always clearly attributed;
- where I have quoted from the work of others, the source is always given. With the exception of such quotations, this thesis is entirely my own work;
- I have acknowledged all main sources of help;
- where the thesis is based on work done by myself jointly with others, I have made clear exactly what was done by others and what I have contributed myself;
- parts of this work have been published as shown in the List of Publications

Signed: .....

Date:...../...../.....

Chapter 1

Introduction

1.1 Optical fibre lasers

Optical fibres have been utilised for the transmission of coherent light since the invention of the laser. The improvements to optical fibres in the early 1970s led to their use for communications, from which the development of the fibre amplifier was inevitable. Their ultra low loss over distances of kilometres made them the obvious successor to the copper electrical cables previously used in communications. Since fibre amplifiers were first fabricated in the early 60s [1, 2], numerous devices have been created with different active ions for an array of purposes.

One major attraction of the optical fibre is its simplicity. In order to create a fibre laser all that needs to be done is to add rare-earth ions to the core, which creates a gain medium with low threshold and good beam quality. Commercial fibres are generally fabricated out of silica, and since the development of Modified Chemical Vapour Deposition (MCVD) [3] fibre lasers have been routinely fabricated. MCVD uses vapourised halides reacting with oxygen to form the required glasses, at very high temperatures. A rotating glass tube is heated along its length and as the chemicals enter the hot area, glass particles are formed, which attach to the inside of the tube. The MCVD technique is capable of creating very low loss, single mode, rare-earth doped preforms for the fabrication of fibre lasers.

The preform is finally drawn, by stretching it, into a thin fibre a few hundreds of microns in diameter.

The attraction of fibre lasers comes from the high beam quality, high gain and thermal management. The small core dimensions mean that the light is well confined and only the fundamental mode can propagate. Extremely high gains are possible due to the very long interaction lengths used in fibre lasers. The small fibre dimensions mean that the poor thermal conductivity of glass has a less severe effect than with bulk glass lasers, due to the higher surface to volume ratio.

1.2 High power fibre lasers

The true potential of optical fibre lasers was only realised with the successful demonstration of the diode-pumped fibre laser [4]. Fibre lasers are dependent on optical pumping that must be focused into the very small dimensions of the fibre, which can only be achieved with high efficiency through the use of laser sources. The development of cladding pumping [5] was the key to increasing the output power from fibres, from a watt to hundreds of watts. The use of double clad fibres enables multimode pump sources to be used, for which the powers are increasing constantly as progress is made in diode laser technology.

The competition in the field of high power lasers comes primarily from bulk solid state lasers, which are non-waveguiding and rely on external optics or self focusing to shape the resultant beam. They are usually crystals doped with rare earths, and generate far higher powers than currently achievable in fibre lasers. The crystals required for bulk lasers are extremely expensive, and as the cost of diode pump sources falls, high power fibre lasers are becoming serious competitors for many applications.

High power laser output is dependent on coupling the maximum pump light into the core. This is generally achieved using double clad fibre, and the breaking of the symmetry of the fibre to ensure maximum overlap with the core. If the core is central in the fibre and there is no symmetry breaking, only the fundamental

pump mode will have a significant overlap with the core, and the pump absorption will be low. By using an off centre core, or more commonly the use of milled flats on the preforms (as described further in section 2.2.2) there is mode mixing and the pump absorption increases dramatically. Another factor is the launching of pump light into the fibre, which is achieved through end pumping, V-groove pumping [6], or the use of the "GT-wave" system [7].

Current high power laser sources such as CO_2 gas lasers, diode lasers, solid state lasers and fibre lasers, all have surpassed the kW output power barrier. Commercial CO_2 lasers can produce laser powers over $15kW$ [8], diode lasers can produce up to $1kW$ from a commercial diode stack [9], solid state lasers have outputs up to $6kW$ [10] and fibre lasers with single mode output powers of up to $1.3kW$ [11] have been attained. The high beam quality combined with high power from fibre lasers makes them very attractive for many applications such as industrial welding, cutting or range finding.

1.3 Novel geometries for high power fibre lasers

The advances currently achieved for high power fibre lasers consist of advances in pump coupling to standard fibres, or the fabrication of large mode area low numerical aperture fibres. These techniques have allowed power levels to surpass $1kW$ from a fibre laser with almost single mode output. Whilst these techniques can continue to increase the output powers attained from fibre lasers, there will come a point when different techniques are required to progress further. This thesis is concerned with the design and fabrication of fibre lasers with non-standard geometries to enable the advancement of high power lasers further than current techniques are capable of. The fabricated fibres are then tested, and the resultant feedback is used to improve the next generation of the fibre laser.

Chapter 2 introduces optical fibres, laser devices, and fibre properties. It also details current fabrication techniques for optical fibre lasers, used in the ORC and elsewhere. The technique of combining outputs from a number of laser emitters is also addressed, as a technique for the simple scaling of laser output powers.

Chapter 3 is an investigation performed into the use of a helical core fibre to solve potential problems with current power scaling techniques. The properties inherent to the fibre are introduced and derived. The fabrication process developed for firstly the preform, and then the fibre are detailed, implemented and improved. The results achieved from the first test fibres to the working helical-core fibre laser are then presented. Finally, the potential direction for the project is suggested.

In chapter 4 the multiple core ribbon fibre is proposed, along with beam combination techniques for a high power laser solution. Firstly, the theory behind the advantage of the fibre shape is explained, then the theory of spectral beam combination is examined. The fabrication process used to develop the ribbon fibre is detailed, explaining difficulties and solutions found during the course of my work. The results achieved from the fibre laser are presented along with preliminary results for the spectral beam combination of the laser outputs. Work on an alternative fabrication technique is finally presented, as a possibility for further work.

The beam combination technique is a promising technique for the scaling of power with little modification of the fibre, and a circular multicore fibre is examined in chapter 5. The technique is firstly explained in detail, with attention drawn to its advantages. The technique used for the fabrication of the fibre is detailed, and results achieved from 'proof of principle' fibres are presented. The fabrication of a scalable model is then described, and the results achieved from this presented. Finally the use of spliced multimode fibre and tapered fibres are tested, as a method for the improvement of the resultant beam quality.

The cladding pumped rod, as introduced in chapter 6, is a laser close to the boundary between fibre lasers and bulk lasers. Firstly the advantages of the cladding pumped rod over both fibre lasers and cladding pumped lasers are described. The fabrication of the rod is explained, along with the proposed method for operation. Results achieved from the cladding pumped rods are then presented, followed finally by the future direction of the project.

Chapter 7 outlines the achievements and conclusions of the work described. Future directions and projects are also proposed.

1.4 References

[1] E. Snitzer. Optical maser action of Nd in a barium crown glass. *Physical Review Letters*, 7(12):444–446, 1961.

[2] C. J. Koester and E. Snitzer. Amplification in a fibre laser. *Applied optics*, 3(6):1182–1186, 1964.

[3] S. B. Poole, D. N. Payne, and M. Fermann. Fabrication of low loss optical fibres containing rare earths. *Electronics Letters*, 21(17):737–738, 1985.

[4] E. Snitzer. Rare earth fibre lasers. *Journal of the Less Common Metals*, 148:45–58, 1989.

[5] J. Kafka. Laser diode pumped fibre laser with pump cavity. *US patent 4,829,529*, 1989.

[6] L. Goldberg, J. Koplow, and D. Kliner. High efficiency 3W side-pumped Yb-fibre amplifier and laser. *Proceedings of the Conference on lasers and electro-optics*, USA:11–12, 1999.

[7] S. U. Alam, J. Nilsson, P. W. Turner, M. Isben, A. B. Grudinin, and A. Chin. Low cost multi-port reconfigurable erbium doped cladding pumped fibre amplifier. *Proceedings of the European Conference on Optical Communication*, Germany:5.4.3, 2000.

[8] Trumpf laser division. Product specifications. *Website - http://www.trumpf-laser.com/208.index.html*, 2005.

[9] M. Anter. High-power diode lasers offer efficient answer. *Opto and Laser Europe*, May:25–30, 2005.

[10] R. Poprawe and W. Schultz. Development and application of new high-power laser beam sources. *RIKEN Review focused on Laser Precision Microfabrication*, 50:3–9, 2003.

[11] Y. Jeong, J. K. Sahu, D. N. Payne, and J. Nilsson. Ytterbium-doped large-core fibre laser with 1.36kW continuous-wave output power. *Optics Express*, 12(25):6088–6092, 2004.

Chapter 2

Fibre lasers

2.1 Introduction

Since the development of the laser in the early 1960's its uses have become numerous, and it now impacts on many aspects of everyday life. The rise in applications has provided a platform for many different types of lasers to be developed, each with their own special properties. For example bulk lasers with high powers and high repetition rates, or fibre lasers with excellent beam quality. Various types of lasers have properties which are ideal for specific applications, but all emit light through the same laser operation. The fabrication of such devices varies with method but generally they consist of the same ingredients of an active medium, a cavity and a pump source. The process by which lasers operate is described in section 2.2.1 along with the equations governing their characteristics. The high power fibre laser and current techniques for increasing output power are outlined in section 2.2.2. The polarisation of the beam produced by a laser is important in many applications such as biological interactions, and the polarisation of light in optical fibres is addressed in section 2.2.3.

The scaling of pump powers is achieved routinely through the combination of outputs from a number of separate sources. The combination can be done in a coherent manner with the sources being phase related, or in an incoherent manner with the light from independent sources. In section 4.2.1 the coherent combina-

tion of laser sources is introduced with examples of diode and fibre combination techniques. Incoherent beam combination is addressed in section 4.2.2.

The fabrication of fibre lasers consists of two steps, firstly the fabrication of a preform, then the stretching of this preform into a fibre. This process is extensively used to create fibres for the communications industry, where pulses of light propagate thousands of kilometres through the core. The basic fabrication process had to be adapted for the incorporation of rare earths to create an active medium, allowing fibre lasers to be fabricated. There are three main methods for the fabrication of optical fibres, Outside Vapour Deposition (OVD), Vapour Axial Deposition (VAD) and Modified Chemical Vapour Deposition (MCVD). OVD and VAD are described in section 2.3.1 and MCVD in section 2.3.1; comparing the advantages and disadvantages of the methods used within the ORC and elsewhere. Laser operation in fibre lasers is achieved by doping the core with rare-earth ions which is performed though solution doping [1], the process for which is outlined in section 2.3.1. Drawing the resultant fabricated preform into a fibre is described in section 2.3.2.

2.2 Lasers

2.2.1 Laser systems

Laser amplification operates though the process of stimulated emission to produce identical photons, and thus cause a signal to be amplified. Atoms are able to interact with photons in two ways, by the absorption or the emission of photons with respective upward or downward transition between its energy levels. Energy must be conserved during these processes, thus the photon energy equals the difference between the two energy levels. There are then two types of photon emission from an atom in an excited state: spontaneous and stimulated emission, as shown in figure 2.1. Spontaneous emission occurs independently of the number of photons in the mode, with a probability dependent on the transition cross-section. Stimulated emission however, relies on the presence of a photon to stimulate the emission of a photon into the same mode with the polarisation, frequency, direction and phase of the original photon. It is this stimulated

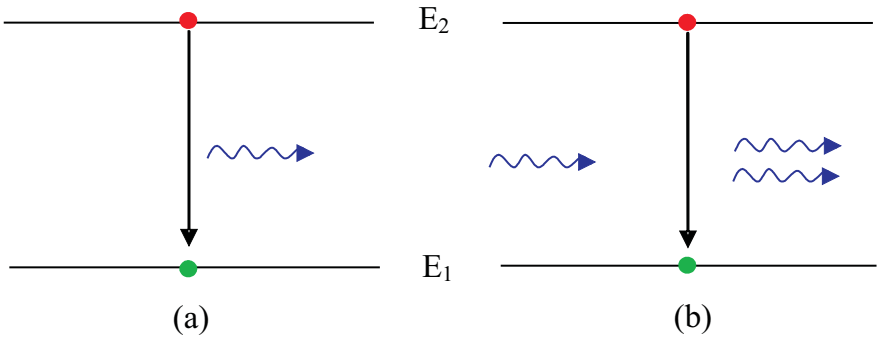

Figure 2.1: a. Spontaneous emission of a photon from an excited electron. b. Stimulated emission of a photon with the same properties as the incident photon.

emission which can be used to amplify a signal of a specific wavelength. Spontaneous emission also occurs in amplifiers and generates signals which are not in the same phase as the final photons, which can then be amplified and is known as Amplified Spontaneous Emission (ASE). Since the energy level of the atomic transition must be equal to the energy of the photon, there is only a small band of frequencies which can be amplified. In general the ions are held within a crystal lattice or silica matrix, which has the effect of broadening the energy levels and thus increasing the amplifiers' operating bandwidth. Amplification does not occur however unless there are more atoms in the excited state than in the lower state. If this were not the case, light passing through the medium would be more likely to be absorbed than to stimulate emission. This is known as population inversion.

The two most important laser systems are the three and four level laser systems. In real laser systems there can be many more levels involved in the act of lasing, but they can be simplified to either the 3 or 4 level case. The energy levels of a ion within a glass host such as silica, are split into a distribution of levels known as Stark levels. The distribution of the number of ions in each Stark level is governed by thermal distribution, and thus the number of ions in higher energy Stark levels decreases according to the Boltzmann distribution [2]. Generally, a four level laser system is one in which the laser transition ends above the ground state, whilst a three level system ends in the ground state. Since the ground state is involved in the lasing transition, a population inversion can only be achieved when over half of the atoms are excited from the ground state. Most of the work achieved with rare-earth ions uses four level or quasi-four level transitions since a population inversion is easily attained. A quasi-four level system is one which has the lasing

transition as the ground state, but at a high Stark level and is therefore only sparsely populated through the thermal distribution. The population inversion can therefore be achieved far easier than for three-level transitions.

Three-level laser system

A three level laser system has level 1 lying at or close to the ground state so that the energy difference is small compared with kT, and is always populated by a significant portion of the atoms. The disadvantage of this type of laser is that it is more difficult to maintain a population inversion due to the ground state being one of the lasing levels. For the probability of a photon to stimulate the emission of another photon to be greater than that of being absorbed, requires that more than half the atoms are in the excited state.

The number of atoms in the energy level can be described by the rate equations for each level, and assuming continuous wave operation, solving for the steady state situation. As shown in figure 2.2, the pumping from ground state gives a probability of transition of R_p, and the rate of decay γ_{xy} is inversely proportional to the lifetime τ_{xy} where x is the initial level and y is the final energy level. The change in population density for different levels is thus:

$$\frac{dN_2}{dt} = RN_0 - \frac{N_2}{\tau_{21}} \tag{2.1}$$

$$\frac{dN_1}{dt} = \frac{N_2}{\tau_{21}} - \frac{N_1}{\tau_{10}} - (N_1 - N_0)\, W_{10} \tag{2.2}$$

$$\frac{dN_0}{dt} = -RN_0 + \frac{N_1}{\tau_{10}} + (N_1 - N_0)\, W_{10} \tag{2.3}$$

Where N_x is the population in state x, RN_0 is the pump rate from level 0 to level 2, τ_{xy} is the lifetime from level x to level y, and $(N_1 - N_0)\, W_{10}$ is the stimulated emission rate.

In an ideal three level laser system, the non-radiative decay from level 2 to level 1 is extremely fast, such that $\tau_{10} \gg \tau_{21}$ and the population of level 1 is far greater

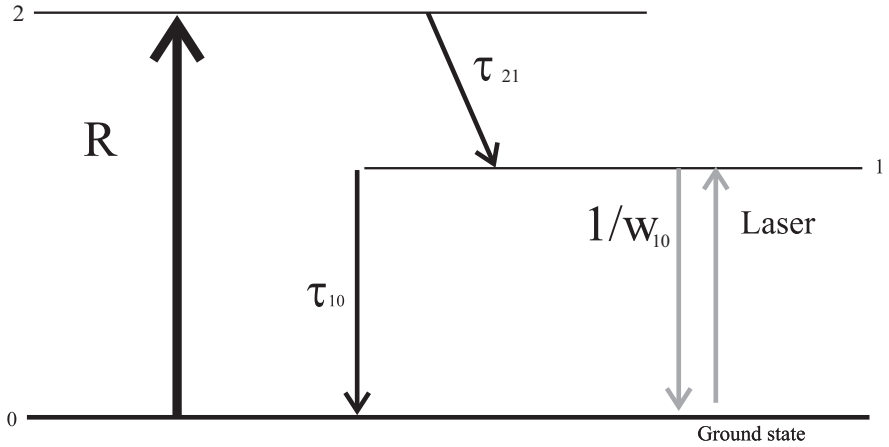

Figure 2.2: Diagram of the energy levels for a three level laser system. The atoms are excited into the second energy level at rate R, and decay rapidly to level one. From level one they can either decay through spontaneous emission or through stimulated emission to the ground state. Unless more than half the atoms are excited into level one, then lasing can not occur.

than level 2[3]. And this can then lead to the population inversion of:

$$\frac{N_1 - N_0}{N} = \frac{R - \frac{1}{\tau_{10}} - W_{10}}{R + \frac{1}{\tau_{10}} + W_{10}} \tag{2.4}$$

Since the number of ions excited in a pumped fibre can be expressed as:

$$RN = \frac{I_p \sigma_A}{h v_p} N \tag{2.5}$$

Where I_p is the intensity of the pump, and σ_A is the absorption cross-section at frequency v_p.

Assuming that $W_{10} \ll \frac{1}{\tau_{10}}$, this leads to the requirement that:

$$I_p > \frac{h v_p}{\sigma_A \tau_{10}} \tag{2.6}$$

This shows that due to the small area of a fibre, only very small pump powers are required to reach threshold. This type of laser is one that is very useful for the telecommunications industry. A fibre amplifier which operates in the 1.5 μm region is the erbium doped fibre amplifier (EDFA) which is a three level laser system. The EDFA was a major breakthrough due to the possibility of all optical

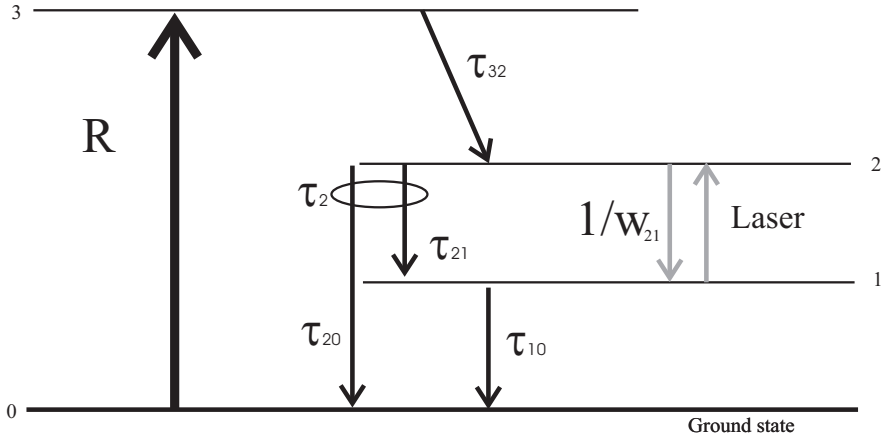

Figure 2.3: Diagram of the energy levels for a four level laser system. The atom are excited into the third energy level at rate R, and decay rapidly to level 2. From level two they can either decay through spontaneous emission (the two on the left) or through stimulated emission on the right. Most will then decay to the ground state.

amplification. Previously the light signals were converted to electrical signals, amplified and then converted back into light pulses. Although this process was adequate for low pulse repetition rates, at the higher rates possible with optical fibres, the electronics became a bottleneck.

Four-level laser system

A four level laser system is shown in figure 2.3. In this configuration atoms are excited into level 3, and then rapidly decay into the long lived level 2 through the emission of a phonon. The decay from this long lived level to level 1 is the laser transition. The lifetime of level 1 is very short, and decay occurs back to the ground state where the process repeats. The long life of level 2 and short life of level 1 means that even for low pump powers, a population inversion can be achieved.

Figure 2.3 shows the energy levels for a four level laser system. The equivalent rate equations to the three-level rate equations given previously are

$$\frac{dN_3}{dt} = R\left(N_0 - N_3\right) - \frac{N_3}{\tau_{32}} \tag{2.7}$$

$$\frac{dN_2}{dt} = \frac{N_3}{\tau_{32}} - \frac{N_2}{\tau_{21}} + \left(N_1 - N_2\right) W_{21} \tag{2.8}$$

$$\frac{dN_1}{dt} = \frac{N_2}{\tau_{21}} - \frac{N_1}{\tau_{10}} - (N_1 - N_2)\, W_{21} \tag{2.9}$$

$$\frac{dN_0}{dt} = \frac{N_1}{\tau_{10}} - R\,(N_0 - N_3) \tag{2.10}$$

Where N is the number of atoms in an energy level, τ is the life time of a state, and W_{21} is the probability that an atom absorbs a photon.

However, we make the assumption that $N_3 \approx N_1 \approx 0$ thus only the ground and upper lasing levels need be considered. Thus for even very low pumping intensities there will be an population inversion, and it is the loss in the cavity which will determine the lasing threshold.

Light amplification

The principle of amplification can be used to make an optical oscillator, which consists of an active medium and a cavity, and is often referred to as a laser. A typical laser consists of the gain medium positioned between two mirrors of very high reflectivity. There are two requirements for laser action: a gain condition, and a phase condition. The phase condition is that there must be an integer number of wavelengths in one round trip. The gain condition is defined by the small signal gain coefficient γ_0 which must be greater than the cavity loss.

$$\gamma_0(v) = N\frac{\lambda^2}{8\pi\tau_{21}}g(v) \tag{2.11}$$

Where $g(v)$ is the normalised transition cross section, τ_{21} is the transition lifetime between levels 2 and 1, and N is the total number of atoms.

Equation 2.11 leads to the equation for threshold population difference N_t, which is the point at which lasing can occur.

$$N_t = \frac{8\pi}{\lambda^2 c}\frac{\tau_{21}}{\tau_p}\frac{1}{g(v)} \tag{2.12}$$

Where τ_p is the photon lifetime in the resonator.

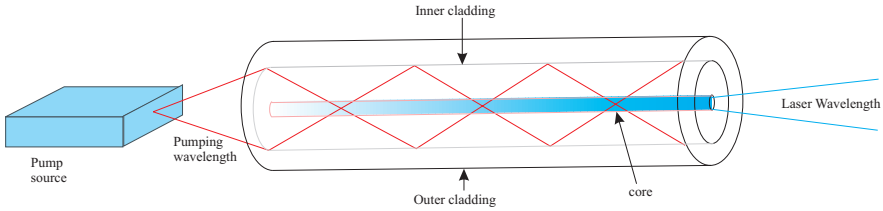

Figure 2.4: Simple schematic of the pumping of a double clad optical fibre laser.

In a laser the gain decreases with increased photon flux density, resulting in steady state being attained when the loss equals the gain.

In the same way that optical fibres can be used as fibre amplifiers, they can also be used to form lasers. By using mirrors or fibre Bragg gratings to form a cavity, a laser is easily formed from a doped optical fibre.

2.2.2 High power fibre lasers

Fibre lasers are attractive due to their low threshold and high efficiencies. Their performance is limited due to the powers that are attainable in the small dimensions which are inherent in optical fibres. The first aspect of fibres is the pumping method which can be either core pumped or cladding pumped. Initial fibre lasers were constructed with core pumping in mind, which necessitated single mode pump sources if single mode output was required. The development of double clad fibres [4] led to the wide availability of pump sources, which enabled fibre lasers' powers to increase rapidly.

The double clad fibre, as shown in figure 2.4, consists of the central doped core, a surrounding inner cladding, then a protective outer cladding. Both the core and inner cladding are generally made from glass, with the outer protective layer being plastic. The outer coating has a lower refractive index than the glass it surrounds, causing the pump light to be confined in the inner cladding. The pump will reflect within the inner cladding, periodically crossing the core, where part will be absorbed by the rare earth, although the absorption is low in comparison to the core pumped case due to the pump light being spread across the core and the cladding, reducing the intensity.

The design of conventional cladding pumped fibres also reduces the overlap of the pump light with the core. Since the inner cladding will be highly multimoded at the pump wavelength, the propagation of light through the fibre can be thought of in a ray-optic picture. It is clear that skew rays will not pass through the centre of the fibre (and thus the core), as shown in figure 2.5. To reduce this problem, the axial symmetry of the fibre must be broken and this is done by either having an offcentre core, or by making flats on the fibre [5, 6]. These both increase the amount of light crossing the core and thus the absorption of the pump.

The high pump powers achievable using cladding pumping means that the signal power can also be extremely high. Published output results from fibre lasers with a single moded core have exceeded 100W [7]. However it is thought that this is near the limit for single mode fibres, due to the output facet being damaged at higher power densities [8]. The damage of the output facet by high power densities within the core of the fibre can be reduced by increasing the size of the core. This increases the number of supported modes [9] however, and single mode output is one of the advantages of using fibre lasers. The number of modes supported by an optical fibre is determined by the V number of the fibre which is defined as:

$$V = \frac{2\pi}{\lambda_0} a (n_1^2 - n_2^2)^{\frac{1}{2}} \tag{2.13}$$

Where λ_0 is the wavelength, a is the core radius, n_1 is the core refractive index, and n_2 is the cladding refractive index.

The approximate number of modes supported, N_{mode}, goes as

$$N_{mode} \approx \frac{V^2}{2} \qquad for\ V \gg 1 \tag{2.14}$$

It is well documented however, that bend loss for higher order modes is much larger than that for the lower order modes [10]. This means that by bending the fibre we can use a larger core to obtain higher powers, but still maintain single mode operation. Section 3.2.3 addresses in more detail the use of bend loss in mode selection.

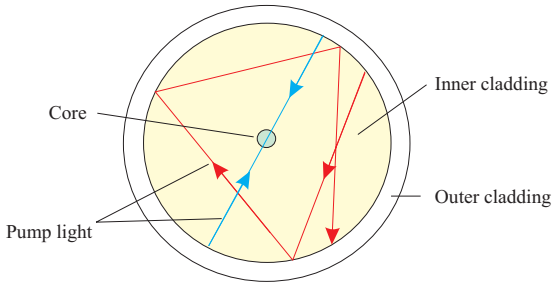

Figure 2.5: Path of pump light if not directly through core.

2.2.3 Birefringent fibres

Birefringence occurs naturally in many crystals, where there are two axes of differing refractive index. This makes it possible to manipulate polarised light, for instance by rotating the polarisation or separating the polarisations. In any optical fibre, it is possible to find a fast and a slow axis, which are orthogonal and determine the birefringence of the fibre. The position of these axes are defined by asymmetries in the fibre. This asymmetry is very small in normal fibre, and thus the birefringence is also very small. If we deliberately cause an asymmetry in a fibre we can induce a larger birefringence, which can then be used for maintaining polarisation along the fibre length. In a linearly birefringent optical fibre, when linearly polarised light is launched with one polarisation in line with one of the axes it will remain linearly polarised throughout a length of the fibre. This occurs since the light aligned along either of the axes has a specific k-vector, and there must be some perturbation to the fibre for the k-vector to change and thus make the polarisation rotate. If light is launched at an angle to these axes then the light will propagate in both polarisation states. The light at the end of the fibre will still be polarised, but due to the different velocities in the two states it will be in an arbitrary polarisation. Small temperature or stress perturbations will also change the polarisation at the end of the fibre, making the output very difficult to use.

Current designs for linearly birefringent fibres include bow-tie fibres, elliptical core and PANDA fibres (see figure 2.6). One further method for inducing a circular birefringence is to use a helical fibre. It has been shown [11] that a core following a helical path can maintain linearly polarised light, and this will be outlined in section 3.2.2

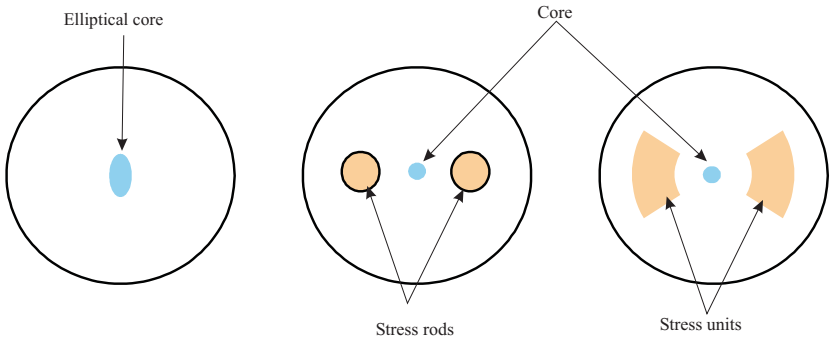

Figure 2.6: (a) An elliptical core to cause a small birefringence. (b) Stress rods inserted into drilled hole in preform to cause birefringence due to differing expansion coefficients. (c) Stress units made during MCVD process perform, induce stress as stress rods.

By combining two orthogonal polarisations, the power can be increased without increasing either the spectral or spatial width. Therefore polarisation maintaining fibre lasers can be used to increase power in a laser beam. Lasers of a definite polarisation are also used in biological applications, where only one polarisation will interact with a molecule.

2.3 Fibre fabrication process

2.3.1 Preform fabrication

The three main methods for creating preforms are through Vapour-phase Axial Deposition (VAD), Outside Vapour Deposition (OVD) and Modified Chemical Vapour Deposition (MCVD). All of these methods create glass from the same chemicals by the reactions as given in equations 2.15 and 2.16 through the process of Chemical Vapour Deposition (CVD).

$$SiCl_4 + O_2 \rightleftharpoons SiO_2 + 2Cl_2 \tag{2.15}$$

$$GeCl_4 + O_2 \rightleftharpoons GeO_2 + 2Cl_2 \tag{2.16}$$

The reagents are fed into an oxyhydrogen burner in VAD and OVD with the resultant soot deposited as a soot preform. This soot must then be dried in the presence of Cl_2 gas to remove the excess water, and then consolidated into a transparent glass preform. MCVD passes chemicals through a tube, which is then

heated and glass is deposited on the inside of the tube. MCVD is the technique used in the ORC for the fabrication of preforms.

Halides such as the aforementioned $SiCl_4$, $GeCl_4$ or $POCl_3$, are used as the initial reagents for all three preform fabrication techniques. These are chosen due to their high vapour pressures [12] at room temperature, and the fact that the vapour pressures for transition metal halides are many orders of magnitude lower. This virtually eliminates transition metal impurities in CVD, which can be a large source of loss.

Vapour Axial Deposition and Outside Vapour Deposition

The VAD and OVD techniques both use flame hydrolysis for the formation of the silica soot, and deposit this onto a porous soot preform. The techniques differ in that OVD deposits the soot onto a target rod which is later removed, and VAD starts the deposition on a target rod but once started deposits directly onto the porous preform.

The reactions are given in equations 2.15 and 2.16, and occur in the flame at temperatures above 1500^oC. Another important reaction is

$$2H_2O + 2Cl_2 \leftrightharpoons 4HCl + O_2 \tag{2.17}$$

In this reaction the water produced from the oxyhydrogen flame consumes the Cl_2 created in the oxidation reactions, allowing those reactions to continue. The glass particles start to form about $10mm$ from the burner and coalesce to form larger soot particles, which then adhere to the target surface.

In the OVD process there are two steps before the preform is ready to be drawn into a fibre. First is the deposition of soot on the outside of a target rod. This is done by passing the halide vapours through an oxyhydrogen burner directed at the rod, which creates and then deposits the glass soot as shown in figure 2.7. The rod is rotated whilst traversed back and forth in front of the burner, depositing an even layer of soot [13]. The first layers deposited are the core layers, and the porous preform is built up layer by layer. Once the porous preform has been completed, it is removed from the target rod. Once the porous preform has been

removed from the target rod, it must be dried to remove the residual water which would otherwise cause losses in the fibre. This is achieved by heating in a furnace, and passing helium, oxygen and chlorine through the preform via the hole left by the rod. Once the preform has been dried, it is ready for the second step, which is the sintering of the porous preform into a bubble free preform. This is achieved by passing the porous preform through a furnace at which stage the hole formed when the target rod was removed can be collapsed if required.

The VAD method was originally designed for the continuous manufacture of preform resulting in very long lengths [13]. The preform is created initially on a seed rod, and then onto the base of the porous preform as it is drawn upwards as shown in figure 2.8. Multiple burners are used to allow control over the reagents and thus the refractive index profile. The soot preform is dried by setting the whole process in a controlled atmosphere and heating the soot. During the heating process the temperature is increased which makes the soot particles become less viscous, and collapse into a solid preform due to the surface tension. This method is complex and thus difficult to control, and to maintain a uniform diameter along the length of the preform requires careful optimisation. This method however, has been refined and the high quality preforms and low loss fibres are fabricated in this way.

The disadvantage with the OVD technique of preform fabrication is the complexity of the system. Corning currently use the process for fibre fabrication [14], and rare-earths can be incorporated though solution doping (described in section 2.3.1). Once the complex and specialised system is in place to fabricate fibres through the OVD technique, the technique is flexible and remains a successful technique for preform fabrication.

The main drawback in the VAD technique is the difficulty in incorporating rare earth ions. The solution doping method (described in section 2.3.1) causes ions to be deposited throughout the entire preform and thus absorption of the pump will occur across the whole fibre. It also suffers from having to dry from the outside in, thus the highest concentration of OH will be in the core once the preform has been fabricated.

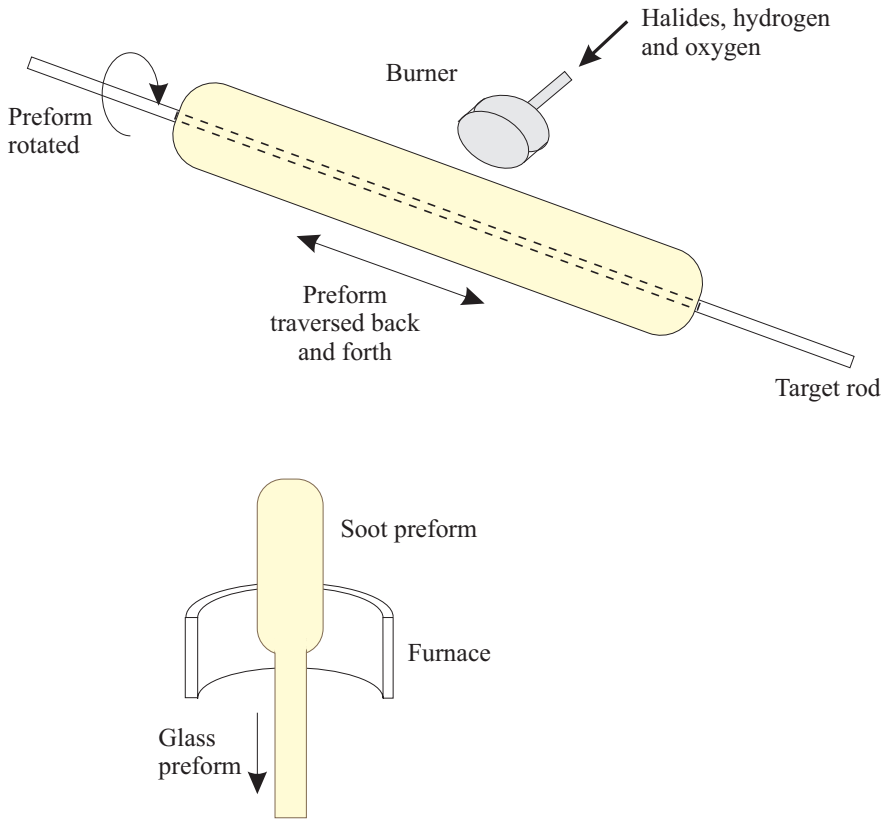

Figure 2.7: Schematic of the OVD preform fabrication process

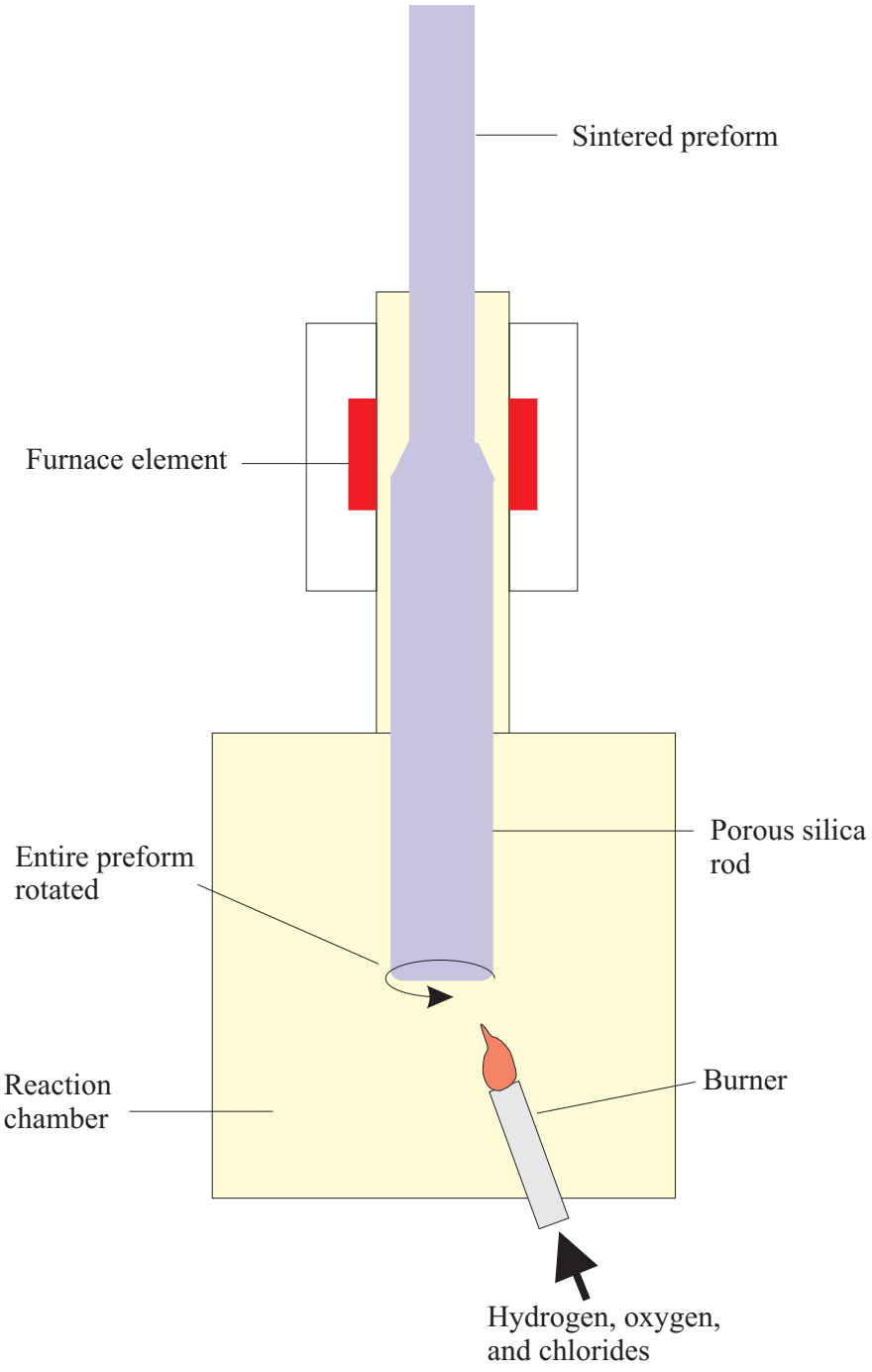

Figure 2.8: Schematic of the VAD preform fabrication process

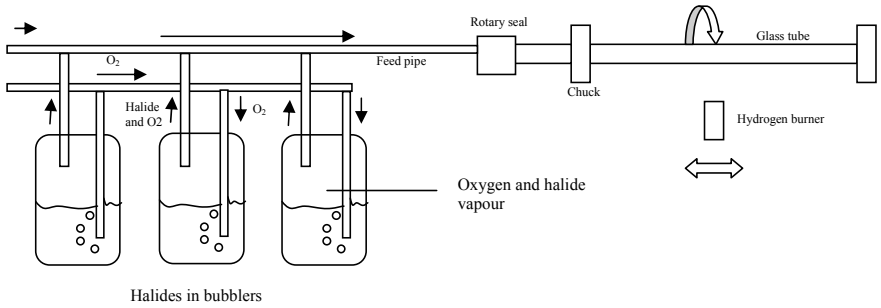

Figure 2.9: Diagram showing the MCVD apparatus. The bubblers feed the tube with gases and halide vapour through the rotary seal. A traversing heater causes the halides to react with oxygen and the oxides to be sintered onto the surface of the tube.

Modified Chemical Vapour Deposition

MCVD uses halide compounds, due to their high vapour pressures, to deposit high purity oxides within a glass tube. A typical MCVD setup is shown in figure 2.9, showing the chemical supply system on the left and the glass working lathe on the right. The principle is that halides react with oxygen at high temperatures to form oxides such as SiO_2 (silica) etc, which are deposited on the inside of a glass tube.

The apparatus required for creating preforms through the MCVD process can be split into two parts, the chemical delivery section and the glass working lathe. In the chemical delivery section, halides for the MCVD are stored in bubblers within a sealed glove box. A bubbler consists of a sealed glass container in which the halides are held, with three glass pipes entering the chamber, as shown in figure 2.10. One of these is the inlet for the oxygen, which has a plate at the base where the oxygen is passed through the halide as small bubbles. Another pipe is the outlet for the oxygen mixed with halide vapour, and the final pipe is the inlet for refilling with halide. The oxygen bubbled into the halide displaces oxygen and halide already in the bubbler, and due to the large surface area of the bubbles the quantity of halide vapour is kept at equilibrium. The bubblers used within the University of Southampton consist of four compounds, $SiCl_4$, $GeCl_4$, BBr_3 and $POCl_3$, which can be used in any combination to obtain the required glass compound. The rate at which oxygen is passed through the bubbler can be controlled, and determines the quantity of halide transferred to the glass working lathe. The control system is through computer and mass flow controllers, which allows the transfer of halides vapour carried by oxygen, pure oxygen, nitrogen,

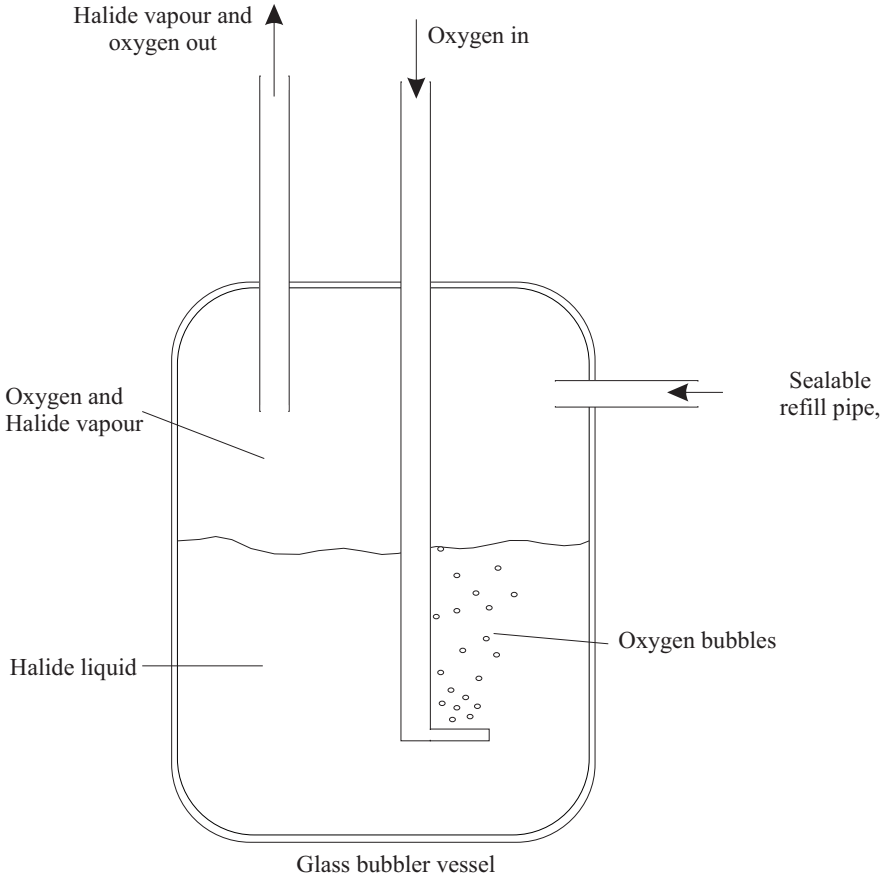

Figure 2.10: Diagram of bubbler for chemical vapour deposition. The oxygen flows in at a certain rate and oxygen with halide vapour is pushed out of the vessel. Bubbling the gas through the liquid creates a large surface area and thus the high vapour pressure is maintained.

helium, chlorine or any combination therein that is required. The gases are mixed together in a single pipeline before being transferred over to the glass working lathe.

The second part of the apparatus, the glass working lathe has rotating clamps that hold that glass to be worked upon, and a burner which can traverse along the length of the glass being held. It also has a rotary seal at one end to allow the passage of gas into tubes held in the clamps, and an extract at the other end to remove the hazardous gases produced, or used, in the processing. For the fabrication of preforms, three tubes are connected together in the lathe; a start-up tube, a deposition tube, and a soot tube. These are welded together to form a long airtight tube through which the chemical pass. The deposition tube is where the chemicals will be deposited as a glass, and is fabricated to high specifications to be free of impurities and deformities. The start up tube is primarily to allow the

chemicals to reach the deposition tube without wasting the expensive material. The soot tube collects the reacted chemicals which have not been attached to the deposition tube, and keeps the gas flow unblocked (as detailed later in this section). All tubes are cleaned before connection by de-ionised water and then acetone to remove any contaminants on the inside surfaces. The burner traverses in the direction of glass flow along the preform to heat the glass tube. The burner is supplied with oxygen and hydrogen in the correct ratio by the control system, which can be set by the user at a certain flow rate or to attain a set temperature as measured by the pyrometer. The pyrometer is connected to the burner and is focussed on a point slightly behind the middle of the burner, which is the hottest point due to the forward movement of the burner.

The first step in the fabrication of an MCVD preform is to use a flow of sulphur-hexafluoride(SF_6) which etches approximately $100\mu m$ of silica from the inside of the tube. This removes the layer where the diffusion of OH^- will have occurred and helps to ensure that the inside of the tube is perfectly smooth. The next stage is the deposition of cladding layers, which are of very high purity and thus serve as a barrier between the core and the deposition tube which could possess small amounts of impurities. The cladding layers also reduce the scattering losses from irregularities on the tube wall, and allows the fabrication of complex fibre designs to be realised [15]. The burner traverses down the tube in the same direction as the gas flow, creating a hot zone which lags behind the centre of the burner. It is in this hot zone that the chemicals react, and there is the formation of glass soot particles which are deposited on the tube further downstream. The soot is pushed onto the wall of the tube by thermophoresis [13], which is the process by which particles suspended in a gas with a temperature gradient will move in the direction of decreasing temperature. The temperature gradient is formed by the hot gas flowing into the unheated tube past the burner, where the gas near the wall is cooled, giving a high temperature in the centre and low at the wall of the tube. Due to the high velocity of the gas particles at higher temperatures, the soot particles are pushed towards areas of lower temperature. As the hot zone passes over the deposited glass soot, it is consolidated into a glass film over the inside of the tube. This process is repeated as many times as required for the cladding layers, and then for the core layer, but using different dopants.

The use of different dopants leads to changes in both the refractive index of the

deposited layer and the temperature at which the deposition can occur. Boron, phosphorous and germanium dopants all decrease the required deposition temperature, with phosphorous and germanium increasing and boron decreasing the refractive index. Boron and phosphorous are regularly used to dope silica since the resultant refractive index is the same as for silica, but the reaction temperature is 200^oC lower [15], allowing more layers to be deposited without tube shrinkage.

Once the required layers have been deposited, the final stage is the collapse of the tube at a very high temperature into the final preform. The collapse of the tube into a solid rod must be carefully controlled to ensure no deformation of the tube and no alteration of the chemical composition. The tube collapses down due to the surface tension of the glass, and the decreased viscosity of the glass. The collapse rate should not be too high, either by using low tube pressure or high temperatures, since the tube is not perfectly circular and this can cause elliptical cross sections. The chemical composition is also altered by the temperatures involved, especially in the case of germanium doped cores. The germanium incorporation is governed by equation 2.16, which has equilibrium to the left, inhibiting its deposition. This is a factor during the collapse, when GeO_2 is evaporated whilst SiO_2 remains behind producing a central dip in the refractive index of the preform. This can be eliminated by passing $GeCl_4$ through the tube during collapse [13], or by etching the surface prior to the final stage of collapse [13].

The prevention of water incorporation into optical fibres is extremely important since the intrinsic fibre losses are lowest around $1.55\mu m$ region, which is where a number of OH absorption bands occur. $SiOH$ has sharp absorption bands at $950nm$, $1250nm$ and $1390nm$ with relative intensities of 1:2:40 [15]. $P-OH$ has an absorption band at $1600nm$ which is a broad absorption band, and can also cause losses in the $1.3\mu m$ region [15]. The existence of $P-OH$ can be reduced by eliminating P_2O_5 from the preform, but the losses from $SiOH$ can only be controlled by reducing the water content of the fibre. The water can enter the preform through contamination in the gas stream (through impure chemicals or a leak in pipelines) or diffusion from the original deposition tube. The amount

of OH can be controlled through the reaction [13]:

$$H_2O + Cl_2 \leftrightharpoons 2HCl + \frac{1}{2}O_2 \tag{2.18}$$

$$H_20 + [Si - O - Si]_{solid} \leftrightharpoons 2[SiOH]_{solid} \tag{2.19}$$

Water is absorbed into the silica, whilst HCl is not, thus the quantity of $SiOH$ can be reduced by the presence of Cl_2 during preform fabrication. A significant quantity of Cl_2 is released through the oxidation of the chlorides during the deposition process, and most of the water present is removed as HCl. In the collapse stage, the use of extra Cl_2 can reduce the OH levels, and thus the loss in the fibre. It must be remembered however, that the presence of Cl_2 in the tube will alter the equilibrium state of equation 2.16 and encourage evaporation of the germanium dopant.

The other source of OH contamination is through diffusion from the deposition tube. This can be controlled by using tubes with very low OH content, and having a thick barrier between the tube and the core. The tubes used for the deposition in the ORC are F300 Suprasil grade, created for the purpose of optical fibre fabrication. The glass has levels of trace metals in the sub-ppb range, typical OH content less than $0.2ppm$ and ovality better than 1 in 200. This OH level would give a loss of $9.6dB/km$ at the largest absorption peak of $1390nm$. Barrier thicknesses in the region of $8-10\mu m$ (measured in the final fibre) have been shown to be necessary for tubes with $250ppm$ concentration, with thinner barriers needed when the OH level was dropped to $\approx 1ppm$ [13]. In standard preform fabrication in the ORC, the barrier thickness approaches $8\mu m$ and therefore more than a sufficient barrier against OH diffusion.

Solution doping in MCVD

An essential process for making fibre lasers is the incorporation of rare-earth ions into fibre preforms [16]. The low vapour pressure of the inorganic rare-earth compounds makes it difficult to use the standard MCVD method for the chemical delivery of rare-earth dopants. This lead to the solution doping technique, which allows the addition of rare earth ions to be incorporated into the MCVD process. This technique has lent itself well to use with MCVD, due to the core being the only doped layer and the ease of use. Solution doping has three stages, soot

formation, solution doping, and consolidation. The first stage starts in the same way as for the regular MCVD process, until the layer which will contain the rare earth metals is to be deposited. This silica layer is generated at a lower temperature, so that whilst the soot is formed and deposited, the temperature of the tube is not high enough to consolidate these particles. The result is a layer of porous silica into which the rare earths can be added in solution. The temperature of deposition of the soot layer is critical, if the temperature is too low the soot tends to disassociate from the tube during sintering, if the temperature is too high the absorption of the rare-earth is impaired as the soot becomes sintered as it is deposited [1].

After the tube is removed from the lathe, a solution of a rare-earth compound is created and is pumped slowly into the tube, as shown in figure 2.11. The solution generally consists of a rare-earth chloride dissolved in methanol, there can be any combination required of rare-earths to tailor the core dopants. The porous silica layer is only loosely attached to the interior of the tube and care must be taken whilst transferring the preform from lathe to solution doping clamp not to dislodge any particles. The solution is pumped in slowly for the same purpose, a fast flow could dislodge particles and cause refractive index changes or bubbles to form later in the preform fabrication process. The tube is soaked for about an hour to ensure that complete diffusion of the rare-earth has occurred [1], the tube is then drained slowly and left to dry completely. The drying stage is critical for the successful sintering of the rare-earth doped soot, since any remaining methanol can combust leaving a residue or the wet soot can disassociate from the tube.

The final stage is the consolidation, or sintering, of the soot into a transparent glass layer. The temperature required for sintering can be critical due to evaporation of the chlorides before the oxidation reaction occurs. For high aluminium concentrations (giving preforms with an NA of 0.14 and above) the temperature can be very high, at low concentrations (NA less than 0.1) the oxidation reaction must be performed separately to the sintering. A temperature of around 1400^oC is used which is not high enough for complete sintering of the silica soot, but oxidises the chlorides into the far more stable oxides. Once the oxides are incorporated into the soot, consolidation and then collapse can continue as usual, although care must be taken not to use too high temperatures where silica can

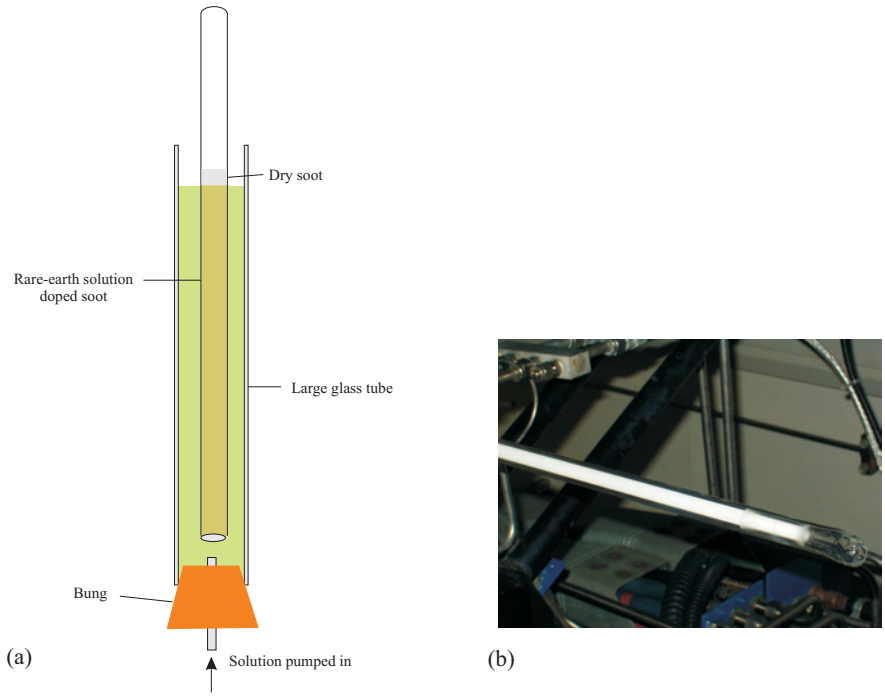

Figure 2.11: (a)Diagram of the aparatus used for the solution doping of silica soot deposited though the MCVD process. The preform is suspended in a tube, and the rare earth/$AlCl_3$ mixture dissolved in methanol is slowly pumped in, so as not to dislodge the fragile soot. (b) Photograph of tube, with rare-earth doped soot, drying on a lathe.

evaporate. The complications encountered whilst fabricating low NA preforms are addressed further in section 3.3.1.

In principle this whole process can be repeated for as many layers as desired, before the tube is collapsed down. In practice the exact refractive index is highly dependent on the deposition temperature, which in turn is dependent on the wall thickness. The wall thickness is altered by the addition of the previous solution doped layer and the degree of collapse whilst sintering, making more than two solution doped layers with the same refractive index extremely time consuming. Unfortunately it is not possible to measure the refractive index during fabrication, thus perfecting the method would require extensive testing and the expensive fabrication of many preforms.

Preform processing

In some cases it is necessary to alter the preform, to improve the properties of the resultant fibre. This is known as pre-processing and involves machining the preform, for instance to improve the birefringence or break the symmetry. This is done in a number of ways; in the creation of highly birefringent fibres, holes are drilled either side of the core; for breaking the symmetry flats are milled into the side of the preform (as shown in figure 2.12). The glass must be polished after this has been performed, usually through fire polishing, since the surfaces are rough and will cause fragile fibres if left untreated.

The cladding to core area ratio for most rare earth doped preforms is around 250:1. To reduce this, preforms can be etched with hydrofluoric acid, reducing the cladding diameter.

2.3.2 Fibre drawing

Figure 2.13 shows a schematic of a typical drawing tower. The preform is mounted in a chuck with x-y positioning stages for aligning the preform in the centre of the furnace. The furnace heats the preform until the viscosity lowers to the point at which it is possible to stretch the end and obtain a fibre. Argon is pumped into

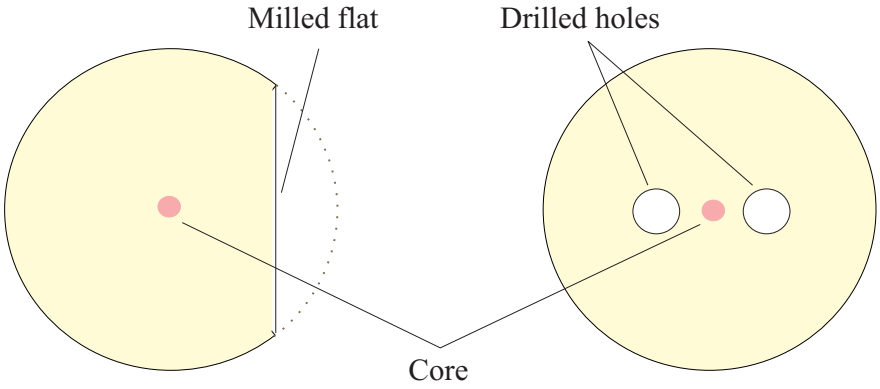

Figure 2.12: Two methods of preprocessing preforms. The milled flat is used to break the circular symmetry of the cladding to improve pump absorption, and the drilled holes are used to induce birefringence in the core.

the furnace to prevent the heated glass reacting with the atmosphere. During fibre drawing the preform is lowered into the furnace as the fibre is drawn out, according to the conservation of mass:

$$\frac{v_p}{v_f} = \frac{d_f^2}{d_p^2} \tag{2.20}$$

where v_p and v_f are the feed and draw speeds respectively, and d_p and d_f are the preform and fibre diameters respectively.

Below the furnace is the laser diameter gauge, which is used to monitor the fibre diameter and then deliver feedback to adjust the draw speed as necessary. The gauge uses a focused laser and a detector opposite to scan across the side of the fibre, when the beam is incident on the fibre there is no signal received at the correct point on the detector and hence the diameter can be determined. Once the fibre has passed through the diameter gauge, $1.5m$ from the base of the furnace, it enters a coating cup containing a viscous acrylate fluid which coats the fibre. The bottom of the cup has a small hole varying between $250\mu m$ and $1mm$, which depends on the size of coating required. The fluid coated fibre is then passed through a curing unit (usually heat or ultraviolet light) where the coating is solidified. The coating forms a hard protective coating over the fibre, allowing it to be handled and bent without the risk of breakage. The fibre then passes round the capstan, which provides the force to draw the fibre and is then wrapped onto a drum with lengths varying from a few metres to tens of kilometres. As the light passes through an optical fibre, the light can be absorbed by atoms or scattered out of the fibre due to imperfections. This causes a loss in the fibre,

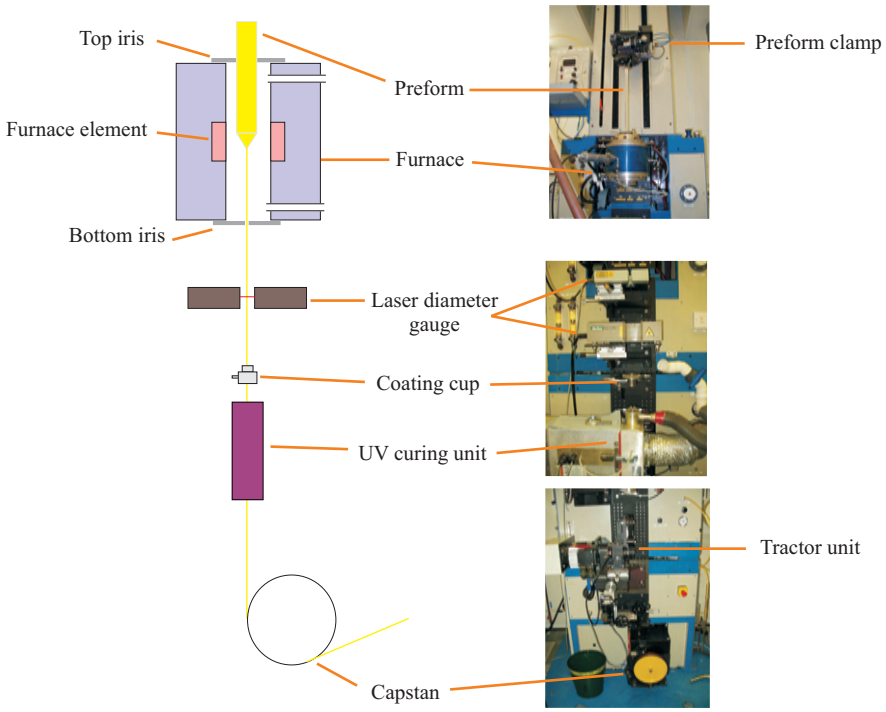

Figure 2.13: A simple drawing tower schematic shown next to photos of the drawing tower using in the ORC. The preform is fed into the furnace from the top, and fibre is drawn out of the bottom by the use of a capstan. The fibre can be coated with protective media before it reaches the capstan.

due to imperfections and impurities present in the preform.

The coating of optical fibres has been extensively investigated as this was a limitation in the fast drawing of optical fibres [17, 18, 19]. Industrial drawing of optical fibres for communications produce fibre in the region of kilometres per minute, which puts a large strain on the coating process since it requires the adherence of viscous liquid to a fast moving solid. The problems were solved by the use of the pressurised coating system [20], along with heating the coating material to reduce the viscosity [19], and tailoring the die geometry [21]. For many standard fibres fabricated within the ORC a non-pressurised coating cup can be used, where the cup holds the coating material and a die at the base controls the coating thickness. This method works well for drawing speeds of $5 - 20m/min$ and fibre diameters less than $\approx 250\mu m$, but for larger fibres or other drawing speeds, the pressurised system must be used.

Whilst drawing the fibre it has been noticed that there is a small contribution to loss, dependent on the tension of the fibre during fibre drawing [22]. The tension

is controlled by the viscosity of the glass and speed of drawing. Due to the large glass transition temperature the viscosity varies over a large range, and drawing temperatures can range from 2100^{o}C to as low as 1750^{o}C. The optimum tension for low loss in fibres has been found to be 30g [15]. If the preform has been processed prior to drawing, then the temperature must be kept low to maintain the shape. The surface tension of the glass increases with temperature whilst the viscosity decreases, so the preform tends towards a circular profile. The amount of deformation is dependent on the time taken in the hot zone of the furnace and the temperature of that hot zone, as has been studied by Furusawa et al. [23].

In addition to the drawing of fibres, the drawing tower can be used to cane cylinders or tubes into rods with diameters varying from 500μm to a few mm. These canes are left uncoated and can be stacked together to form new preforms such as holey fibre preforms. The upper drawing speed of these canes is determined by the rate at which the rods cool, which decreases as the diameter increases. A low furnace temperature is also used to keep the tension on the rod whilst drawing.

2.4 Beam combination

Methods for combining light from separate cores fall into two categories, coherent and incoherent techniques. This section describes techniques for beam combination, in section 2.4.1 coherent methods are addressed, and in section 2.4.2 incoherent beam combination is addressed. The section 2.4.3 will mention 2 mirror beam shaping which is the method used to reform the light from a diode bar stack before fibre pumping, rather than a beam combination technique.

2.4.1 Coherent beam combination

Evanescent field coupling

An approach which allows for the light to be coherently combined, is to allow the modes inside the cores to overlap with one another. This creates a super mode across all the cores in the fibre, which means the output of each core is coupled

to the adjacent cores and can then be coherently combined. The cores must be very close to one another for the fields to overlap, and any perturbation in this separation will cause instabilities in the supermode.

A fibre fabricated by M. Wrage et al. [24] shows the effect of imperfections in the fibre on the energy exchange between cores, and is illustrated in figure 2.14. The fibre consisted of 38 doped cores, in a ring near the edge of the cladding. The core diameter was $6.9\mu m$, with the distance between adjacent cores of $2.7\mu m$. The results showed that the coupling constant between adjacent cores is unaffected by perturbations to the geometry of the cores, however the energy exchange is altered, causing a discrepancy between experiment and theory.

The phase of the light from the cores must be controlled to a precision of less than a wavelength to allow coherent combination. This is less of a problem for a single fibre than it is for multiple laser elements, however it requires only small temperature fluctuations in the cores to cause temporal instability. The coupling effect due to evanescent field overlap is small, which means that although the cores are coupled, they are not phase locked and external optics are required to ensure that an in-phase super-mode is selected rather than an out of phase super-mode.

A method for increasing the coupling, and hence forcing the selection of an in phase super-mode, was performed by Beach et al. [25], using an antiguiding waveguide. The fibre design is shown in figure 2.15, where the refractive index is constant across the rectangular core area, hence the light from the cores are able to interact with all other cores. The degree to which the difference in refractive index of the cores and the surrounding medium affects the formation of the super-mode has been investigated, and shown to have little adverse effect to within predicted fabrication tolerances [26]. The performance of the fibre is extremely dependent on the fabrication of the preform, the quoted example used soft glass to facilitate the preform design and transfer to an all silica design would be difficult, particularly when current fabrication issues are considered as mentioned in section 4.5.3.

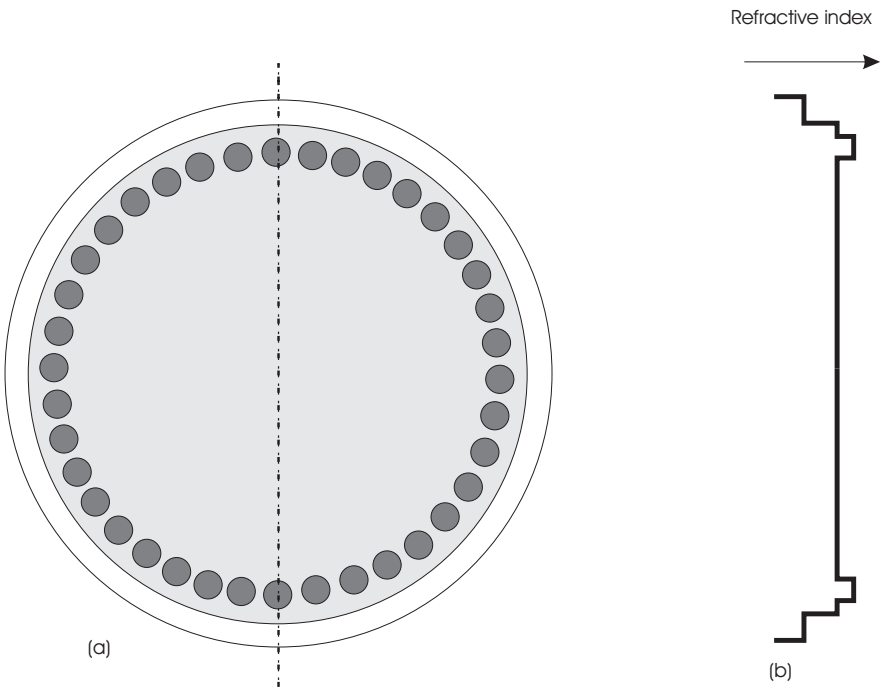

Figure 2.14: a) Cross-section of a Multi-core fibre fabricated by Wrage et al. [24]. b) Refractive index profile through the dotted line shown on the cross section

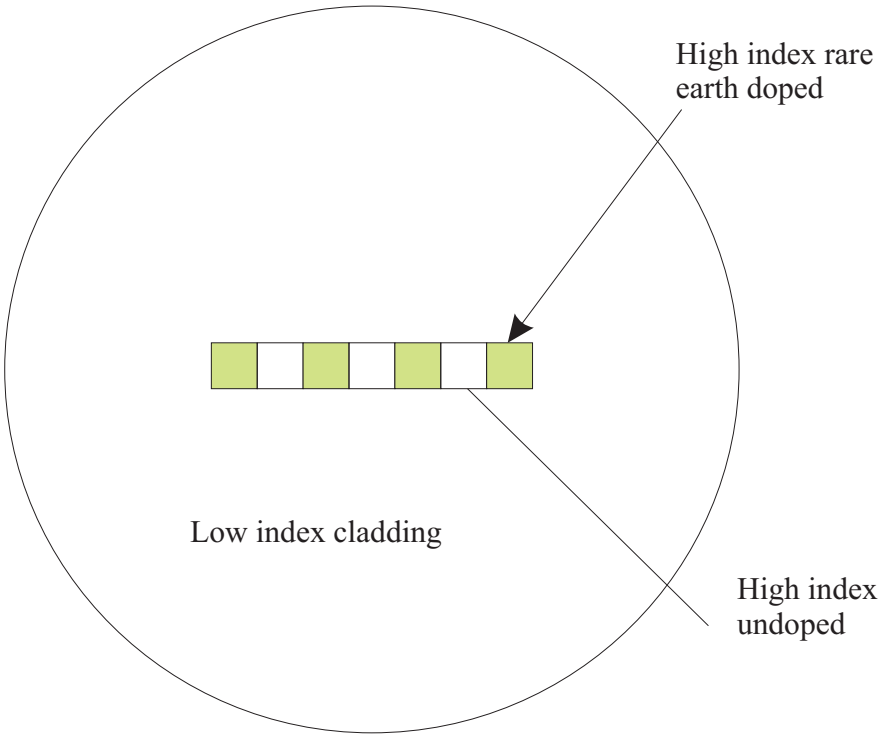

Figure 2.15: Diagram showing the face of the fibre fabricated by Beach et al. The central rectangular core has a uniform low index cladding, with alternating sections of active and inactive regions.

Diffractive coupling

A well established method for enabling the mode-locking of a number of diodes is to use diffractive coupling of the laser array [27]. This method was first demonstrated as a method for forcing the in-phase supermode of an evanescently coupled laser system to lase [28]. However it was shown by Mehuys et al. [27] that if the elements were designed to be optically isolated except in the diffractive coupling region, then operation in the fundamental supermode can be achieved. The setup used for the experimental demonstration is shown in figure 2.16, where the array elements were ridge waveguides with a strong effective index guiding to suppress evanescent coupling. The waveguiding regions were $4.5\mu m$ wide with centre-to-centre spacing of $9\mu m$. Fundamental supermode operation was demonstrated, with extra lobes corresponding to the first and second diffraction orders. By altering the diffraction width from $80\mu m$ to $150\mu m$, a higher order supermode was excited, shown by the absence of the central peak of the fundamental supermode.

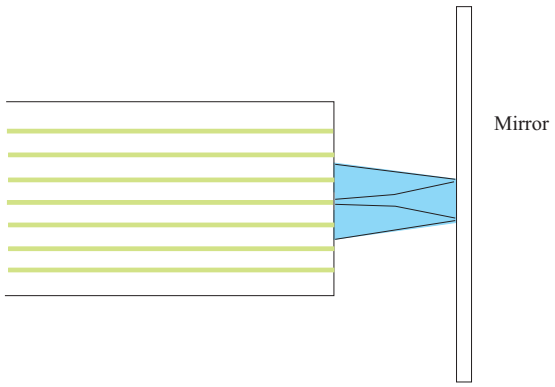

Figure 2.16: Figure showing a beam from an emitter, reflected back and spread due to diffraction from leaving the active medium

1-to-N-way resonators

1-to-N-way resonators operate on a principle which was developed to form Talbot resonators [29]. Talbot resonators utilise a multimode waveguide to phase lock the emissions from a number of emitters and reflect the light back into these emitters, as shown in figure 2.17(a). To understand the principle behind Talbot resonators the propagation of single mode beam in a multimode cavity must be

examined. As shown in figure 2.18, at certain distances the light is split a number of ways across the waveguide due to the interference of the propagation wave [30]. If the peaks at the $L/8$ distance were replaced by optical fibres, it can be seen that light from a single source can be coupled into 8 fibres, each with the same mode. For a laser system with a Talbot resonator at one end and a number of emitters at the other, the fibres would be forced by the Talbot effect to be coupled in-phase. For a Talbot resonator the waveguide length is $L/4$, and the light is reflected back on to the emitters. For the 1-to-N-way resonator, the waveguide is L/N in length, and the light is directed into a single wave guide from multiple waveguides, as shown in figure 2.17(b). By reflecting both ends of this system, all other lasing modes are eliminated and only the supermode will remain.

Both the Talbot resonator and 1-to-N-way resonator systems require high precision in the manufacturing, with the Talbot resonator being extremely sensitive to slight perturbations. The 1-to-N-way system has the advantage of being slightly more stable, and has better coupling between all cores due to the combination into a single beam.

The Talbot resonator was first applied to the case of a multicore optical fibre with a ring of 18 rare-earth doped cores [31]. This showed that self imaging through the Talbot effect could be applied in a similar way to a circular array of emitters, allowing Wrage et al to select the in-phase supermode, albeit in a superposition with two adjacent modes. Later work investigating the use of Talbot resonators using an annular waveguide [32], and through structured mirrors [33], both of which were able to suppress independent lasing of the cores. The use of structured mirrors showed a greatly improved in-phase supermode, when a diffracting spot was used to beam shape the resultant beam.

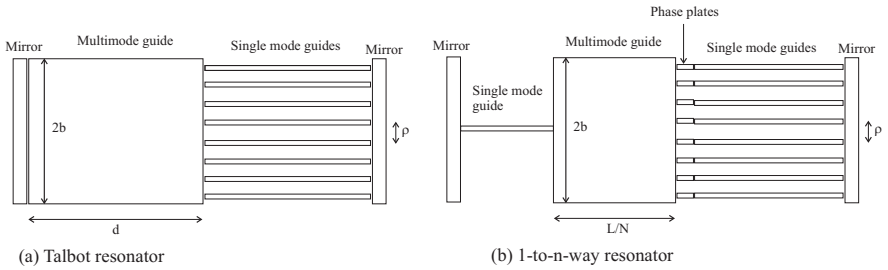

Figure 2.17: a) Diagram of Talbot resonator. Where $d = \frac{\rho^2}{\lambda}$ or half this value. b) Diagram of 1-to-N-way resonator. Where $L = \frac{(2b)^2}{\lambda}$, and there are also phase plates between the multimode guide and the singlemode array

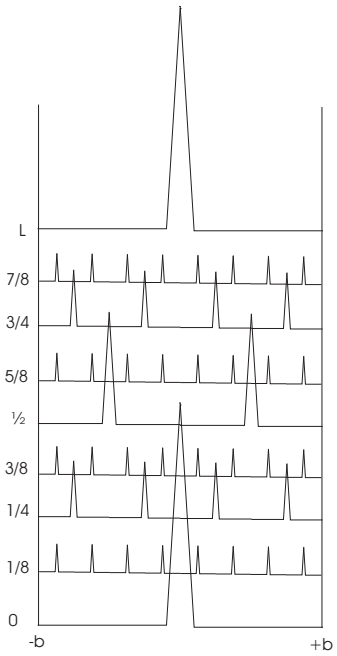

Figure 2.18: Intensity profile at various propagation distances for a guided single mode beam, entering a multimode guide. The distance is measured as a fraction of L, where $L = \frac{(2b)^2}{\lambda}$.

2.4.2 Incoherent beam combination

Spectral beam combination

The Spectral Beam Combining (SBC) technique was developed from a device for use in wavelength division multiplexing applications for telecommunications [34]. The SBC technique combines incoherent laser arrays with different wavelengths to gain spatial brightness, at the cost of spectral brightness. A proof of principle experiment was performed with four Yb-doped fibres [35] and figure 2.19 shows a schematic of the SBC technique. The lens acts to direct the light of a specific wavelength from each fibre, to the same spot on the grating. The angles of incidence are calculated such that the out-coupled beams are overlapped and copropagational. The outcoupling mirror ensures that only light along its axis will contribute to the laser cavity, and thus the fibres will have a wavelength defined by their spatial position [36].

This technique allows a large number of different fibre lasers outputs to be com-

bined and focused into an almost diffraction limited spot. The spatial brightness is dependent on the number of fibres used and the efficiency of the optical devices used in the system. The spectral width increases with the number of fibre lasers used, with the width and spacing of the individual wavelengths such that there is little cross talk between adjacent lasers.

It is the SBC technique that will be used for the combination of light from the cores of the multicore fibre, and will be examined in detail in section 4.3.4.

Multiple core M^2 combination

In some applications such as industrial welding or laser pumping, it is not necessary to have a diffraction limited output, a beam with M^2 of less than 10 with very high power is suitable. One property required by all applications is the stability of the output. The output from large core fibres is unstable due to the high powers stored in the cores, and is susceptible to pulsing hence damaging the output facet of the cores. To avoid this, single mode cores with very stable outputs can be used and arranged in such a manner where there is no over lap between the cores. M^2 is the relationship between the divergence of a beam with a certain waist, compared to the divergence of a Gaussian beam of the same waist.

$$w_0 = \frac{M^2 \lambda}{\pi \Theta_0} \tag{2.21}$$

Where w_0 is the beam waist radius, and Θ_0 is the far field divergence angle.

From equation 2.21 it is clear that since divergence and beam waist are inversely proportional, M^2 can be thought of as a measure of the waist size given a certain divergence. For a number of cores arranged with no mutual coherence, this means that the M^2 is simply the ratio between the diameter of the area the cores cover (D) and the area of a single core (d) multiplied by the M^2 of the single core as shown in figure 2.20.

This method can be used to make high power sources with very stable beam outputs, with good beam qualities useful for many industrial applications.

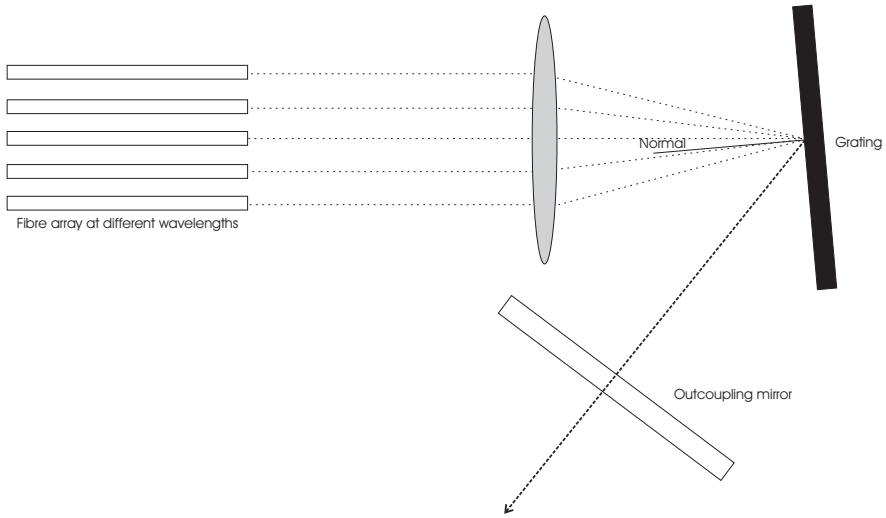

Figure 2.19: Fibres with slightly differing wavelengths are focused onto a diffraction grating. The beams are combined and selected via the outcoupling mirror which forms part of the laser cavity.

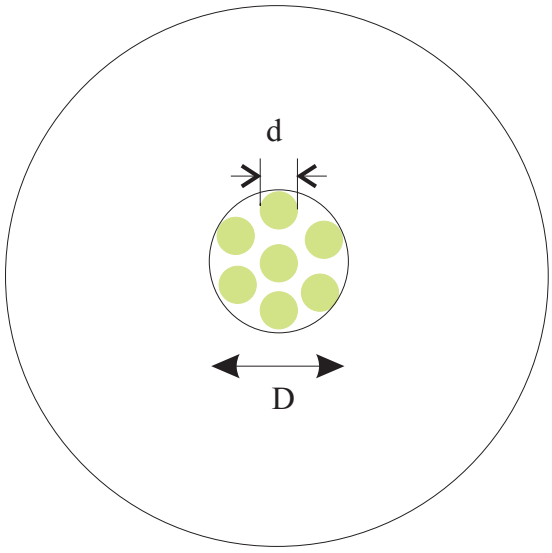

Figure 2.20: The beam quality from an array of incoherently combined cores can be expressed as the total diameter of the area covered by the cores, divided by the diameter of an individual core, multiplied by the M^2 of the individual cores.

2.4.3 2 mirror beam shaping

Two-mirror beam shaping is a technique designed to alter the beam quality from a laser diode bar array in order to improve the launch efficiency when coupling into fibres [37]. The principle of 2-mirror beam shaping is to 'chop up' the incident beam and rearrange it in a more suitable shape for fibre coupling.

Two mirrors are positioned as shown in figure 2.21 and are of very high reflectivity. The beam can be thought of in terms of a number of separate beams, the dimensions of which are determined by the mirror spacing and angle of incidence of the beam. The first section of the beam passes both mirrors and is unaltered. The second part of the beam passes over mirror A, reflects off first mirror B and then mirror A, and is repositioned under the first section of the beam. This process repeats for all sections of the beam, and thus reformats the beam shape without altering the beam divergence. This results in the M^2 values being altered, reducing one and increasing the other, along with the shape of the beam. This technique can be applied to the multicore fibre, by replacing the single incident beam with a number of separate laser beams from the cores in the fibre, and for example convert a line of 9 cores into a group of cores in a 3 by 3 matrix.

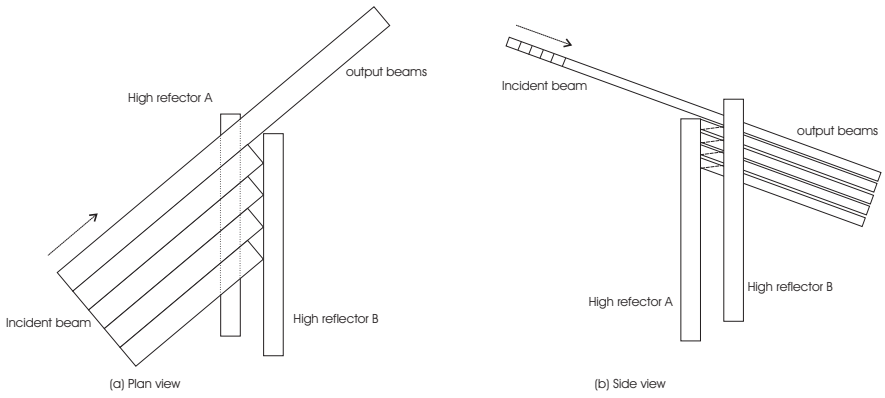

Figure 2.21: Two mirror beam shaping technique. Shown in a) is the plan view, showing the first part of the beam missing both mirrors. b) shows the side view of the beams being manoeuvered under each other

2.5 References

[1] J.E. Townsend. The development of optical devices doped with rare-earth ions. *PhD Thesis. University of Southampton, Faculty of Electronics and Computer Science*, 1990.

[2] M. J. F. Digonnet. *Rare earth doped fibre lasers and amplifiers,*. Basel: Dekker, 1993.

[3] L. Reekie, R. J. Mears, S. B. Poole, and D. N. Payne. Tunable single-mode fiber lasers. *Journal of Lightwave Technology*, 4(7):956–960, 1986.

[4] L. Zenteno. High power double clad fibre lasers. *Journal of Lightwave Technology*, 11(9):1435–1447, 1993.

[5] J. Xu, J. Lu, L. Lu, and K. Ueda. Influence of cross-sectional shape on absorption characteristics of double-clad fibres. *Proceedings of the Conference on Lasers and Electro-optics*, 1:520–521, 2002.

[6] K. Ueda, H. Sekiguchi, and H. Kan. 1kW cw output from fibre embedded lasers. *Proceedings of the Conference on Lasers and Electro-optics*, postdeadline:CPDC4, 2002.

[7] V. Dominic, S. MacCormack, R. Waarts, S. Sanders, S. Bricknese, R. Dohle, E. Wolak, P.S. Yeh, and E. Zucker. 110W fibre laser. *Electronics Letters*, 35:1158–1160, 1999.

[8] H. Zeller, U. Williamowski, A. Tunnermann, H. Welling, S. Unger, V. Reichel, H.R. Muller, J. Kirchof, and P. Albers. High-power cw neodymium doped fibre laser operating at 9.2W with high beam quality. *Optics Letters*, 20:578–560, 1995.

[9] A. Ghatak and K. Thyagarajan. *Introduction to fibre optics*. Cambridge: University Press, 1998.

[10] A. Altintas and J.D. Love. Effective cut-offs for modes on helical fibres. *Optical and Quantum Electronics*, 22:213–226, 1990.

[11] R. D. Birch. Fabrication and characterisation of circularly birefringent helical fibres. *Electronics Letters*, 23(1):50–52, 1987.

[12] L. Tingye. *Optical fiber communications*. New York: Academic press inc. pp 3, 1985.

[13] L. Tingye. *Optical fiber communications*. New York: Academic press inc. pp 97-179, 1985.

[14] J.Wang, D. T. Walton, and L. A. Zenteno. All-glass high NA Yb-doped double-clad laser fibers made by outside-vapour deposition. *Electonics Letters*, 40(10), 2004.

[15] L. Tingye. *Optical fiber communications*. New York: Academic press inc. pp 6, 1985.

[16] S. B. Poole, D. N. Payne, and M. Fermann. Fabrication of low loss optical fibres containing rare earths. *Electronics Letters*, 21(17):737–738, 1985.

[17] S. Ravinutala and C. Polymeropoulos. Entrance meniscus in a pressurized optical fiber coating applicator. *Experimental Thermal and Fluid Science*, 26:573–580, 2002.

[18] D. Jacqmin. Very, very fast wetting. *Journal of Fluid Mechanics*, 455:347–358, 2002.

[19] C. Y. Zhao and S. H.-K. Lee. Physical considerations of a pressurized optical fibre coating process. *Journal of Materials Processing and Manufacturing Science*, 8:53–73, 1999.

[20] S. Sakaguchi and T Kimura. High-speed drawing of optical fibres with pressurised coating. *Journal of Lightwave Technology*, 3:669–673, 1985.

[21] P. W. France, P. L. Dunn, and M. H. Reeve. Plastic coating of glass fibres and its influence on strength. *Fibre and Integrated Optics*, 2(3-4):267–286, 1979.

[22] H. Schonhorn, H. N. Vazirani, and H. L. Frisch. Relationship between fiber tension and drawing velocity and their influence on the ultimate stength of laser-drawn silica fibers. *Journal of Applied Physics*, 49(7):3703–3706, 1978.

[23] K. Furusawa. Fabrication, characterisation and application of novel holey optical fibres. *PhD thesis. University of Southampton, Faculty of Electronics and Computer Science*, 2001.

[24] M. Wrage, P. Glas, M. Leitner, T. Sandrock, N. N. Elkin, A. P. Napartovich, and A. G. Sukharev. Experimental and numerical determination of coupling constant in a multicore fibre. *Optics Communications*, 175:97–102, 2000.

[25] R. J. Beach, M. D. Feit, S. C. Mitchell, K. P. Cutter, R. Wilcox, S. A. Payne, R. W. Mead, J. S. Hayden, D. Krashkevich, and D. A. Alunni. Phase-locked antiguided multiple-core ribbon fiber. *IEEE Photonics Technology Letters*, 15(5):670–672, 2003.

[26] R. H. Page L. D. Brasure R. Wilcox R. J. Beach, M. D. Feit and S. A. Payne. Scalable antiguided ribbon laser. *Journal of the Optical Society of America B*, 19(7):1521–1533, 2002.

[27] L. Eng W. K. Marshall D. Mehuys, K. Mitsunaga and A Yariv. Supermode control in diffration-coupled semiconductor laser arrays. *Applied Physics Letters*, 53(13):1165–1167, 1988.

[28] M. Jansen S. Wang, J. Z. Wilcox and J. J. Yang. In-phase locking in diffraction-coupled phased-array diode lasers. *Applied Physics letters*, 48(26):1770–72, 1986.

[29] R. G. Waarts D. Mehuys, W. Streifer and D. F. Welch. Modal analysis of linear Talbot-cavity semconductor lasers. *Optics Letters*, 16(11):823–825, 1991.

[30] J. Banerji, A. R. Davies, and R. M. Jenkins. Comparison of Talbot and 1-to-N-way phase-locked array resonators. *Applied Optics*, 36(7):1604–1609, 1997.

[31] M. Wrage, P. Glas, D. Fischer, M. Leitner, D. V. Vystsky, and A. P. Napartovich. Phase locking in a multicore fiber laser by means of a Talbot resonator. *Optics Letters*, 25(19):1436–1438, 2000.

[32] M. Wrage, P. Glas, D. Fischer, M. Leitner, N. N. Elkin, D. V. Vysotsky, A. P. Napartovich, and V. N. Troshchieva. Phase-locking of a multicore fiber laser by wave propagation through an annular waveguide. *Optics Communications*, 205:367–375, 2002.

[33] M. Wrage, P. Glas, and M. Leitner. Combined phase locking and beam shaping of a multicore fiber laser by structured mirrors. *Optics Letters*, 26(13):980–982, 2001.

[34] I. H. White. A multichannel grating cavity laser for wavelength division multiplexing applications. *Journal of Lightwave Technology*, 9(7):893–899, 1991.

[35] C.C. Cook and T.Y. Fan. Spectral bean combining of Yb-doped fibre lasers in an external cavity. *Advanced Solid State lasers*, 26:163–166, 1999.

[36] E. J. Bochove. Theory of spectral beam combining of fibre lasers. *IEEE Journal of Quantum Electronics*, 38(5):432–445, 2002.

[37] W. A. Clarkson and D. C. Hanna. Two-mirror beam-shaping technique for high-power diode bars. *Optics Letters*, 21(6):375–377, 1996.

Chapter 3

Helical core fibre laser

3.1 Introduction

The light emitted from a fibre laser is generally arbitrarily polarised. There are a number of methods for making fibre which maintain linearly polarised light such as PANDA fibres [1], elliptical core [2], bow tie fibres [3], or helical core fibres as described in section 2.2.3. With the exception of the helical core fibre, all of these use distortions or stress in the core to induce a linear birefringence. The helical fibre is an optical effect, which has since been compared with Berry's phase phenomenon for objects with spin proceeding down a helical path [4], which will be addressed in section 3.2.1. A fibre laser fabricated with polarisation maintaining properties can provide an output polarised in a single direction, which is useful for sensors or beam combination.

The helical core fibre also has the property of an inherent bend loss, which can be used for mode selection, this is examined in section 3.2.3. The fabrication of helical core fibres is significantly different from conventional fibres which requires designing and optimisation, this will be addressed in section 3.3. The accuracy of the theoretical bend loss prediction is critical for the successful fabrication of a helical core fibre laser, therefore the predictions are tested in section 3.4. The results from a fabricated core-pumped helical core fibre laser are presented in section 3.5 and from a cladding-pumped helical core fibre laser in sections 3.6

and 3.7.

3.1.1 History

Helical core fibres have been fabricated previously in Southampton in 1985 [5]. The purpose of the helical core was to detect current flowing through a wire by wrapping the polarisation maintaining helical core fibre round it and detecting changes to the angle of polarisation. The polarisation would rotate due to the Faraday effect, where the magnetic field surrounding the flowing current in the wire alters the refractive indices of the glass seen by circularly polarised light, and causes a phase change [6]. The fibres were fabricated by spinning an off-centred core preform whilst drawing it into fibre.

There has been a large amount of theoretical work investigating propagation loss in bent optical fibres. One of the first investigations was performed by Snyder and Love [7], deriving the bend loss for fibres through a Kirchoff-Huygens diffraction integral. Since then expressing the field outside the fibre as a superposition of cylindrical outgoing waves [8], and analysing radiation modes adapted from slab waveguides [9] have been used and are all essentially in agreement, within the limit that the bend radius is large.

3.1.2 Benefits

The highest power attained by a single core fibre with near Gaussian beam is $1.3kW$, and was achieved by bending a large core fibre [10]. The fibre used was 600 μm in diameter, which could easily bend into the radius required to strip modes higher than the fundamental. As power levels are increased further there is the need for more pump light and thus larger cladding dimensions are required into which it can be coupled. As fibres become larger they will then become difficult to bend to the required curvature or be fragile when bent to the required radius, hence limiting the scope of this technique. Helical core fibres have the advantage that the required core curvature can be built into the fibre, so there is no need for further bending.

The helical path of the core also makes the fibre circularly birefringent. This means that it will maintain linearly polarised light with the polarisation in any direction, this phenomenon is discussed in section 3.2.1. The helical core fibre can form the basis of fibre lasers with single polarisation or single-mode output.

3.2 Analysis of helical fibre

3.2.1 Polarisation rotation

There are a number of papers [11] [12] which show that the rotation of polarisation in a helical core fibre is a purely geometric effect, which it is possible to derive the extent of the rotation without resorting to quantum mechanics. One such method for deriving the rotation of polarised light in a fibre uses the Serret-Frenet set of co-ordinates [13]:

$$\hat{J}_t = r' \qquad \hat{J}_n = \hat{J'}_t/\kappa \qquad \hat{J}_b = (\hat{J'}_n + \hat{J}_t)/\tau$$

$$\tau = \frac{2\pi P(z)}{S^2(z)} \tag{3.1}$$

The vector $r(s)$ describes the path of the helical core, with s being the length along this path, τ is the torsion in the fibre, κ is the curvature, and $S = (4\pi^2R^2+P^2)^{1/2}$, where R is the offset and P is the pitch length.

Figure 3.1 shows a diagram of a helix within a fibre and an unwound helix, both indicating the dimensions of S, R, P, and the pitch angle θ.

The first two Serret-Frenet co-ordinates therefore, are the tangent to the core, and the normal to the path directed at the centre of the fibre respectively. By using results from Ross [14], the polarised light in a helical fibre lags behind the rotation in the Serret-Frenet frame by:

$$\varphi_t = -\int_0^S \tau(s')ds \tag{3.2}$$

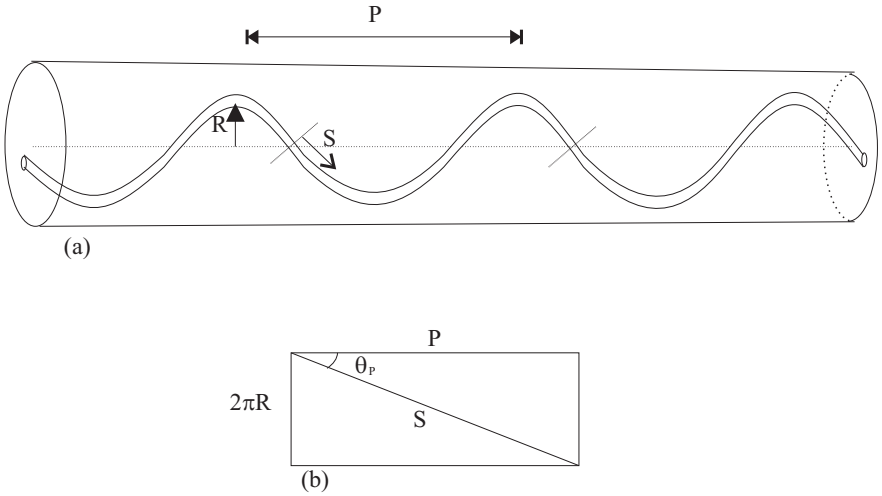

Figure 3.1: Diagram of a helix and the directions for measurements. (a) Shows a helix as it would be inside a fibre. (b) Shows an unwound helix, giving a better indication of the relationship between all the parameters

Whilst the fibre normal rotates by:

$$\varphi_n = 2\pi \int_0^S \frac{1}{S(s')} ds \tag{3.3}$$

The geometric phase is simply the sum of these:

$$\varphi_r = \int_0^s \frac{2\pi}{S(s')} - \tau(s') ds' \tag{3.4}$$

By inserting the definition for τ given earlier and using the identities $z = s\cos\theta_p$ and $\cos\theta_p = \frac{P}{S}$, this gives us:

$$\varphi_r = 2\pi \int_0^z \left[\frac{1}{P(z')} - \frac{1}{S(z')} \right] dz' \tag{3.5}$$

By making the assumption that the fibre geometry is uniform, P and S are independent of z. This makes the total rotation of the polarisation:

$$\varphi_r = 2\pi (\frac{1}{P} - \frac{1}{S}) \int_0^z dz' = \frac{2\pi z(S-P)}{PS} \tag{3.6}$$

This effect is purely due to the geometry of the fibre and therefore not affected by stress or small temperature fluctuations. Any shear or stress on the fibre will induce an amount of circular birefringence, but will be swamped by the larger geometrical birefringence in a properly designed fibre. This makes it ideal for the construction of a circularly birefringent fibre, as it has a built-in pitch and offset as shown in figure 3.2.

A fibre which is circularly birefringent can maintain linearly polarised light. This is due to the fact that linearly polarised light, passing through a helical fibre, can be split into right and left circularly polarised components. These propagate through the fibre and, due to the birefringence in the fibre, move at different velocities. As for linearly birefringent fibres mentioned in section 2.2.3, the two polarised components have different energies from the circular birefringence, and therefore will be maintained. The two components therefore see a different local refractive index, which causes a change in phase as the light progresses down the fibre. Once the two components are combined the result is that the angle of the linearly polarised light rotates along the length of the fibre.

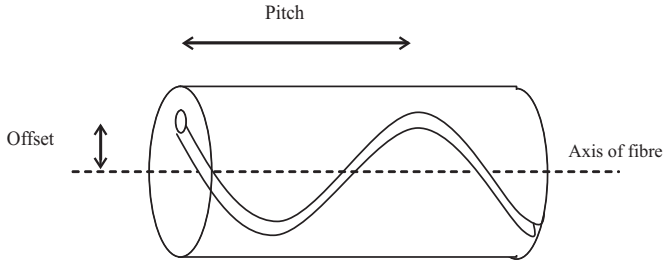

Figure 3.2: Side view of a helical core fibre indicating the lengths of pitch and offset refered to in this report

The angle at which the light is polarised once it exits the fibre is dependent on the length of the fibre, and the inherent properties of that fibre. This has no advantage over standard polarisation maintaining fibres since either additional optics are required to be aligned with that angle, or the fibre must be cut to a precise length. Once the light is reflected back through the fibre however, the light emitted from the launching end will be in the same polarisation state as the original beam. Figure 3.3 shows the helical core fibre with the end faces as seen from the exterior of the fibre. The light proceeding forwards through the fibre experiences a rotation, due to the helical path, in a clockwise direction,

lagging behind the helical frame by the geometrical phase. The light reflected back through the fibre also experiences a rotation, due to the helical path, in a clockwise direction and since the fibre is now reversed, it is anticlockwise in the frame of reference of the original beam. This means that the light emitted from the launch end of the fibre will be in the same polarisation state, enabling the formation of a laser cavity and canceling any variation in the circular birefringence due to temporal stress or temperature.

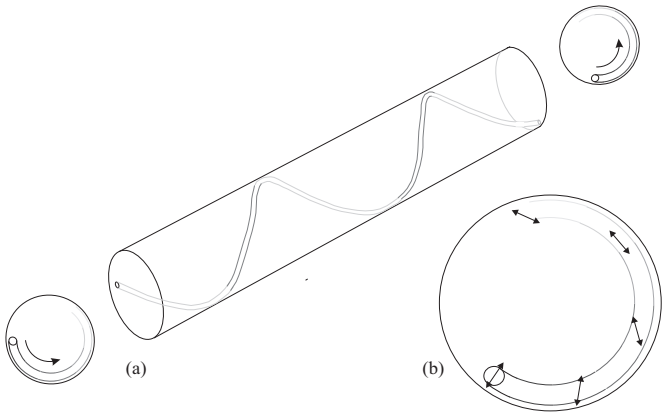

Figure 3.3: (a) A short section of helical core fibre with the end on views showing that the light experiences anticlockwise rotation as it proceeds through the fibre in both directions. (b) View of the end face of the fibre showing an exaggerated example of the rotation of polarised light as it travels along the core.

3.2.2 Birefringence

The magnitude of the birefringence induced in a helical fibre is calculated by using equation 3.6 and the relation [15] that the beat length $L_b = \frac{2\pi}{\delta\beta}$ and $\Delta n_{LR} = \frac{\lambda_0 \delta\beta}{2\pi}$, giving the equation:

$$\Delta n_{LR} = \frac{\lambda}{PS}(S - P) \tag{3.7}$$

where $\delta\beta$ is the propagation constant Δn_{LR} is the difference in refractive indices for left and right circular light.

In order for a fibre to exhibit a large circular birefringence either the pitch length must be decreased, or the core offset increased. The effect of increasing the

birefringence is to reduce the length over which the polarisation of the light is rotated by 2π. The equation for this rotation length is given by [16]:

$$L_z = \frac{SP}{S-P} \approx \frac{P^3}{2\pi^2 R^2} \qquad for P \gg R \tag{3.8}$$

For a fibre such as has been demonstrated [5] with a pitch length of 1.5mm and an offset of $170\mu m$, the predicted rotation length would be $5.9mm$ and for a similar fibre with a different offset of $200\mu m$ the rotation length would be $4.3mm$.

The degree of birefringence that the fibre exhibits can be accurately controlled by careful design of the preform and by controlling the drawing process, and so create polarisation maintaining fibre. It is important to note that the conditions for which the birefringence of a helical core fibre is increased, also raise the bend loss of the fibre. The exact relationship between the birefringence and bend loss is investigated in section 3.2.3.

From the above equations it is useful to derive the relation between the rotation length and the birefringence, which is simply:

$$L_z = \frac{\lambda}{\Delta n_{L,R}} \tag{3.9}$$

Typical birefringences for linearly birefringent fibres are: $4.2 * 10^{-4}$ for elliptical core fibres and $5.9 * 10^{-4}$ for fibres with stress rods. The maximum offset for a $125\mu m$ helical core fibre would be around $50\mu m$ due to the space between the core and the edge of the cladding, and the diameter of the core. This fibre would then require a pitch length of $0.8mm$ to attain a birefringence of $1 * 10^{-4}$, close to the levels of birefringence employed in linearly birefringent fibres. A larger fibre is needed, with an increased offset, to reduce the pitch length required to satisfy the condition that $P \gg R$.

3.2.3 Bend loss

The bend loss of a fibre is the amount of light propagating through the core which is lost due to a bend which a fibre goes through, defined by the radius of curvature, as illustrated in figure 3.4(a). In the case of a multimode fibre,

the bend loss can be simply thought of as the change in angle at which light is propagating due to being incident on the interface at a changed angle. In a single mode fibre however, light has a Gaussian distribution of which the ends of the tails propagate outside the core as shown in figure 3.4(b), the tails on the outer surface of the curve must travel at a higher speed than the light in the centre. Once the light in the tail matches the higher speed of light in the lower refractive index of the cladding, the light can escape into the cladding and is lost. It is simple to see that at large radii of curvature, only a small fraction of the tail will be as fast as light in the cladding, whilst for small radii of curvature a large fraction will be lost to the cladding. Similarly, with a lower NA there is more field outside the core and so the loss due to bending increases.

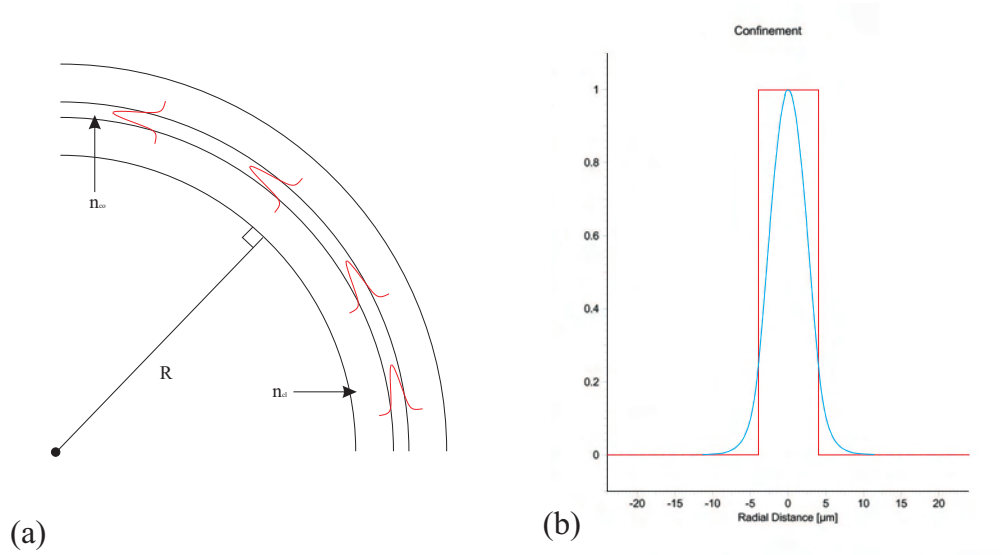

Figure 3.4: Fundamental mode of a single-mode optical fibre. (a) The bend radius R is the distance from the centre of the fibre to the point of origin of the bend. Light in the outer wing of the fundamental mode must travel faster than the light in the core and thus can couple to the modes of light travelling in the cladding. (b) The mode distribution in a single-mode fibre superimposed on the refractive index profile of the core, showing the intensity of the light in the wings of the Gaussian distribution.

A number of methods have been used to calculate the loss for bent optical fibres including analysing radiation mechanisms, whispering modes of a curved metal surface and using the Kirchhoff-Huygens diffraction integral. The final method mentioned, calculated by Snyder et al. [17], has also been calculated for the case of helical fibres, where there is an added factor to the loss equation, from interference between progressive loops of the helix. The bend loss for helical core

fibres is one of the reasons why the design is suited for high power single mode lasing operation. A limitation in current fibre lasers is saturation in the gain medium, so to obtain higher powers larger cores are preferable. Large cores lead to a larger number of supported modes, and this is measured by the normalised frequency V of the fibre. Fibres with V values over 2.4 are multimode, with the number of modes increasing for higher values. In helical core fibres the bend losses for higher order modes are orders of magnitude higher than for the fundamental mode, meaning that the core can be very large whilst still maintaining single mode operation [18]. It has been shown that helical core fibres with normalised frequencies of up to 25 can be made to only support the fundamental mode [16]. For a device to be viable for use in fibre lasers, the loss for the fundamental mode should be of the order of a few tenths of a dB/m. This is defined by the pump losses and the small signal gain, and dictates the required device length. The bend loss equation for bent single mode fibres has been derived [17] as:

$$\alpha(dB/m) = 4.343\left(\frac{\pi}{4rR}\right)^{1/2}\left(\frac{U}{VK_1(W)}\right)^2\frac{1}{W^{3/2}}e^{\left[\frac{-2W^3}{3k_0^2r^3n_1^2}R\right]} \tag{3.10}$$

where r is the core radius, $k_0 = \frac{2\pi}{\lambda_0}$, V is the normalised waveguide parameter, U and W are normalised modal parameters, K_1 is the modified Bessel function and n_1 is the refractive index of the core

This however doesn't take into account the constructive interference between modes on adjacent parts of the helix. Love and Snyder [7] amended equation 3.10 to take into account the helical interactions, which come into play as the pitch becomes smaller or the offset becomes larger. The equation now looks like:

$$\alpha(dB/m) = 4.343\left(\frac{2}{r}\right)^{1/2}\left(\frac{\pi^2RV^{5/2}}{\Delta^{1/4}P^{3/4}U^2(1+\delta)^{1/4}}\right)^2 e^{\left[\frac{-2\Delta^{1/2}SW^2}{3\pi rV(1+\delta)^{1/2}}R\right]} \tag{3.11}$$

where $\delta = 2\left(\frac{\theta_p^2}{\theta_c^2}\right)\left(\frac{V^2}{W^2}\right)$, $\theta_c = \arccos\left(\frac{n_{cl}}{n_{co}}\right)$, $\theta_p = \arctan\left(\frac{2\pi R}{P}\right)$ and $\Delta = \sin^2\left(\frac{\theta_c}{2}\right)$

Using this equation figure 3.5 was plotted, showing the sensitivity of the loss with changes in the pitch, the offset and the numerical aperture.

The dependence on wavelength, as shown in figure 3.6 is weaker than for the other parameters, with a variation of $6dB/m$ over the ytterbium emission bandwidth. The sensitivity to numerical aperture and pitch length are crucial, since variations of 2.5% can double the attenuation.

3.2.4 Core area scalability

The attainment of greater than 1kW from a single fibre with M^2 nearly 1, by Jeong et al, used fibre with a diameter of $600\mu m$ and core diameter of $40\mu m$. For the demonstration of tens of kWs from a single mode fibre it is essential to be able to couple more pump light, therefore the cladding dimension will need to be increased. Past inner cladding $1mm$ diameter it becomes increasingly more difficult to bend the fibre to the degree needed to suppress higher order modes. Table 3.1 shows the required bend radius for some example fibre dimensions, by using equation 3.16 referred to in section 3.4.6.

Fibre Diameter(μm)	Core Diameter (μm)	Bend radius required (mm)
600	30	18
800	40	21
1000	50	25
1500	75	34

Table 3.1: Table showing the bend radius required for the bend loss for the fundamental mode to be less than $1dB/m$ whilst the next highest order mode is greater than $10dB/m$

The upper limit for the bend radius achievable using a helical core fibre is far higher than for large bent fibres, which makes it ideal for pushing the limits of power attained from a single core fibre. The limit for helical core fibres is defined by the requirement that the pitch length be far greater than the offset to reduce the degree to which subsequent helical loops interfere with each other. For the equivalent fibre to the last example in the table an equivalent loss is achieved at a pitch of $28\mu m$ and offset of $600\mu m$ for a fibre with a diameter of $1500\mu m$ and core diameter of $75\mu m$.

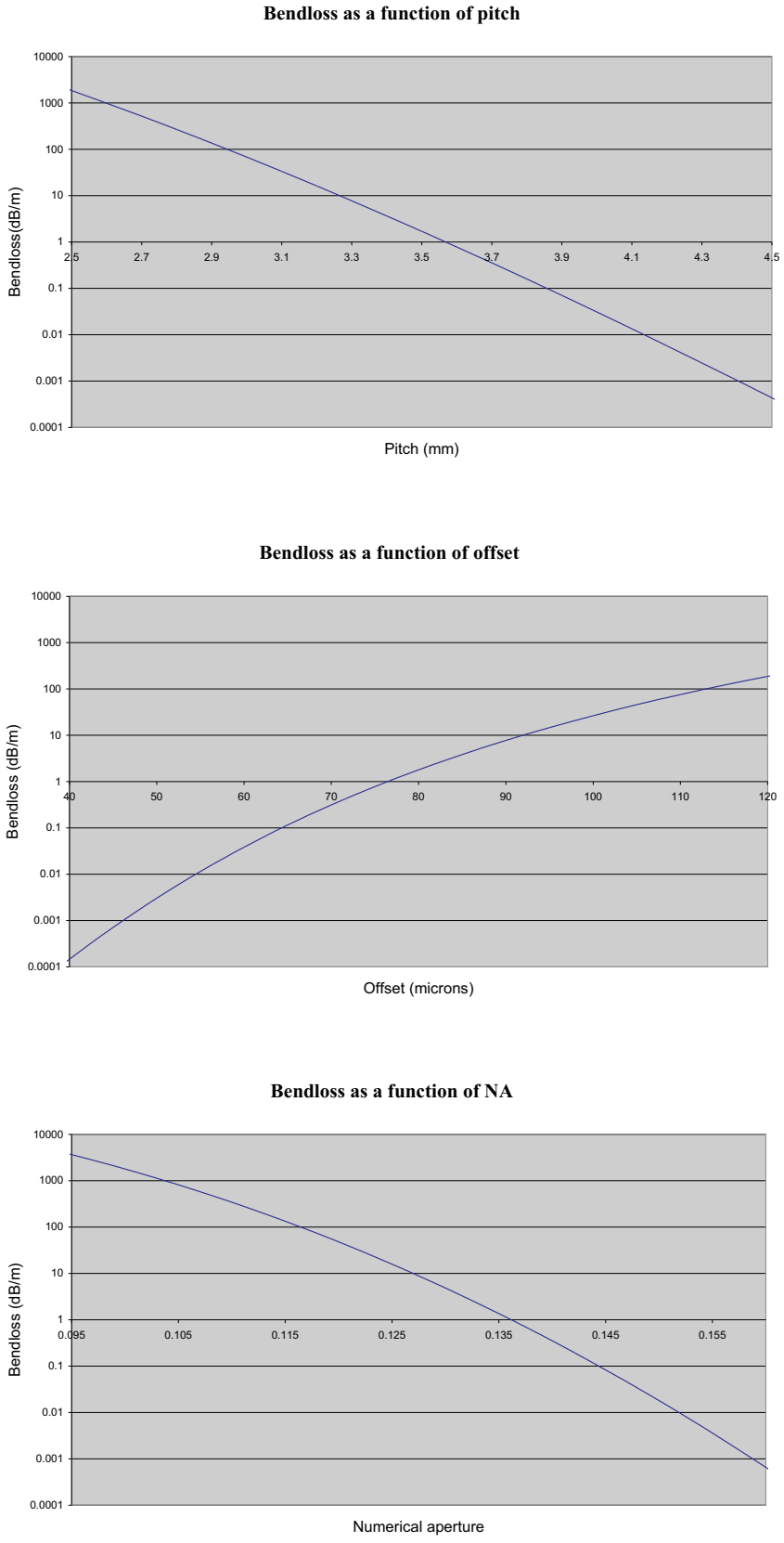

Figure 3.5: Graph showing the relative effects of pitch, offset and NA on the bend loss of the fibre. The basic fibre parameters used were a core diameter of $30\mu m$, offset of $75\mu m$, pitch length of $3.6mm$ and an NA of 0.135.

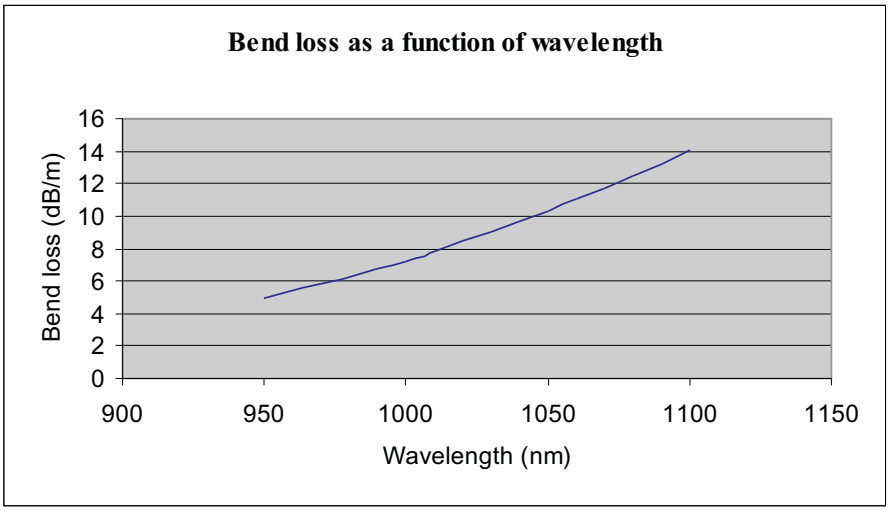

Figure 3.6: Graph showing the effect of variation in wavelength on bend loss

3.2.5 Fabrication methods

One method for creating a helical core fibre is to make a preform with an off-centre core, and then spin either the preform or the fibre whilst drawing. The fabrication of very low birefringence fibre by spinning the preform whilst pulling, smooths out any intrinsic birefringence in the preform [19]. The previous technique used at Southampton for the fabrication of helical core fibres [5] was the rotation of the preform whilst drawing in the drawing tower. Spinning the preform has some draw backs which are; the possible deformation due to a viscous cylinder rotating at high speed, and any oscillation due to imperfect alignment of the preform segments.

3.3 Helical-core fibre fabrication

3.3.1 Low NA, ytterbium doped preforms

An example preform refractive index profile for the standard aluminium-ytterbium doped preform with an NA of 0.14 is shown in figure 3.7. Preforms with NAs of 0.09 or lower, fabricated in the same way as for the higher NA, end up with a central dip in the refractive index profile. Modeling of this preform shape in a commercial fibre design software package shows that the fundamental mode

becomes a ring, as illustrated in figure 3.8 and this degrades the resultant beam quality. The refractive index shape shown for the preform with NA of 0.14 has very good characteristics for the propagation of the fundamental mode. The

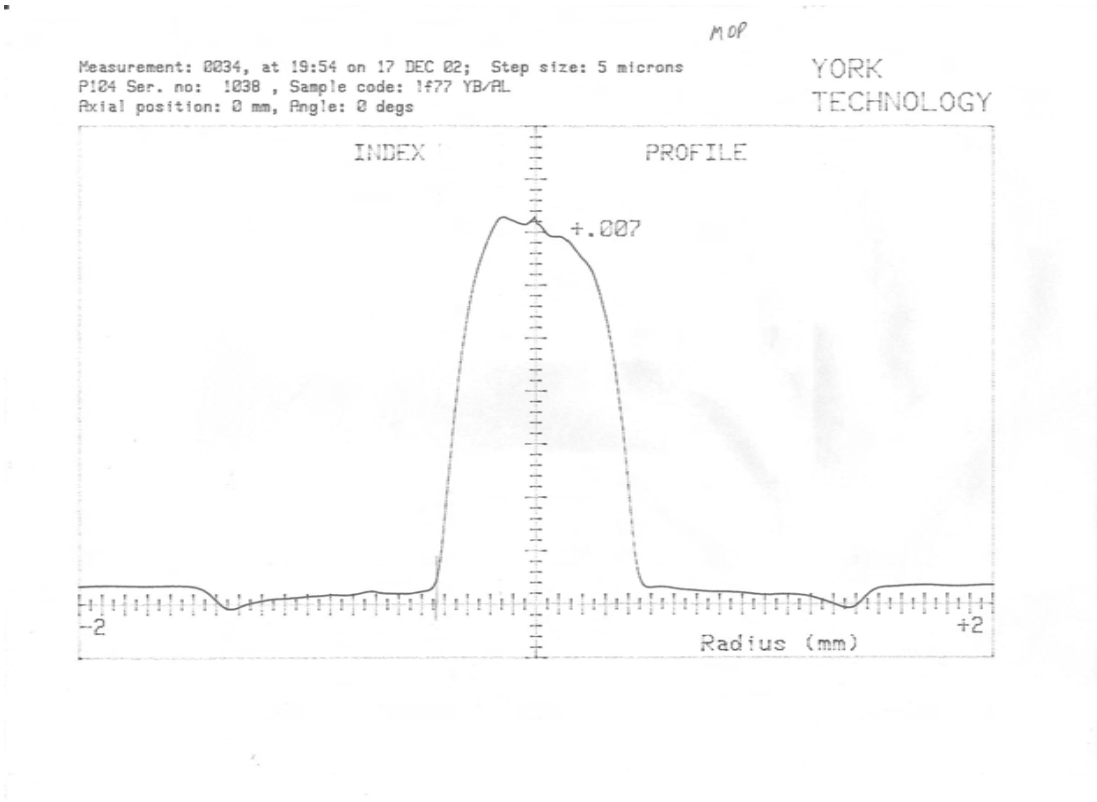

Figure 3.7: An example of the fabrication technique for Al/Yb doped preform with an NA of approximately 0.14. A high temperature is used to consolidate the doped soot, and a high flow rate of $SiCl_4$ is used to deposit the soot. The refractive index profile shows a smooth curve, with no central dip.

process by which the doped core glass is formed from a doped soot is achieved in two steps; first the reaction of the chlorides, $AlCl_3$ or $YbCl_3$ for example, with oxygen to make the glass compound, then the consolidation of both the formed glass compound and the silica soot into a glass layer with no air gaps. The reaction of the chloride with oxygen is the most critical aspect of the process, since the reaction occurs at a temperature of $\approx 1300^oC$, whilst the evaporation temperature of $AlCl_3$ is only 500^oC. Therefore a large amount of the $AlCl_3$ will evaporate before reacting with the oxygen to form Al_2O_3 with an evaporation temperature much higher than the glass transition temperature of silica. The cause of the central dip was investigated using different flow rates of silicon tetrachloride, to alter the thickness of the deposited soot. The dip in the preform refractive index profile, was completely eradicated by using a flow rate of $80sccm$ rather than the

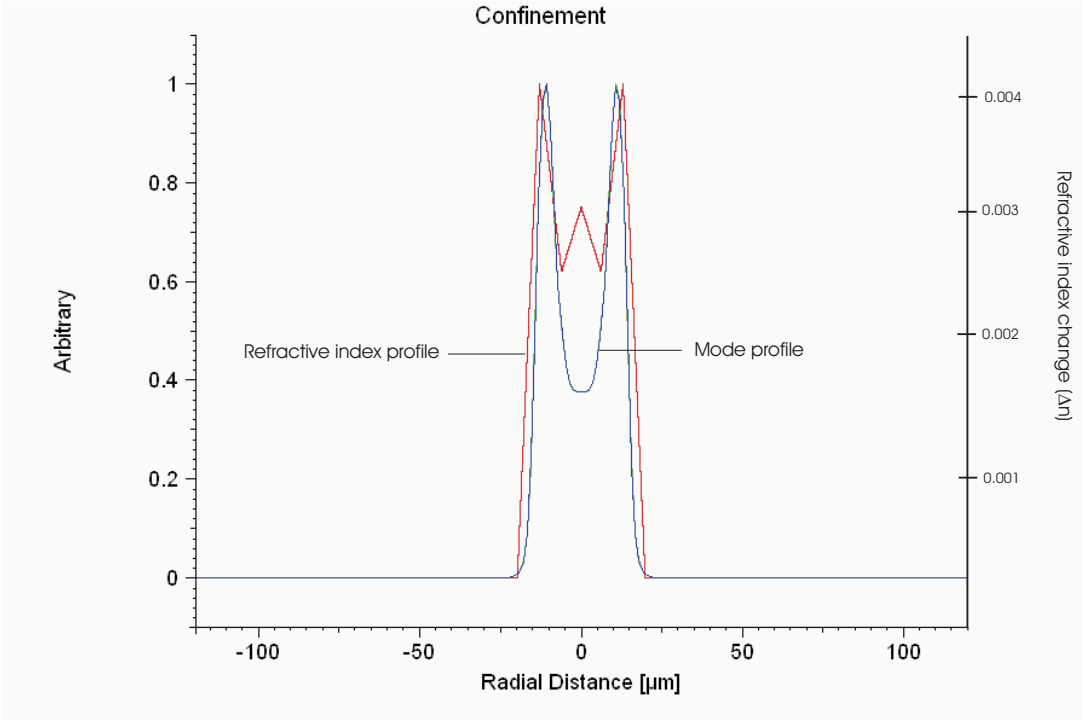

Figure 3.8: The dip in the refractive index profile causes the distortion of the fundamental mode, reducing the beam quality available from a fibre laser

usual $150sccm$, as shown in figure 3.9.

Two fibres were fabricated using exactly the same temperatures and flow rates, with the exception of the flow of $SiCl_4$. The elimination of the central dip by reducing the thickness of the wall layer implies that the cause could be due to the lack of dopant diffusion through the thick layer, and evaporation due to insufficient temperature for oxidation of chlorides. High NA preforms have large concentrations of aluminium and therefore the aluminium can diffuse through the preform to reduce the impact of the lost aluminium at higher oxidation temperatures. For low NA preforms there are much lower concentrations of aluminium and a reduced diffusion effect, therefore the layer thickness must be less to account for this effect. The effect of the non-uniform aluminium concentration is enhanced by the effect of refractive index differences on the NA; in order to halve the NA from 0.15 to 0.075, a change in refractive index from 0.008 to 0.002 is required. This causes small variations in refractive index to have larger effects on low NA preforms than high NA preforms. During the collapse process, the temperature increases to temperatures where Al_2O_3 will not evaporate while SiO_2 will start to evaporate, care must be taken to ensure that a peak is not formed

by using too high a temperature. Using the technique of thin layers and low temperature fabrication, preforms with an NA of 0.07 can routinely be made, and preforms with NAs as low as 0.04 have been fabricated with no central dip.

3.3.2 Preform cores

The fabrication of an offcentre core preform is actually based on a standard core taken from a conventional preform. This may be achieved in two ways, by drilling the core with a small amount of the surrounding cladding out of the preform, or by etching the preform diameter down using hydrofluoric acid. Drilling the core from the preform requires a few hours, however the precise alignment of the drill is critical to ensure that the core is exactly central in the extracted rod of glass. Etching the preform to the required diameter will yield a rod with the core precisely in the centre, however the process takes a number of days and the etching can be irregular along the length of the preform. An HF bath is used in the ORC, however this suffers from evaporation of HF , which causes two problems; firstly the level drops so that the recirculation fails, secondly the concentration drops, increasing the required etching time. With HF in solution, with less than 50% by volume concentration of HF, the amount of glass etched in 24 hours was approximately $100\mu m$ from the surface. The use of a raised temperature will increase the reaction rate, but will also dramatically increase the evaporation and is therefore not generally used. The extracted cores from these preforms are then inserted into the off-centred preform by either stacking with other silica rods or inserting into a rod of silica.

3.3.3 Stacking

Initial attempts to fabricate off-centre preforms used the stacking of a large number of silica rods to control the positioning of the core. Stacking is advantageous in that the off-centre preform length is limited only by the length of the initial preform, assuming etching is used to extract the full length of the original core. The first test fibres used three to five rods and hence the preform formed was not circular. This meant that the weight was not uniformly distributed about

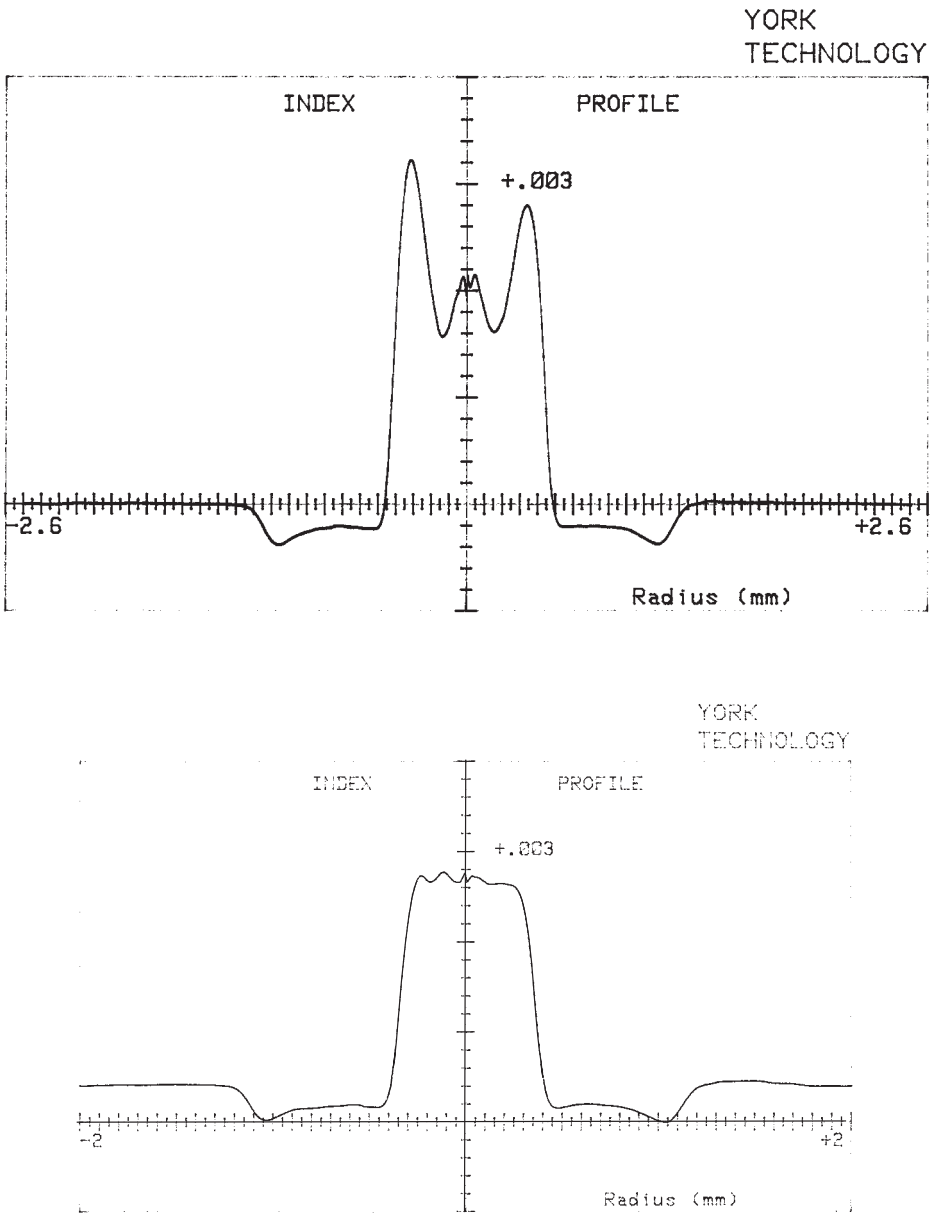

Figure 3.9: Two refractive index profiles are shown, one with a silica flow of 150*sccm* during the soot layer deposition, the other with 80*sccm* and with all other parameter the same. The dip produced is due to the uneven evaporation of $AlCl_3$

the axis of rotation causing the preform to be unstable whilst pulling into a fibre. Thinner rods were added into the air gaps for later attempts to ensure that the preform was more circular, and therefore more stable whilst spinning.

3.3.4 Drilling

The problem of contamination from the stacking technique led to the development of drilling a hole into a silica rod and inserting an etched core into this. Using drilling however, limits the length of the off-centre preform to the length of the drill bit used. Drilling is also limited by the fact that rather than cutting the hole, an ultrasonic drill is used to grind out a ring in the glass. The coolant flows through the centre of the drill which has increasing amount of glass inside, therefore as the depth of the drilled ring increases the flow of coolant becomes restricted, resulting in the danger of the grinding tip overheating. The drill bit for an ultrasonic drill consists of a steel tube with a short cylinder of diamond impregnated abrasive material fixed to the end. If this impregnated material is heated it can disintegrate, or under extreme circumstances become detached from the steel tube and lodged in the drilled hole.

The insertion of the core and collapse into a solid preform requires that both surfaces are smooth, or else there will be the risk of small pockets of air being trapped at the interface. The surface of the glass after the hole has been drilled is very rough, and there are often small parts of the diamond paste used to cut it left on the surface. To remove these, a combination of HF etching, cleaning and fire polishing is used. The surface is first cleaned using acetone and isopropanol, then it is immersed in 50% strength solution of HF for half an hour to remove the inner surface from the hole. This is then cleaned again using the solvents, and if there are any contaminants remaining, then the process is repeated. Once the surface has been prepared, it must be fire-polished into a smooth surface to avoid air bubbles in the final preform. This is performed on a glass working lathe, at temperatures of around 1900^oC, repeatedly passing the burner over the rod until the surface is smooth. The process is similar to that of the consolidation of silica soot in section 2.3.1, the surface becomes less viscous as it increases in temperature and the forces of surface tension smooth any roughness. The rod also must be fire polished, even if it has been etched the process is not

completely uniform and the core will have a small degree of surface roughness. Fire-polishing the outer surface of a rod is simpler than the inside of a tube, and can be performed vertically using the drawing tower furnace to ensure the rod will not become distorted under its own weight.

Once both core-rod and hole are smooth the rod is inserted and collapsed on the lathe. The preform is collapsed on the lathe prior to drawing since the hole in the preform would not seal whilst pulling due to the centripetal acceleration caused by the spinning preform. Tests were performed which showed that whilst holes would seal at low revolution rates, around $200rpm$, for higher rates, up to $1000rpm$, holes would remain on the inner side of the rod. The 'rod in hole' preform is collapsed by attaching another section of rod with a hole drilled in the same position as the original rod, to provide an escape route for the air during the process. The other end is attached to a blank rod with the same diameter as the drilled rod, as shown in figure 3.10. The purpose of the rods at either end are to ensure that a constant temperature is maintained to the very end of the off centre preform, ensuring that there is minimal loss of length of fibre. A tube directly connected to the off-centre preform would have a mass per volume far lower than the solid rod, it would therefore heat quickly to above the glass transition temperature and be unable to support that end of the preform. Once the air gap is sealed, the preform is ready for drawing into a helical fibre.

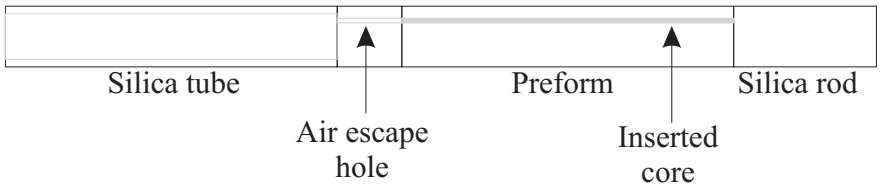

Figure 3.10: To collapse the gap around the inserted core there must be support capable of withstanding the high temperatures whilst still allowing the air to escape.

3.3.5 Helical core fibre drawing

Drawing helical core fibres requires an alteration to the drawing tower in order to spin the preforms, this was developed as part of this work. The device used during this thesis is shown in figure 3.11. A number of spinning systems were considered, varying from simple drill to air-bearing mounted chucks. To test

the method however, it was decided to use a mechanical stirrer with a digitally controlled rotation rate, and smooth ramp-up operation. This device was able to spin preforms up to $1500rpm$ with no distortion of the free end of the preform, which provides a large range of pitches. The device is not designed to operate near the high temperatures used in fibre drawing, therefore the preform is designed such that there is a large amount of light removed at the change in diameter and the end extends out of the stirrer, so most of the light is directed away from the device.

The pitch of the fibre is determined by the rotation rate of the preform and the speed at which the fibre is being drawn, related by:

$$P = \frac{v_D}{\omega} \tag{3.12}$$

where P is the pitch, v_D is the fibre drawing speed and ω is the angular velocity in revolutions per minute. The offset is determined by the placement of the rod with the core inside the stack and the final diameter of the fibre.

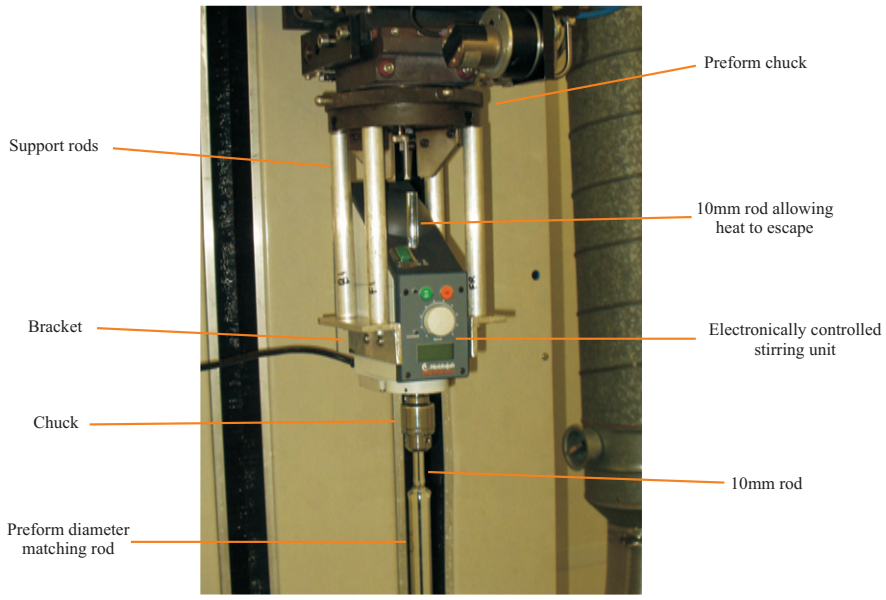

Figure 3.11: The device used for spinning was a commercial stirrer, which had to be attached securely to the preform mount to limit vibrations and movement. The top of the preform must extend out of the device due to the large quantity of heat transmitted as light through the glass

The mechanical stirrer has a $10mm$ chuck to grip objects, this is smaller than the

diameter of commonly fabricated preforms which are around $11mm$. The preform must therefore be mounted on a $10mm$ rod with another section with a diameter of the spun preform, which is required to have a length of $150mm$ to account for the distance from the top of the furnace to the hot zone. The general preform design for helical core fibre drawing is shown in figure 3.12. The alignment of every section is critical since any deviation from the centre of mass will cause the preform to vibrate in the furnace. As detailed in section 2.3.2, the fibre is coated $1.5m$ after leaving the furnace, $1.5m$ above the capstan which supplies the force pulling the fibre. The position of the coating cup is of course critical and is aligned whilst a fibre is being pulled, to ensure that an even coating is applied around the fibre. The alignment for helical fibres is exactly the same, so the coating should be the same for helical fibres as it is for normal fibres. In the case of helical fibres, the alignment of the off centre preform can cause there to be a slight vibration of the end of the preform. This means that the ideal position of the coating cup is changing as the preform is rotated, and can cause an uneven coating. The problem of coating fibres has been extensively studied in telecoms

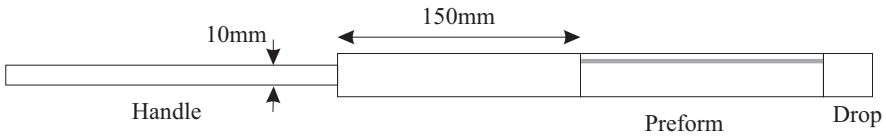

Figure 3.12: A handle of 10mm diameter is gripped by the chuck of the spinning device, a blank silica rod of the same diameter as the off-centre preform is used to position the preform correctly in the furnace.

applications, where hundreds of kilometres of fibre are being pulled at kilometres per minute. The results of these, although not directly applicable to the case of helical core fibres, can give an idea of the problems and solutions to the coating of these fibres and are addressed in section 2.3.2. It has also been noticed during the pulling of very large diameter fibres with coating, that the fibre has a tendency not to be central in the coating. There is a centralising force [20] whose strength depends on the drawing velocity and the angle of the taper in the die. This effect reduces for large fibres as the temperature of the fibre at the coating cup is increased, and thus the viscosity of the fluid is also decreased. There is a stronger force due to the thickness of the fibre to keep it perfectly straight, therefore any variation in the position on the capstan or position of preform will cause the fibre not to pass through the centre of the hole, giving an uneven coating. Therefore the pressurised coating system must be used to increase the centralising force, as

shown in figure 3.13.

The pressurised coating system uses two small apertures which the fibre passes through, with a chamber between filled with coating material. The coating material is fed into the chamber under a pressure of a few hundred millibars, which allows the fibre to be coated as it exits the underside of the coating cup. This system increases the centralising force, and helps to maintain uniform coating well for industrial uses. The system works well for small diameter spun fibres, but large diameter spun fibres still have too much lateral movement, which causes them to stick to the side of the hole. In order to control this, the top seal of the pressurised coating system can be made smaller than the diameter of the exiting hole, to fix the position of the fibre as it passes through the aperture. If a 600

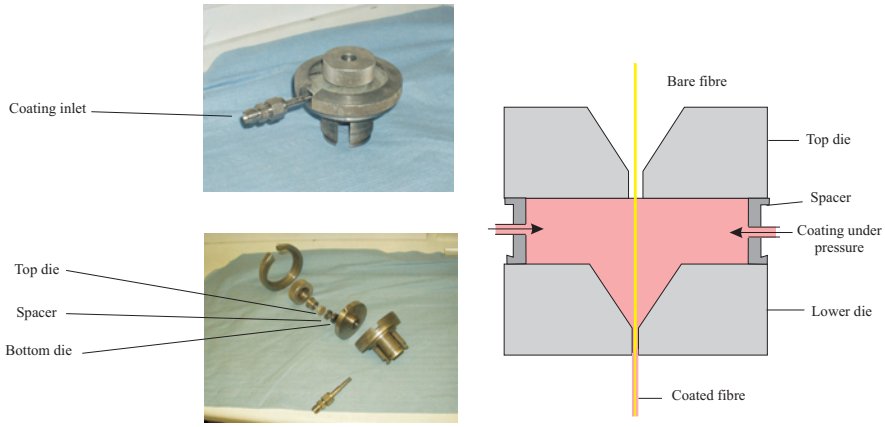

Figure 3.13: The pressurised coating system forces coating on to the fibre which increases the force keeping the fibre central in the apertures. The existence of two apertures makes it possible for the first aperture to be used as a guide for the fibre position into the second aperture.

micron fibre is to be drawn the top aperture can be $750\mu m$ in diameter, with the lower aperture being $1.2mm$ diameter. This limits the maximum deviation at the lower aperture of $225\mu m$ over a distance between the two apertures of $15mm$. Translated to a deviation at the capstan, $1.5m$ from the base of the coating cup, this is a maximum positional change of $22.5mm$. The fibre however, must have at least $50\mu m$ coating on all sides to give the fibre strength and the reduction in size of 30% whilst curing must also be taken into account, which reduces the tolerance at the capstan to $15mm$. This allowable movement is within the tolerance of the capstan system, which has one transverse dimension fixed by the drive wheel, and the other limited by rollers placed $10mm$ apart.

3.4 Germanium doped helical core fibre

3.4.1 Fabricated fibre properties

To test if the system worked and that it was possible to fabricate the required helical core fibres, a test fibre was fabricated with a germanium doped core. The preform was fabricated using the stacking technique, and the fibre was drawn with a pitch length of $2mm$. The fibre had the parameters:

Fibre Diameter	$\sim 250\mu m$
Core diameter	$\sim 14\mu m$
Numerical aperture	0.14
Offset	$\sim 75\mu m$
Pitch	$\sim 2mm$

Table 3.2: Properties of the first fabricated passive helical core fibre

From the results of this fibre as detailed in section 3.4.4, led to the fabrication of fibres with properties as shown in the table below.

As seen in figure 3.14 the core can be observed as it crosses the axis of the fibre and by measuring the distance between successive crossings, the pitch can be measured.

Measuring the distance between successive crossings was used to determine the accuracy of the pitch fabrication, which is dependent on the accuracies of the draw speed and the rotation speed of the preform. A microscope was used with vernier scale attached to measure the distance between 10 successive crossings.

Fibre Diameter	$\sim 250\mu m$
Core diameter	$\sim 14\mu m$
Numerical aperture	0.14
Offset	$\sim 75\mu m$
Pitches	$\sim 2.6, 2.9, 3.3, 3.65 \text{and} 4mm$

Table 3.3: Properties of the set of germanium doped helical core fibres, designed after the results of the first fibre.

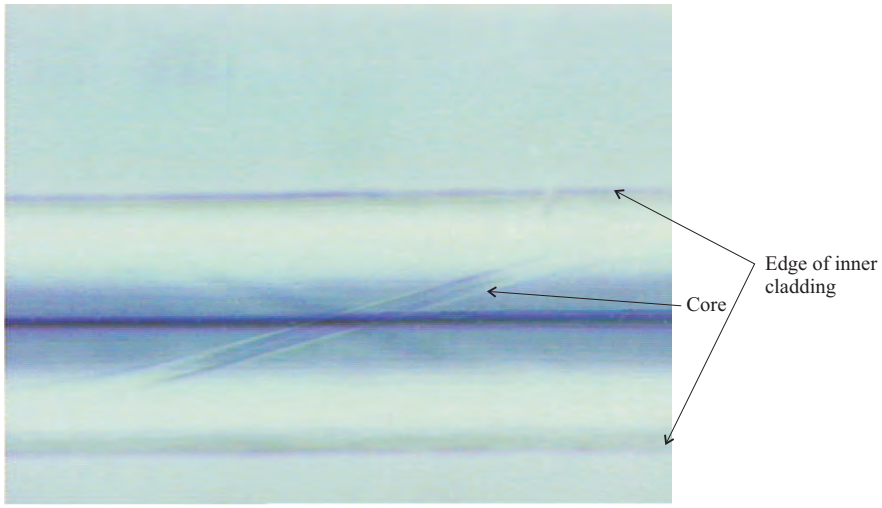

Figure 3.14: Photo taken from the side of a helical core fibre. The colours have been inverted so the dark patch along the centre of the fibre is light reflecting from the edge of the fibre. The core can clearly be seen crossing this dark stripe.

The measurement is therefore accurate to $\approx 0.02mm$ however the point at which the centre can be said to be crossing gives an uncertainty of $\approx 0.1mm$. The results showed that the pitch was as expected from equation 3.12, given the uncertainty in the drawing speed which has no feedback to set the rate, and is therefore accurate to $0.05m/min$.

3.4.2 Setup for measurement of helical core properties

The apparatus used for measuring helical fibre properties is shown in figure 3.15. The core propagates through the fibre at an angle to the axis of the fibre. This angle is given by taking the core as being on the outside of a cylinder. This cylinder has a radius of R and length of P, unwrapping this cylinder yields the pitch angle through simple trigonometry. The angle at which light should enter the fibre is greater than the angle of the core within the fibre due to refraction at the surface, therefore the angle can be expressed as:

$$\sin\theta = 1.458 \sin\left(\arctan\left(\frac{2R\pi}{P}\right)\right) \tag{3.13}$$

To determine the direction of the core, a HeNe laser is directed at one end of the

fibre. A fraction of this light couples to the modes in the core, and by the use of a microscope objective at the output end of the fibre, the position of the core can be located. By rotating the fibre so that the core is at the bottom of the fibre, it is known that the tangent to the core is in a horizontal plane. The fibre can then be fixed in position and the launch angle set. By focusing the light from a Nd:YAG laser into the core, light is emitted from the opposite end at the angle to the axis of the fibre, as calculated in equation 3.13. This light can then be focused onto a beam analyser for beam quality measurements, through a polariser for extinction ratio measurements or onto a power meter for loss measurements. The beam quality measurements can compare the output from the straight section of the helical core fibre and the helical core fibres, since the cores should be multimoded at the wavelengths used. The loss measurements use the cutback method, which results in a graph from which the loss and launch efficiency can be found.

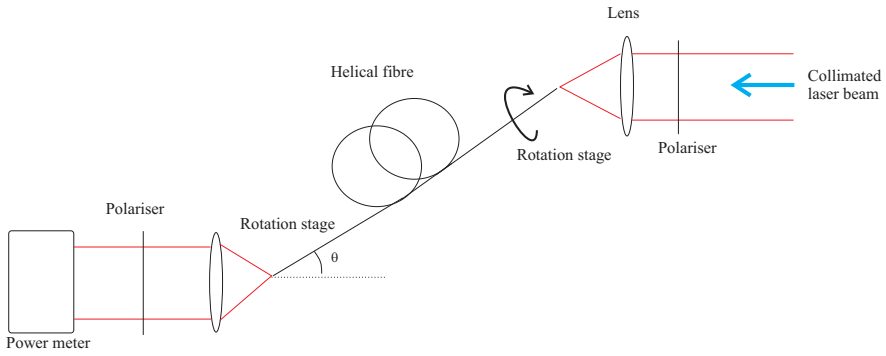

Figure 3.15: Diagram of the apparatus used for measuring the core propagation losses and birefringence in helical fibres. The light is focused into the core at an angle defined by the pitch angle. After propagating through the core the light can be passed through another polariser or onto a power meter.

3.4.3 Birefringence

The measurement of linear birefringence is performed using a polarised light source, and using interference between the two polarisation directions to determine the degree of birefringence. Circular birefringence does not have a polarisation axis to perform this measurement, however the birefringence can be determined by measuring the precession of the angle of linearly polarised light through the fibre, as detailed in section 3.2.2. By cutting short lengths progressively off the fibre and measuring the direction of polarisation, the optical rotation length and

hence degree of circular birefringence can be determined through equation 3.9. The measurements made from the helical core fibre are shown in figure 3.16. The

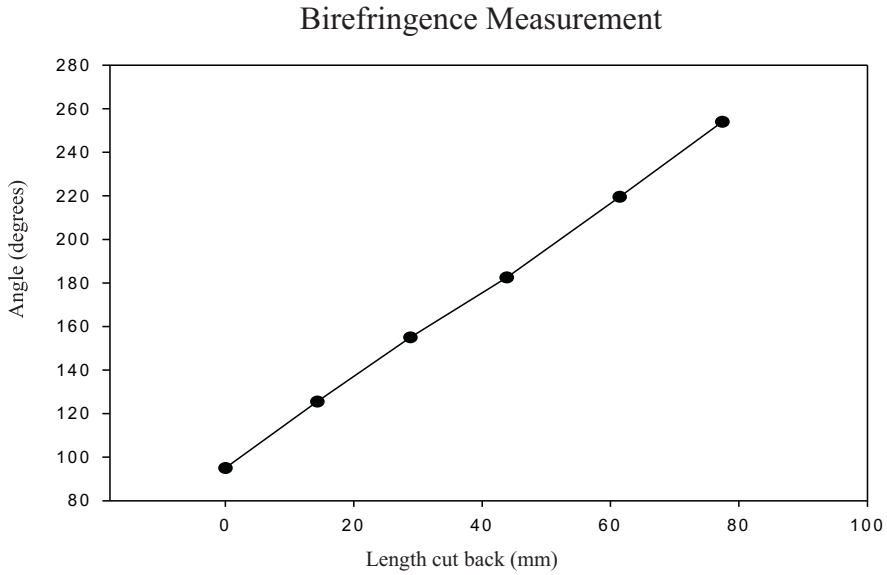

Figure 3.16: Graph showing the measured polarisation orientation as the fibre is progressively cut back. The rotation length for 180^o is found to be 88mm.

results from the application of equation 3.8 is $92mm$, which shows good agreement with the measured value of $88mm$. The method for deriving the circular birefringence seems to fit with the observed results to within experimental error.

3.4.4 Bend loss

The bend loss of the fibre is critical in the fabrication of an efficient helical core fibre laser. The loss for the fundamental mode should be in the region of 0.1dB/m and the next order mode should be in the tens of dB/m. These losses would ensure that the higher order modes would not have enough gain to be amplified, whilst the fundamental mode would maintain a high efficiency. The bend loss equation 3.11, predicted that for the initial fibre parameters (NA-0.14, offset-$75\mu m$, pitch-$2mm$), the bend loss of the fundamental mode would be of the order of $2000dB/m$. The measured results however, showed that the fibre exhibited losses in the region of $5dB/m$. The discrepancy for this fibre indicated that a helical core fibre laser, with high circular birefringence and single mode operation, was achievable. This discrepancy can be ascribed to the condition that the fibre parameters must satisfy the 'slowness criteria' [17] due to approximations

in calculating the bend loss:

$$\frac{R_c}{r} \gg \frac{4\pi V}{W^2\sqrt{2\Delta}} \tag{3.14}$$

Where R_c is the effective radius of curvature of the helix, and r is the radius of the core. This leads to values of a factor of ten greater on the right hand side, so the conditions are not robustly satisfied. The short pitch and large offset, gives an effective radius of curvature is only $1.5mm$ which, combined with the large core radius, means that the equation is unreliable for these fibre parameters.

The measurement of the bend loss for a helical core fibre is complicated by the geometry of the fibre and the sharp variation with wavelength and helical pitch. The alignment of the fibre requires first the rotational alignment of the fibre to ensure that the core is in the same plane as the beam, the correct angle for the fibre face to the incident beam, and finally the standard xyz alignment to focus the beam precisely on the core (as shown in figure 3.17). This means that instead of the usual 3 degrees of freedom there are 5 and, as a consequence, any small movement of the fibre in any direction will sharply alter the power entering the fibre. Coupled with the variation in length of fibre needed to account for the variation in losses, a definitive measurement for bend loss was found to be too time consuming and inaccurate for detailed study. The results show that for long pitches, the loss predictions are accurate, however at smaller pitches, the theory starts to break down.

The region where the theory breaks down, is the region when radiation lost from subsequent helical loops will constructively and destructively interfere. Correction 3.11 to equation 3.10 is meant to account for this effect, however the effect is stronger than is predicted by theory.

3.4.5 Bend loss trend

In order to determine the limitations of the theory, a number of fibres were fabricated to determine the bend loss trend and therefore be able to predict losses for future fibres. The parameters for the fibre are listed in section 3.4.1, and were chosen by assuming that the loss predicted by theory was too high by a factor of 1000, and this correction was applied in order to fabricate fibres with

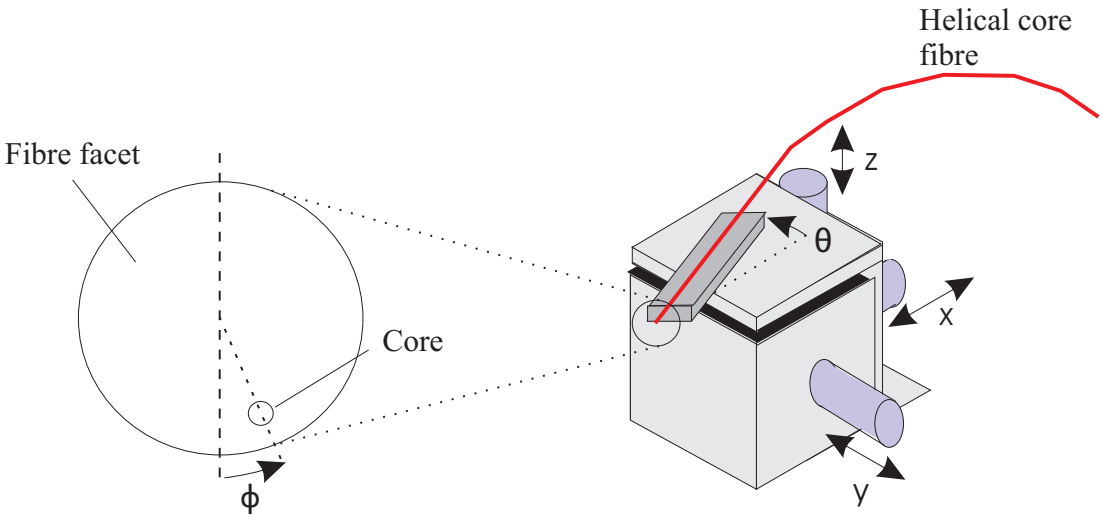

Figure 3.17: Diagram showing the five degrees of freedom which need to be adjusted to achieve high launch coupling. In addition to the standard xyz alignment for fibres, the helical core fibre must be adjusted to the correct angle and the core must be positioned at either the base or top of the fibre.

low fundamental mode losses.

The experimental measurements for the core propagation losses for a fibre with a pitch of $4mm$, offset of $75\mu m$ and NA of 0.14, are shown in figure 3.18. The plot shows an increase in the transmission at short fibre lengths, due to the higher order modes not being fully attenuated. The results showed that a correction factor did not result in the equation accurately predicting the losses in helical core fibres, since the longest pitch length, at $4mm$, was the only pitch capable of transmitting light at $1064nm$. Light from the HeNe laser operating at $633nm$ was able to pass through the tightest pitch of $2.6mm$, whilst light from an $808nm$ source could pass through the $3.6mm$ pitch fibre. This indicates a very strong dependence on wavelength, which is predicted correctly by the theory [7].

3.4.6 Marcuse et al. bend loss evaluations

An alternative method for calculating the bend loss was proposed by Marcuse et al. [8] as mentioned in section 3.1.1. The advantage of this technique is the ease with which the losses for higher order modes can be calculated. The equation derived is [21]:

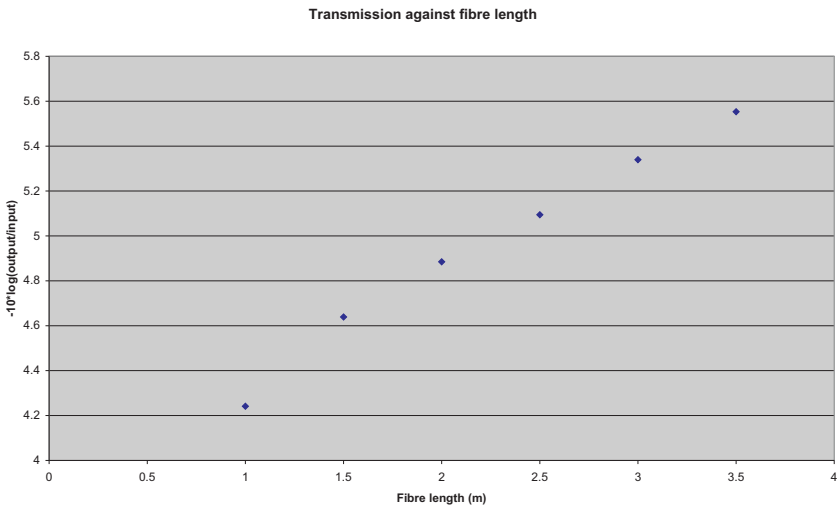

Figure 3.18: Graph showing the transmission of light through the helical core expressed as the log of transmitted over input power, against the length of fibre used. The fibre had a pitch length of $4mm$, an offset of $75\mu m$ and an NA of 0.14.

$$\alpha(dB/m) = 4.343 \frac{\kappa \pi^{\frac{1}{2}} e^{\left[\frac{-2\gamma^3 Q}{3\beta^2 sin^2\theta}\right]}}{e_v V^2 \left(\frac{Q}{sin^2\theta}\right)^{\frac{1}{2}} K_{v-1}(\gamma\rho) K_{v+1}(\gamma\rho)} \tag{3.15}$$

The values of κ and γ are dependent on the values of U and W respectively, thus it is useful to convert the equation using the identities $\kappa = \frac{U}{\rho}$ and $\gamma = \frac{W}{\rho}$:

$$\alpha(dB/m) = 4.343 \frac{\pi^{\frac{1}{2}} U^2 e^{\left[\frac{-2QW^3}{3\beta^2\rho^3 sin^2\theta}\right]}}{e_v \rho^{\frac{1}{2}} W^{\frac{3}{2}} V^2 \left(\frac{Q}{sin^2\theta}\right)^{\frac{1}{2}} K_{v-1}(W) K_{v+1}(W)} \tag{3.16}$$

The results from equation 3.16 are shown in figures 3.19, showing the effects of NA, pitch length, offset and core size on the fundamental and first order mode. From the equation it is possible to determine the requirements for a certain design of fibre [22].

The difficulties in measuring the bend loss of the helical core fibres was explained in section 3.4.4, but rough results were achieved using a fibre with $10\mu m$ core diameter, $120\mu m$ offset, NA of 0.13 and various pitch lengths. Using lengths of $3.5mm$, $4mm$ and $4.5mm$ losses of $> 40dB/m$, $\approx 2.5dB/m$ and $< 0.1dB/m$ were measured respectively, with a helium neon laser. Calculations from the

above equation gave expected losses of $660dB/m$, $2.1dB/m$ and $0.003dB/m$ for $3.5mm$, $4mm$ and $4.5mm$ pitches respectively. This indicates that equation 3.16 is suitable for the determining the correct parameters for a fibre with properties useful for helical core fibre lasers.

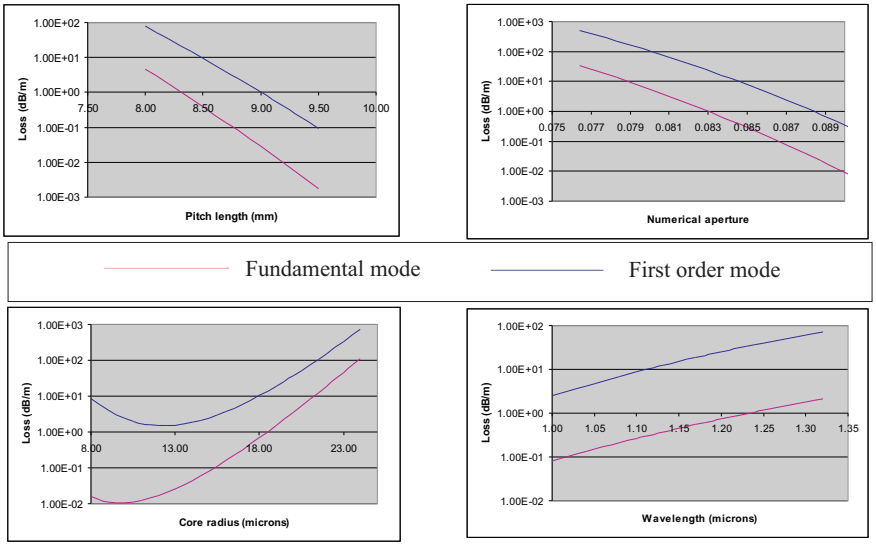

Figure 3.19: The loss of the fundamental and first order modes as a function of Pitch, NA, Core diameter and Wavelength are shown. The base fibre parameters were pitch of $8.8mm$, NA of 0.08, core diameter of $15\mu m$, offset of $100\mu m$ and wavelength of $1\mu m$.

3.4.7 Cladding losses comparison for double clad helical fibres

The fabrication of high power helical core fibre lasers requires the use of cladding pumping to allow the very high pump powers to be used, as explained in section 2.2.2. The loss in the cladding is therefore important and might be a factor for helical core fibres due to the interfaces formed from either the stacking or rod in tube technique of preform fabrication. The cladding losses were measured using a white light source for a number of fibres from three preforms, one with a germano-silicate core, one with alumino-silicate and another of pure silica, all spun at various speeds. Using short lengths of fibre the losses were measured, for a number of rotation rates, for each preform type. Figure 3.20 shows the losses for a number of fibres with different pitch lengths, against wavelength. As the pitch length decreases, the loss increases, indicating that there is an excess loss

associated with the helicity. There are two methods for loss of pump light from the helical fibre, one is the loss due to scattering from imperfections in the glass, and the other is scatter from the helical core itself.

To determine whether the excess losses were due to contaminants on the surface of the stacked rods, preforms with different diameters of pure silica rods were pulled into fibres and the background losses measured for each one. The rods were thoroughly cleaned using de-ionised water, acetone and then isopropanol. The water removes general dirt from the surface, acetone dissolves other contaminants, and the isopropanol will remove the evaporation products of the acetone. Four preforms were fabricated from which fibre was drawn, one consisting of a solid silica rod, one with $1.5mm$ stacked canes, one with $1mm$ stacked canes, and one with $800\mu m$ stacked canes. The resulting losses at $800nm$ were $0.016dB/m$, $0.05dB/m$, $0.19dB/m$ and $0.55dB/m$ for the solid rod, $1.5mm$ canes, $1mm$ canes and $800\mu m$ canes respectively. The increase in losses due to remaining contaminants on the cleaned rods causes dramatic increases in the cladding losses due to scattering. This shows that the stacking technique for a circular preform requires intensive cleaning, such as etching in HF, and improved cleanroom conditions to ensure the minimum contamination of the rods before insertion. Another process

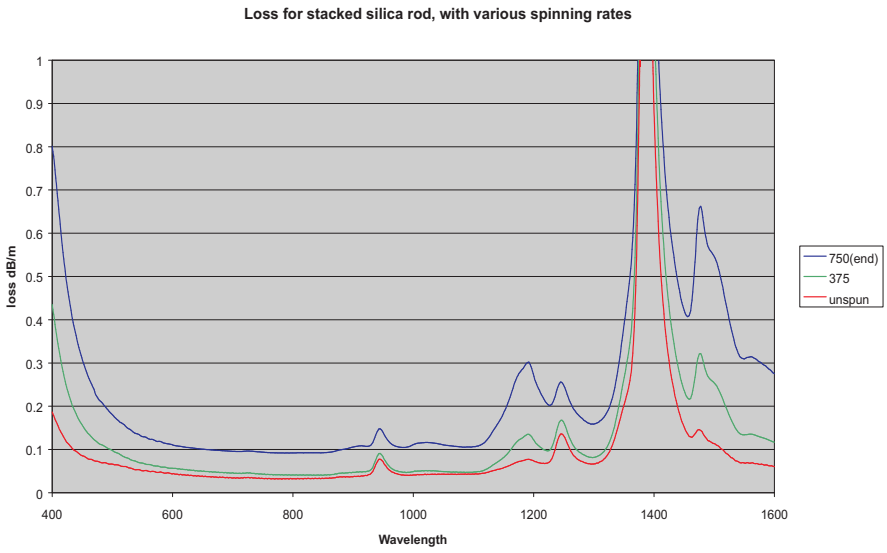

Figure 3.20: Graph showing the effect of spin rotation rate on the loss in the inner cladding. As can be seen the loss increases at $1200nm$ and $1500nm$ as the rotation rate increases, indicating that there are contaminants which increasingly interact with the light as the pitch length is shortened.

by which loss in the cladding of the fibre is increased, is refraction from the light

passing through the core. In a straight core fibre the light passing though the core will be refracted, but the angle at which it propagates along the fibre is unaffected. In the case of the helical core fibre, as shown in figure 3.21, the light refracting from the angled core can emerge at an altered angle of propagation along the fibre, and hence escape from the fibre. This effect can be reduced by having a small refractive index difference or having a long pitch length.

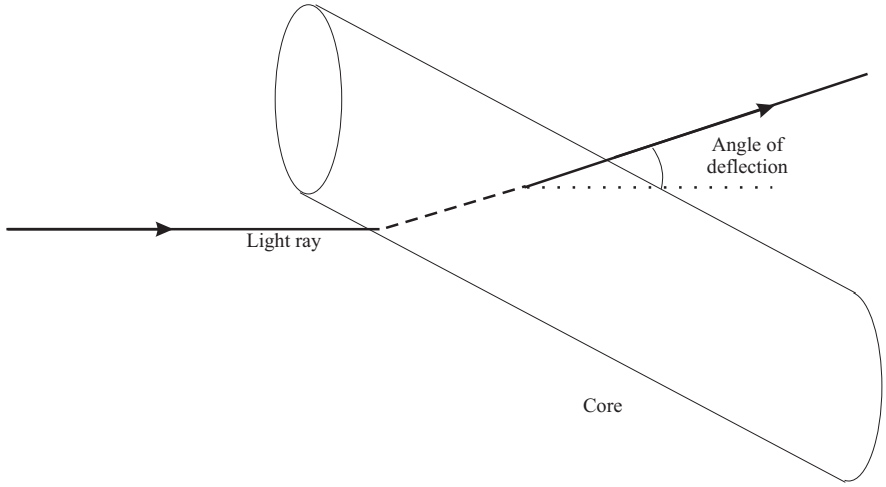

Figure 3.21: Light which enters the core at a grazing angle, will be refracted at both entry and exit, which will impart an angular deflection which can be large enough to allow the light to escape the inner cladding.

3.5 Core-pumped helical core fibre laser

Due to the high losses in the cladding, it was determined that a cladding pumped helical core fibre with high circular birefringence and single mode output was not possible in this project. The problem can be avoided by using a core pumping scheme, but at the cost of available pump power due to the low beam quality of diode sources.

3.5.1 Core pumping setup

The fibre used had a core diameter of $26\mu m$ and 0.14 NA, giving a V-value of ≈ 11. The fibre diameter and core offset were 400 and $130\mu m$ respectively, and the pitch length chosen was $5.17mm$. The setup used to core pump the helical

core fibre is shown in figure 3.22. The set up can be divided into two sections, the pumping of an Yb:YAG rod, and the use of the resultant beam to pump the helical core fibre.

A high power diode source at $940nm$ was used to end pump an Yb:YAG rod using a simple cavity design comprising a plane pump input mirror and a plane output coupling mirror. Both mirrors had high reflectivity at $1030nm$ and the pump input mirror had high transmission at $940nm$. Thermal lensing within the Yb:YAG rod provided the means to create stable resonating modes, and the cavity was capable of producing up to $10W$ with M^2 varying from < 1.1 at low powers, up to 4.4 at the maximum pump power.

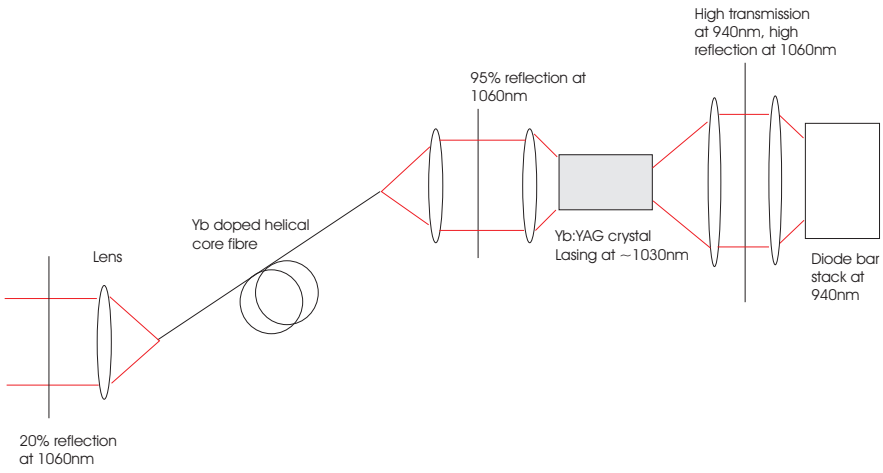

Figure 3.22: Diagram of the setup for a core-pumped helical core fibre. The pump used is a Yb:YAG rod, which provides a beam of good enough quality to enter the fibre.

The output at $1030nm$ was then used to pump the core of the helical core fibre, using an $11mm$ collimating aspheric collimating lens. Due to the core having an incidence angle of 13.3^o the fibre is effectively angle cleaved, and Fresnel reflection cannot be used to provide the feedback for laser operation. The output end of the fibre had an $8mm$ collimating lens and an output coupler with 20% reflectivity at $1060nm$, so reflecting a portion of the light back into the core of the fibre. As in the core propagation experiments, the alignment of the fibre is critical and positioning of the core with respect to the incident beam must be undertaken with care.

3.5.2 Core-pumped helical core fibre results

Using a fibre length of $3m$, the threshold pump power was found to be $100mW$ and the helical core fibre had a maximum output power of $350mW$ at $1047nm$ [23]. The beam had an M^2 less than 1.1 for $2.16W$ input pump power. At higher pump powers the output power decreased due to increased M^2 output from the Yb:YAG rod, reducing the pump brightness. The rejected laser power from the thin film polariser was 10% indicating that the output from the core pumped helical core fibre laser was linearly polarised. The slope efficiency was only 17%, due to the loss associated with the fundamental mode, implying a loss of more than $8dB$ for a complete pass.

Measurements made using similar fibre without ytterbium doping showed that the circular birefringence was in good agreement with the calculated value of $0.5 * 10^{-5}$, and had an extinction ratio of over $13dB$, independently from the orientation of the input. To examine the benefits of the helical structure a length of fibre was made during fabrication with no rotation, to enable the analysis of the effect of the helical core path. In the same configuration as described in section 3.5.1 (albeit with no angle launching at either end), the straight core fibre acted as a multimode fibre with M^2 of 5.5 and with 45% of the light rejected from the thin film polariser.

3.5.3 Analysis of core-pumped helical core fibre

The helical geometry of the fibre was shown to improve the beam quality from 5.5 to less than 1.1, and gave a linearly polarised output. The loss associated with the short pitch length was too high for efficient lasing operation, and by using equation 3.16 the losses for the fundamental and next order modes can be found. The loss for the fundamental mode is predicted to be $0.1dB/m$, whilst the loss for the first order mode is $1.5dB/m$. The apparent loss is due to the beam quality of the output from the Yb:YAG rod, which degrades as the power is increased, reducing the launching efficiency.

3.6 Parameter determination for Cladding pumped helical core fibre laser

To create a cladding pumped fibre laser, the fibre parameters must be chosen such that the core propagation loss is low enough to allow efficient operation, and loss due to refraction from the core is minimised. The core propagation loss is described in equation 3.16, and it has been shown that the loss will be reduced with a higher numerical aperture, longer pitch length, smaller offset, or larger core size. To reduce the loss due to refraction from the core, a lower NA and smaller core are desirable. The exact specifications are further complicated by the requirement of the next order mode to have a high loss, and this can be calculated to an approximate accuracy by equation 3.16.

3.6.1 Fibre specifications

In order to allow high pump powers to be used the fibre diameter was chosen to be $300\mu m$. A short length of fibre is needed to suppress losses due to pump scattering, which requires a large core diameter. We can look at the interaction of core diameter, NA, offset and pitch on the pump and core propagation losses. The pump losses increase with core diameter, pitch, offset and numerical aperture, whilst the core losses increase with core diameter, short pitch lengths, large offsets and lower NA. One important factor to consider is that the maximum Yb concentration decreases as the NA is decreased, due to clustering which is suppressed by the addition of aluminium [24].

To make an efficient cladding pumped helical core fibre, a low NA large core fibre is desirable, with a large core offset and long pitch length. A core diameter of $30\mu m$ was chosen and an offset of $125\mu m$, which combined with an NA of .087 gave loss as a function of pitch as illustrated in figure 3.23. From this a selection of pitches were chosen, 8.8mm, 9.2mm, 9.6mm and a straight core section. The ytterbium concentration was $\approx 7000ppm$ which gave an absorption of $5.8dB/m$ at a pump wavelength of $976nm$, leading to a device length of $2-3m$.

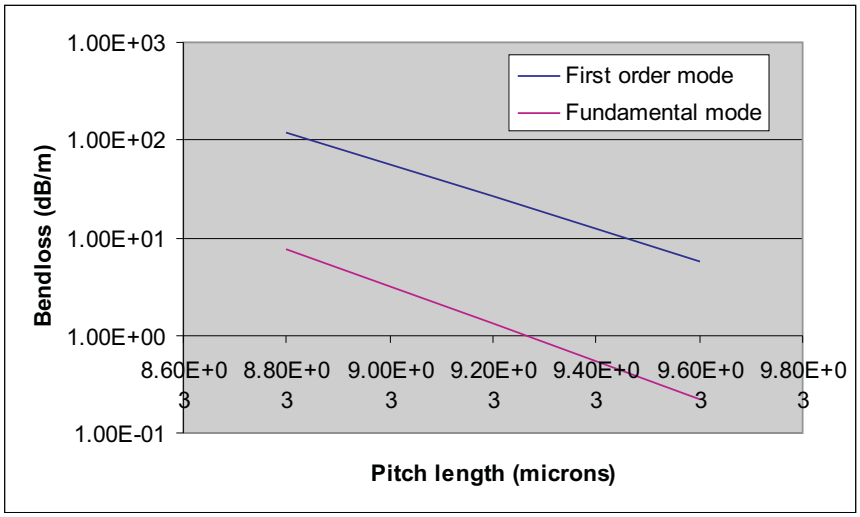

Figure 3.23: Losses calculated for the fundamental and first order modes, for a fibre with an offset of 125 microns, core diameter of 30 microns and NA of 0.087

3.6.2 Cladding pumped fibre laser setup

The experimental setup used to measure the performance of the cladding pumped helical core fibre is shown in figure 3.24. The laser cavity is formed by the fresnel reflection from the output facet of the helical core fibre at the pump input end, and a flat mirror at the other. The mirror is aligned to image the signal directly back onto the core, which means that little residual pump light is coupled back into the fibre.

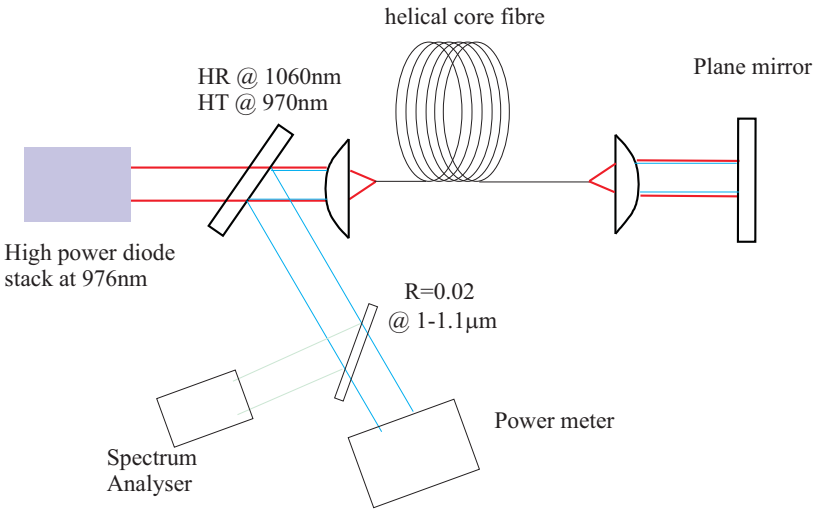

Figure 3.24: Setup for the measurement of the lasing characteristics of the cladding pumped helical core fibre. The output is measured from a single end, with the other output imaged back onto the core.

3.6.3 Fibre performance

Initially the properties of the unspun section of fibre were tested. The M^2 value for the straight core fibre was found to be around 3.3. Using $2.8m$ of fibre with a pitch length of $8.5mm$, the efficiency was measured to be 84% with a maximum output power of $64W$ for $92W$ launched pump power, as shown in figure 3.25 [25].

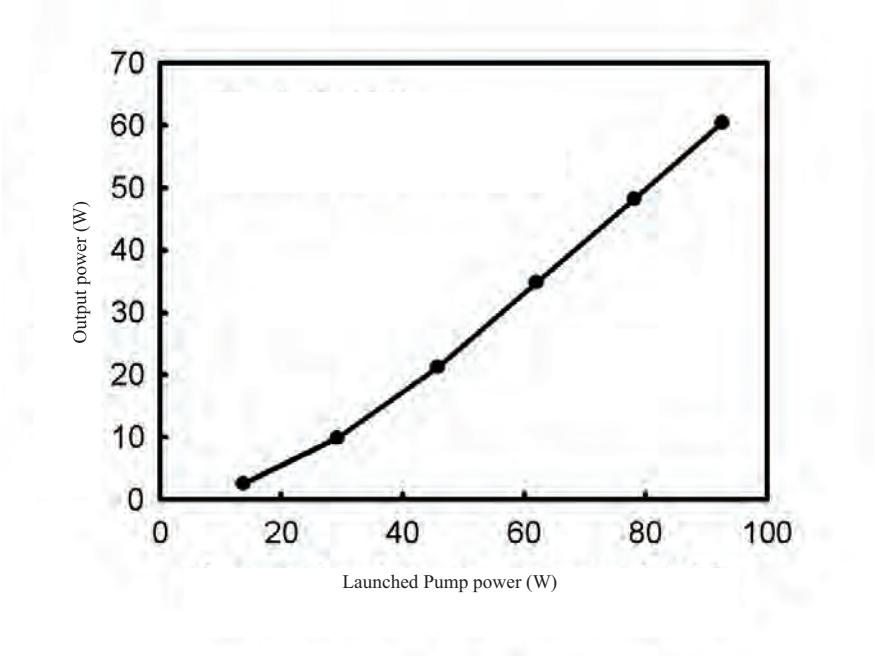

Figure 3.25: Graph showing laser output power against the launched pump power for a fibre with a pitch length of $8.5mm$, core diameter of $30\mu m$, offset of $100\mu m$ and an NA of 0.09.

Figure 3.26 shows the far field laser output from the $8.5mm$ pitch fibre, and the straight core fibre both at lasing powers of approximately $50W$. The improved beam quality of the helical core fibre laser is clear to see, having an M^2 of < 1.4. The $8.8mm$ pitch fibre was also used, and yielded an M^2 of 1.7.

The spectral output of the helical fibre laser is shown in figure 3.27, showing the lasing occurring between $1038nm$ and $1048nm$, lower than for standard ytterbium doped fibre lasers.

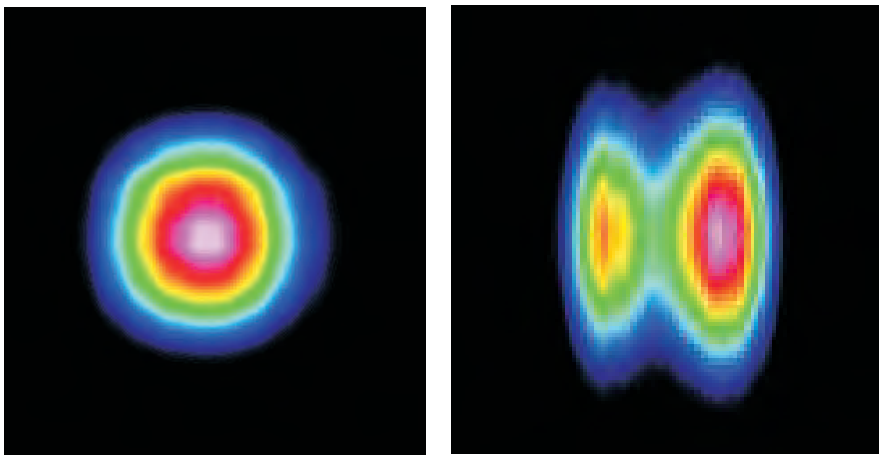

Figure 3.26: Beam scans of output from helical core fibre laser with a pitch of $8.5mm$ on the left and the straight core fibre, with all other parameters the same, on the right. The helical core fibre, with an M^2 of less than 1.4 has an improved beam quality.

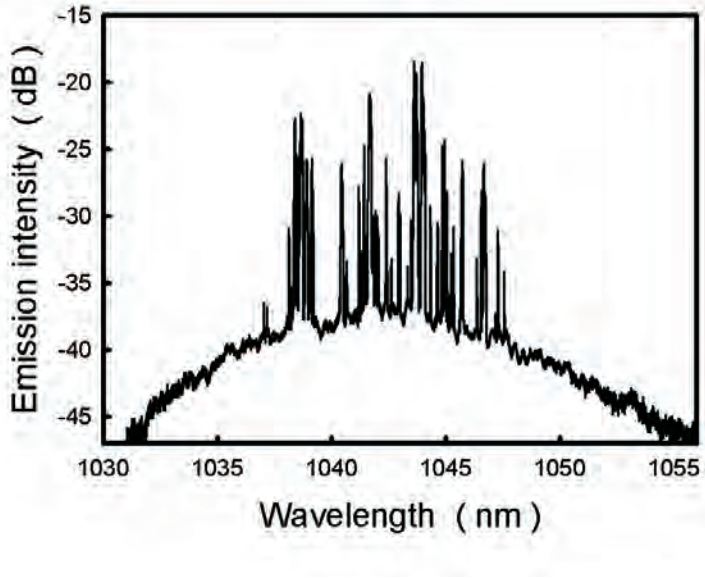

Figure 3.27: Spectral output from the cladding pumped helical core fibre with a pitch length of 8.5mm. The lasing wavelength is lower due to the lower losses associated with shorter wavelengths.

3.7 Large diameter helical core fibre laser

From the successful tests of the $300\mu m$ helical core fibre, it was decided to increase the fibre diameter to $600\mu m$ and the offset to $250\mu m$. The theory would be used to determine the correct pitch, thus confirming the ability to design a fibre to give predictable results. The fibre diameter would also closely match the parameters used by Jeong et al. [10] in the successful demonstration of a 1kW CW fibre laser.

3.7.1 Expected results

Using equation 3.15, and the fibre parameters; $250\mu m$ offset, $30\mu m$ core diameter and 0.08 NA, the required pitch range was determined. The pitch against loss curve is shown in figure 3.28, indicating that a pitch length of $13.3mm$ would give loss for the fundamental mode of $0.5dB/m$, and $10dB/m$ for the first order mode. This should give a highly single mode output, with a high efficiency since the loss due to scattering from the core should be reduced due to the lower core to clad ratio.

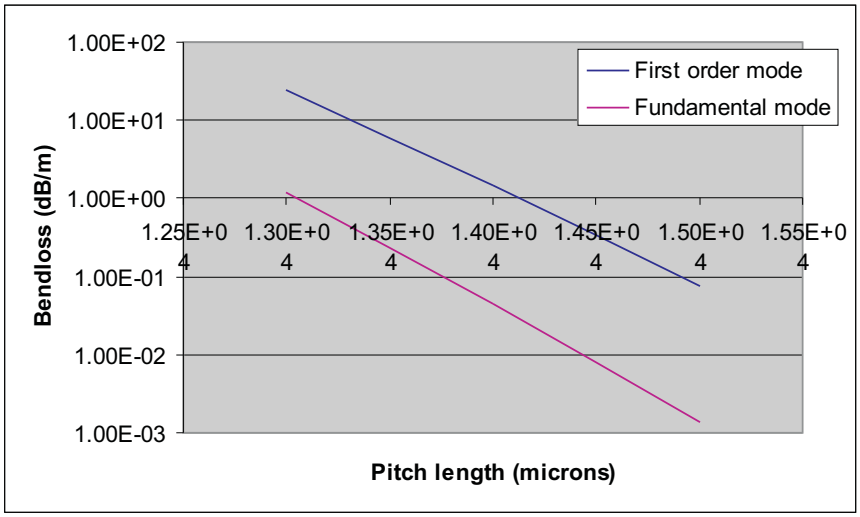

Figure 3.28: Predicted loss for 600 micron fibre, to illustrate that the current theory can predict the fibre parameters required for the successful operation of a cladding pumped helical core fibre

3.7.2 Set up

The setup used to measure the properties of the helical core fibre laser was a standard helical core set up with a single ended output, as used in section 3.6.2. Coupling pump light into the $600\mu m$ core yields a very high efficiency, with over $500W$ possible launched power. The laser cavity is formed using fresnel reflection from the pump input end facet of the fibre, which is not significantly reduced due to the angle of incidence of the core which is 12^o. The device length is 7m, which is due to the reduced core/cladding ratio.

3.7.3 Mode discrimination and efficiency

The M^2 for the straight core section was 3.3, which is as expected since the beam quality is determined by only the NA and the core size, which was not changed from the previous fibre. The M^2 for the fibre with a pitch length of $13.3mm$ was 1.4, which is near single mode. The efficiency was measured at over 70% for low pump powers, however poor coating meant that the fibre fractured at high power and so an exact measurement was not possible.

3.8 Conclusion

The fabrication and operation of helical core fibre lasers has been demonstrated. The fabrication of the helical core fibre required the improvement in both low NA preform fabrication and the development of new fabrication methods for off-centred preforms. The improvement in low NA preforms was achieved through the discovery of the effect of thin soot deposition, and then experimental tests to improve the results further. The drilling technique for preform fabrication has been developed to a stage where off-centred preforms can routinely be fabricated, with no imperfections at the inserted core/cladding interface.

A core pumped helical core fibre has been demonstrated with an output power of $350mW$ and M^2 value of less than 1.1. A cladding pumped helical core fibre has been demonstrated with an improvement in M^2 value from 3.3 in a straight

core, to 1.7 for a fibre with 8.8mm pitch, and to < 1.4 in a fibre with a pitch of 8.5mm. The power attained from the 8.5mm pitch fibre was 60W from an input power of 92W with a slope efficiency of 84%.

The use of bend loss equations to predict the losses for fibres with specific parameters has proved successful. A preform can be fabricated and then the equations developed by Marcuse, used to determine the appropriate pitch for single mode operation. The equation holds for when the pitch length is long, and the effects of adjacent helical passes can be ignored. This limit does not currently restrict the operation of helical core fibre lasers due to the increased losses in the cladding at shorter pitch lengths due to scattering, which inhibits working at those pitches.

3.9 References

[1] K. Okamoto, T. Hosaka, and J. Noda. High-birefringence polarizing fiber with flat cladding. *Journal of Lightwave Technology*, 3(4):758–762, 1985.

[2] R. B. Dyott, J. R. Cozens, and D. G. Morris. Preservation of polarisation in optical-fiber waveguides with elliptical cores. *Electronics letters*, 15(13):380–382, 1979.

[3] M. P. Varnham, D. N. Payne, R. D. Birch, and E. J. Tarbox. Single-polarization operation of highly birefringent bow-tie optical fibers. *Electronics Letters*, 19(7):246–247, 1983.

[4] M. V. Berry. Quantum phase factors accompanying adiabatic changes. *Proceedings of the Royal Society. London Series A*, 392:45–57, 1984.

[5] D. N. Payne M. P. Varnham, R. D. Birch and J. D. Love. Design of helical-core circularly-birefringent fibres. *OFC Proceedings of Optical Fibre Communication Conference*, TUL20:68–69, 1986.

[6] R. W. Wood. *Physical optics*. London: MacMillan, 1988.

[7] J. D. Love and A. W. Snyder. Radiation from single-mode helical fibres. *Electronics Letters*, 23(21):1109–1110, 1987.

[8] D. Marcuse. Curvature loss formula for optical fibers. *Journal of the Optical Society of America*, 66(3):216–220, 1976.

[9] V. V. Shevchenko. Radiation losses in bent waveguides for surface waves. *Radiophysics and Quantum Electronics*, 14:607–614, 1973.

[10] Y. Jeong, J. K. Sahu, D. N. Payne, and J. Nilsson. Ytterbium-doped large-core fibre laser with 1.36kW continuous-wave output power. *Optics Express*, 12(25):6088–6092, 2004.

[11] F. D. M. Haldane. Path dependence of the geometric rotation of polarisation in optic fibres. *Optics Letters*, 11(11):730–732, 1986.

[12] L. H. Ryder. The optical Berry phase and the Gauss-Bonnet theorem. *European Journal of Physics*, 12:15–18, 1991.

[13] L. Lewin, D. C. Chang, and E. F. Kuester. *Electromagnetic waves and curved structures*. London: Peter Peregrinus, 1977.

[14] J. N. Ross. The rotation of the polarisation in low birefringence monomode optical fibres due to geometrical effects. *Quantum Electronics*, 16:455–461, 1984.

[15] A. Ghatak and K. Thyagarajan. *Introduction to fibre optics*. Cambridge: University Press, 1998.

[16] R. D. Birch. Fabrication and characterisation of circularly birefringent helical fibres. *Electronics Letters*, 23(1):50–52, 1987.

[17] A. W. Snyder and J. D. Love. *Optical waveguide theory*. New York: Springer, 1979.

[18] J. P. Koplow, D. A. V. Kliner, and L. Goldberg. Single-mode operation of a coiled multimode fiber amplifier. *Optics Letters*, 25(7):442–444, 2000.

[19] A. J. Barlow, J. J. Ramskov-Hansen, and D. N. Payne. Birefringence and polarization mode-dispersion in spun single-mode fibers. *Applied Optics*, 20(17):2962–2968, 1981.

[20] P. W. France, P. L. Dunn, and M. H. Reeve. Plastic coating of glass fibres and its influence on strength. *Fibre and Integrated Optics*, 2(3-4):267–286, 1979.

[21] D. Marcuse. Curvature loss formula for optical fibers. *Journal of the Optical Society of America*, 66(3):216–220, 1976.

[22] Z. Jiang and J. R. Marciante. Mode-area scaling of helical-core dual-clad fiber lasers and amplifiers. *CLEO US*, pages 1–4, 2005.

[23] P. Wang, L. J. Cooper, R. B. Williams, J. K. Sahu, and W. A. Clarkson. Helical-core ytterbium-doped fibre laser. *Electronics letters*, 40(21):1325–1326, 2004.

[24] K. Arai, H. Namikawa, K. Kumata, and T. Honda. Aluminium or phosphorous codoping effects on the fluorescence and structural properties of neodymium doped silica glass. *Journal of Applied Physics*, 59:3430–3436, 1986.

[25] P. Wang, L. J. Cooper, V. Shcheslavskiy, J. K. Sahu, and W. A. Clarkson. Cladding-pumped ytterbium-doped helical-core fiber laser. *ASSP - Vienna*, 6-9 Feb:MC5, 2005.

Chapter 4

Ribbon fibre laser

4.1 Introduction

The highest single-mode fibre laser output powers are currently achieved using large mode area fibres and using bend loss to suppress any modes other than the fundamental mode. This method has proved highly successful, but will ultimately be limited by the thickness of the fibre and hence the difficulty in bending. An alternative method for the scaling of fibre laser powers, is to use multiple cores. This has the advantage of increasing the effective core area, with no degradation of beam quality. Each core is capable of emitting the same power as in a single core fibre, and thus the power can be multiplied as the number of cores. The outputs from the individual cores must be combined to provide a beam which is useable, which can be achieved in two different ways. The outputs can be made coherent, through for example diffraction coupling [1] or overlapping the evanescent fields [2], which is described in more detail in section 2.4.1. The alternative method of beam combination is incoherent beam combination, exemplified by Spectral beam combination [3] or the use of the effective core area [4], which is detailed in section 2.4.2.

One of the major limitations of conventional fibre is the launching of pump light. For very high pump powers the end face of the fibre gets damaged, rendering the fibre useless. A rectangular fibre more closely matches the shape of the pump

diode stack, increasing launch efficiency and thus reducing the needed power. The shape of the fibre would also allow better contact with the outer cladding for cooling purposes, and reduce the need for water cooling systems, which is explained in further detail in section 4.3. The use of a linear array of emitters has been demonstrated in various guises usually in a circular inner cladding, however there have been no attempts to fabricate a purely rectangular ribbon fibre.

The fabrication of rectangular fibre requires a number of different techniques compared with circular fibres, the process is outlined in section 4.4. An alternative method of fabrication is proposed in section 4.7, which has the potential to reduce the complex fabrication process. The results from the fabricated fibres are given in section 4.5, followed by the conclusion in section 4.8 where analysis of results and the future direction is considered.

4.2 Beam combination

To get high powers from fibres, one can combine the output from a number of cores. This can be achieved in a coherent manner, whereby the emissions of the individual cores are phase locked, or incoherently, where the cores are not phase locked. The next two sections have been addressed in detail in section 2.4, though will be briefly refreshed.

4.2.1 Coherent combination

Coherent combination is attractive because the output can theoretically be single moded with unlimited scaling opportunity. There are a number of methods to phase lock separate cores, including evanescent field mode coupling, and the use of a 1-to-N way resonator.

In evanescent field mode coupling the modes inside the cores overlap with one another. This creates a super mode across all the cores in the fibre, which means the output of each core is coupled and can then be coherently combined. The cores must be very close to one another for the fields to overlap, and any perturbation

in this separation will cause losses from the super mode.

A fibre fabricated by M. Wrage et al. [5] shows the effect of imperfections in the fibre on the energy exchange between cores. The fibre they analysed consisted of 38 doped cores, in a ring near the edge of the cladding. The results showed that the coupling between adjacent cores was unaffected by perturbations in the geometry of the cores however the power exchange was altered, causing the theory not to agree with experiment. The phase of the light from the cores must be controlled to a precision of less than a wavelength to allow coherent combination. This is less of a problem for a single fibre than it is for multiple laser elements, but it only requires only small temperature fluctuations in the cores to make continuous operation difficult.

1-to-N-way resonators work on a principle developed to form Talbot resonators [6]. Talbot resonators use a multimode wave guide to phase lock the emissions from a number of emitters and reflect the light back into these emitters. To understand the principle behind talbot resonators the propagation of single mode beam in a multimode cavity must be examined. At certain distances the light is split a number of ways across the waveguide [7]. If waveguides replace the peaks at the 1/8 L distance (where L is the length of the multimode waveguide), then light from a single source can be coupled into 8 fibres. For a Talbot resonator the waveguide length is L/4, and the light is directed back to the emitters. For the 1-to-N-way resonator, the waveguide is L/N in length, and the light is directed into a single wave guide from multiple waveguides. By reflecting both ends of this system, all other modes are eliminated and only the supermode remains.

Both of these systems require high precision in the manufacturing, with the Talbot resonator being extremely sensitive to slight perturbations. The 1-to-N-way system has the advantage of being more stable, and has better photon mixing.

4.2.2 Incoherent combination

Incoherent combination sacrifices the quality of the beam in someway, in order to get higher powers. Some examples of this are 2 mirror beam shaping, effective core area scaling and spectral beam combination.

Two-mirror beam shaping is a technique designed to alter the beam quality from a laser diode bar array in order to improve the launch efficiency when coupling into fibres [8]. The principle of 2-mirror beam shaping is to 'chop up' the incident beam and rearrange it in more suitable shape for fibre coupling. The two mirrors are placed as shown in figure 2.21, and are of very high reflectivity. The beam can be thought of in terms of a number of separate beams, the dimensions of which are determined by the mirror spacing and angle. The first part of the beam passes both mirrors and is unaltered. The second part of the beam passes over mirror A, reflects off first mirror B and then mirror A, and ends up positioned under the first part of the beam. This process repeats for the length of the beam, and reformats the properties. The M^2 values are altered, reducing one and increasing the other, along with the shape of the beam. This technique can be applied to the multicore fibre, by replacing the single incident beam with a number of separate laser beams from the cores in the fibre.

The Spectral Beam Combining (SBC) technique was developed from a device for use in wavelength division multiplexing applications for telecommunications. The SBC technique combines incoherent laser arrays with different wavelengths to gain spatial brightness, at the cost of spectral brightness. A proof of principle experiment was performed with four Yb-doped fibres [9]. A lens acts to direct the light from each fibre, to the same spot on the grating. The angles of incidence are calculated such that the out-coupled beams are almost overlapped and co-propagational. The outcoupling mirror ensures that only light along its axis will contribute to the laser cavity, and thus the fibres will have a wavelength defined by their spatial position [3].

This technique allows a large number of different fibre lasers outputs to be combined and focused into an almost diffraction limited spot. The spatial brightness is dependent on the number of fibres used and the efficiency of the optical devices used in the system. The spectral width increases with the number of fibre lasers used, with the width and spacing of the individual wavelengths such that there is little cross talk between adjacent lasers.

4.3 Concept

4.3.1 Cladding pumping geometry

The width a beam of light, with a given beam quality (M^2), is given by equation 4.1.

$$W_{x,y} = \frac{2M^2_{x,y}\lambda}{\pi \arcsin(NA)} \tag{4.1}$$

This means that for a diode bar, the ratio of the two beam dimensions is around 1000, whilst for a diode bar stack (as is commonly used to pump fibre lasers) this drops to 340/n, where n is the number of emitters [10]. This indicates that for efficient high power pump sources to be coupled into fibres they should be elongated. The ideal shape would be rectangular, with a large aspect ratio, to closely match the diode pump geometry.

4.3.2 Thermal loss

One of the greatest advantages of fibre lasers is the suppression of thermal effects. This is due to the long interaction length of fibres, and the small distance from the core to the environment enabling efficient cooling. The cooling is very effective for low power levels ($< 10s$ of watts), but for very high power systems more cooling is required. This is particularly true near the pump launch end of the fibre, where the high intensity causes a large heat build up from the energy level transfers in the light amplification process. The circular geometry of optical fibres, although helping by allowing uniform heat transfer, obstructs the efficient removal of heat due to its shape. A ribbon fibre with two large flat surfaces simplifies the heat sinking process, by allowing the fibre to be sandwiched between two metal plates, potentially along the entire length of the fibre.

The circular fibre geometry in standard optical fibres allows even heat distribution in all directions from the core, due to the cylindrical symmetry, suppressing thermal stress by eliminating localised hot spots. A ribbon fibre loses this ad-

vantage but the cores can be distributed along the profile of the ribbon fibre in a uniform fashion, with the distances between cores controlled. This even distribution will allow uniform heating from the cores, thus limiting unwanted thermal stress and potential damage to the fibre.

4.3.3 Scalability

The number of cores that can be put into a ribbon fibre is dependent on the fabrication of a suitable preform. Drilling holes of less than $3mm$ in diameter and with wall thicknesses less than $1mm$ is an unreliable process due to the heating of the drill bit during drilling, as mentioned in section 3.3.4. For power scaling, a large number of cores can be used to maintain a good core to clad ratio and, since the cores are nearer to single mode, they can have a good beam quality. The output of the cores can then be combined with the M^2 of a single core, with only small losses due to the use of extra external optics, as described in section 4.3.4.

4.3.4 Beam combination

The method of spectral beam combination increases the spatial brightness of a beam at the cost of the spectral brightness. It combines an array of emitters, through the use of a diffraction grating in conjunction with a transform lens, to transform the position of each emitter into a separate angle of incidence on the same point on the grating. Figure 4.1 shows a schematic diagram of an example spectral beam combination setup. The lens is designed such that the output from the array of emitters is focused on a particular point on the grating, with each emitter having a different angle of incidence. The outcoupling mirror is aligned such that, in conjunction with the grating, each emitter will lase at a well defined wavelength, dependent on its position in the array.

The relationship between the wavelength and array position is given by

$$d \approx f \frac{d\alpha}{d\lambda} \Delta\lambda \tag{4.2}$$

Where $\Delta\lambda$ is the change in wavelength, d is the positional change along the array,

f is the focal length of the lens, and

$$\frac{d\alpha}{d\lambda} = \frac{1}{a\cos\alpha_0} \tag{4.3}$$

Where a is the grating period, and α_0 is the angle of incidence with respect to the grating normal. The spectral range over the complete array $\delta\lambda_t$ is therefore

$$\Delta\lambda_t = \frac{Da\cos\theta}{f} \tag{4.4}$$

Where D is the total width of the array.

The grating equation is given by

$$\sin\beta - \sin\alpha = \frac{m\lambda}{d} \tag{4.5}$$

Where β is the angle of incidence of the beam with respect to the grating normal, α is the same only for the diffracted beam, m is the order of diffraction and d is the grating spacing. This means that the grating will form a second order diffracted beam at a certain distance from the primary diffracted beam. The distance from the primary diffracted beam and the first minimum is

$$\Delta\left(\sin\alpha\right) = \frac{\lambda}{Nd} \tag{4.6}$$

Where N is the number of grating grooves. This angle translates to a distance at the emitters of $f\frac{\lambda}{Nd}$, which is the limit imposed by the grating for the separation of the cores.

The lens required to focus every emitter onto the same point on the grating has been investigated using different types of lenses [3]. The lenses modeled were a biconvex spherical lens, a plano-convex aspheric lens, a multi-element lens and a plano-parabolic lens. The results showed that the plano-parabolic lens gave excellent coupling efficiency back into the cores, when used in conjunction with a curved emitter array, effectively defocusing the light from emitters further from the lens axis. The multi-element lens showed a much improved performance over that of the single spherical lens.

The use of defocusing of array elements is not possible in the ribbon fibre, however a potentially significant problem is that of core misalignment in the direction perpendicular to the plane formed by the array and beam propagation. The path of an off-axis core in an example spectral beam combination system is shown in

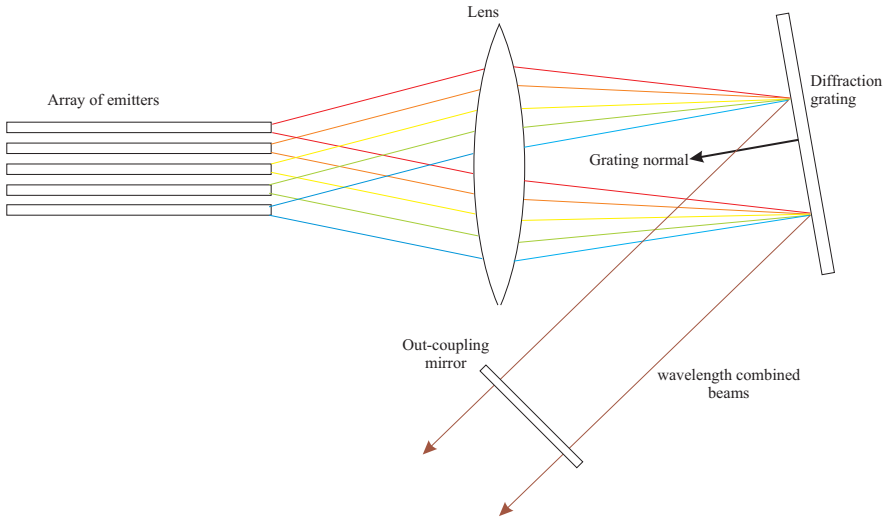

Figure 4.1: Diagram showing the experimental setup used for the Spectral Beam Combination of multiple emitters. The position of the emitter is converted to an individual angle at the focal point on the grating. The outcouping mirror, in conjunction with the grating, defines a different wavelength for every emitter.

figure 4.2. An off-axis beam positioned out of the page would be focused onto the correct spot on the diffraction grating, however with an extra angle into the page. This would mean that the reflected spot on the grating would be offset by the same amount as the original core offset. When the beam is directed back to the fibre, the spot will be focused on a position reflected about the central axis. In such a situation the deviation should be limited to a quarter of the core diameter misalignment to ensure that the coupling efficiency is maintained.

4.4 Fibre fabrication

4.4.1 Initial fabrication tests

The standard of glass used by the ORC for optical fibres is F300 supplied by Heraeus, which has very low OH^- concentration (typically less than $0.2ppm$), and very low contaminants of iron and other impurities. This grade of glass is fabricated as standard in the form of rods and tubes, which are then used to fabricate the silica based fibres in the ORC. The tubes and rods are fabricated using the OVD technique (as outlined in section 2.3.1) and this is therefore inappropriate for the fabrication of a rectangular profile. To obtain sections of

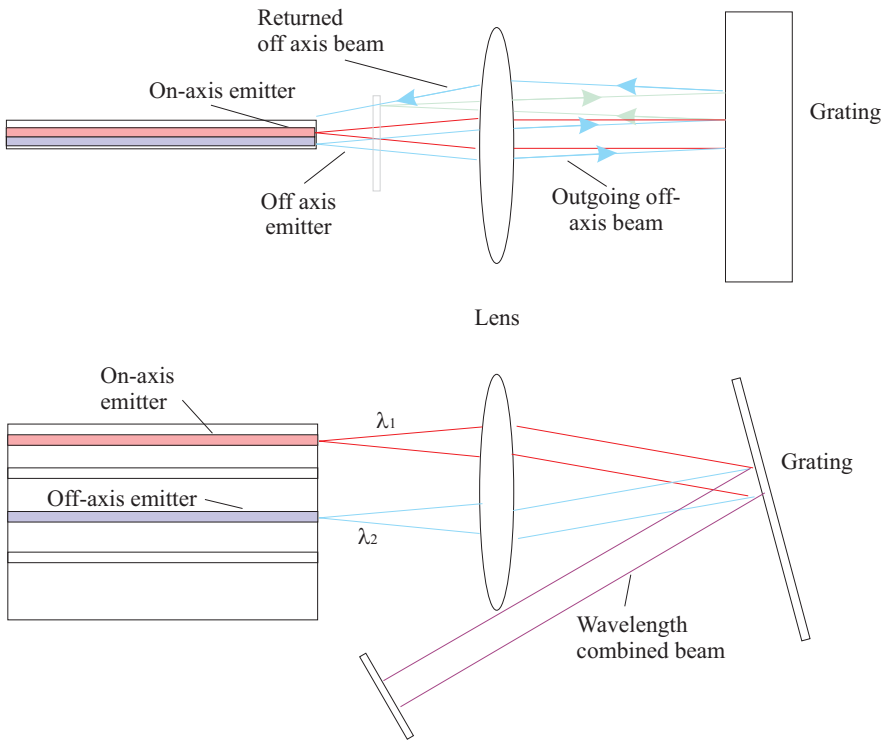

Figure 4.2: A beam propagating from a core which is misaligned perpendicular to the plane of the cores and beam is shown. The beam has a angle which is unaltered by the grating, and on return to the emitter array is in a position which is effectively a reflection across the line of the emitter axis.

rectangular glass, circular F300 grade glass was cut into rectangular sections, as shown in figure 4.3(a). The glass saw uses a circular cutting blade, with diamond impregnated abrasive material as the grinding tool. This abrasive material will cause small chips to form on the corners of the cut glass, as shown in figure 4.3(b). This can be avoided by ensuring that the surface being cut is braced by a firm substance, which is also cut through.

The first tests with rectangular glass used standard silica, which has the same melting point and machining properties as F300 but higher impurities, to ensure that there would be no deformation due to the high aspect ratio. These tests showed that at low temperatures there was little deformation of the glass, with only the sharp corners slightly rounded off due to the surface tension. This would not cause a significant problem with the launching of pump light, since the field intensity is low at the corners of the beam.

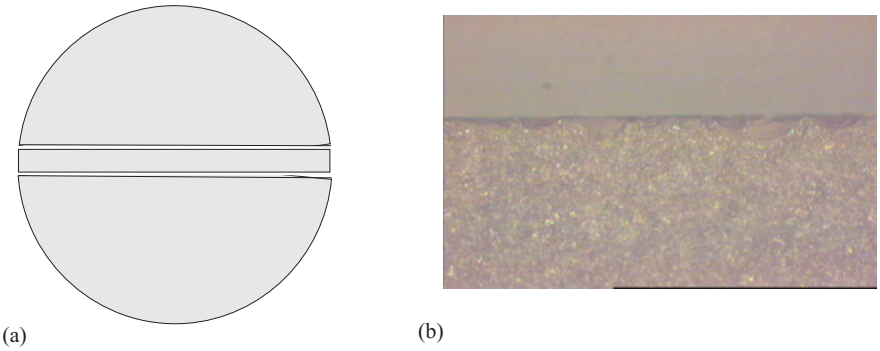

Figure 4.3: (a)F300 quality glass is supplied in rod form, with a diameter of 24mm, which can be cut to form a number of thin slices of 2mm width. (b)The abrasive cutting surface effectively grinds out the material and the chipping that occurs is shown. By having a material to strengthen the glass no chipping will occur at the glass interface.

The glass taken from a $24mm$ diameter F300 rod had dimensions of $24mm \times 3mm$, into which seven holes with a diameter of $1mm$ were drilled. The cores were taken from a standard MCVD preform, with a germanium doped core, which had been stretched and then etched to a diameter of $900\mu m$ to fit the holes. The final fibre dimensions were planned to be $2mm$ by $250\mu m$, with a core size of $14\mu m$. This meant that the preform would decrease by a factor of 12 and therefore the original preform needed to be stretched so that the core diameter would be reduced by a factor of 6.

The air gap between the rectangular glass and the inserted core was expected to

seal during pulling due to the surface tension combined with the lower viscosity of the glass. In order to preserve the aspect ratio, a low temperature during pulling was used, 1950^oC as opposed to 2020^oC used in standard fibre drawing. This meant that the glass surrounding the inserted cores was not sufficiently viscous to completely seal and left air gaps on the side of the cores, as shown in figure 4.4.

To coat the fibres a die was required which would have a rectangular shape close to the dimensions of the fibre being drawn. This was achieved by machining an existing coating die to form a slot, measuring approximately $2mm$ by $400\mu m$. The coating is very viscous, and hence tends towards a circular profile as the fibre leaves the base of the coating cup before entering the curing unit. This caused the coating to collect on the large faces of the fibre with very little on the ends or the corners, as shown in figure 4.5, although not a problem in terms of confining the light, it meant that the fibres were fragile and difficult to handle.

Figure 4.4: A low drawing temperature to maintain the rectangular profile, causes the viscosity of the glass to increase to a point where the air gaps surrounding the inserted core rods are not completely sealed. The fibre has dimensions of $2mm \times 140\mu m$.

The small preform size leads to a limit in the length of fibre drawn. Drawing down from $24mm$ to $2mm$ is a factor of 12, leading to the attainment of $10m$ of fibre from a $70mm$ length preform, this not taking into account losses at the start and end of the drawing. The fibre was planned to have a concentration of approximately $14000ppm$ of ytterbium ions, which over 7 cores of diameter $15\mu m$ gives an effective concentration of $70ppm$ over the entire cladding. The pump sources operated at $920nm$ which, for the absorption of 90% of the power, gives a device length of over $6m$, which means a large amount of work was involved in fabricating a single fibre laser. The laser results from the initial fibres were poor, mainly due to the loss associated with scattering from the air gaps surrounding

the cores.

Figure 4.5: Photograph showing the coating of a rectangular fibre. The coating is thin at the corners of the fibre, which leads to structural weakness. The fibre has dimensions of $1.8mm \times 150\mu m$.

4.4.2 Demonstration of a multi-core ribbon fibre laser

The fibre dimensions were $1.90mm \times 0.26mm \times 2.7m$ with the cores of diameter $20\mu m$, with a numerical aperture of ~ 0.1. The ytterbium concentration was approximately $10000ppm$, calculated by drawing fibre from the original preform fabricated through MCVD and solution doping. The fibre was pumped at $930nm$ with an incident power of $45W$, and a cutback measurement with $100mm$ of fiber gave a power reading of $26.5W$ indicating a pump coupling efficiency of $\sim 60\%$. The residual pump light power from the output end of the 6m of fiber was $7.2W$ with the laser output power being $\sim 440mW$ at $1.054 - 1.071\mu m$. The laser threshold was noted to be $\sim 35W$ incident power. The poor quality of the fibre can be ascribed to the loss of pump light due to scattering from air gaps around the cores, which also blocked light from reaching the cores.

To eliminate the holes in the final fibre, the drawing temperature was tested using low grade silica at a higher temperature, whilst maintaining the aspect ratio of the original preform. This showed that pulling at a temperature of 1980^oC would seal the holes completely, whilst not deforming the fibre to a significant degree. The next generation of fibres were pulled with no air gaps and gave promising

results, although hampered by the lack of devices fabricated, as illustrated in figure 4.6.

Figure 4.6: Photograph of the end face of a ribbon fibre with no air holes. The germanium doped cores can clearly be seen, and there were no air holes anywhere in the length of the fibre drawn.

The time required for the fabrication of a single ribbon fibre device took in the order of a few weeks, due primarily to the material processing required. An alternative method for fibre ribbon fabrication was suggested, using a number of square fibre lasers. This method involved making square fibres, stripping the ends and fixing them together in a line as shown in figure 4.7. In order to fabricate square fibres, a standard MCVD preform was taken and milled into a square shape, with care taken to ensure that the core was perfectly central. This was then fire polished to ensure that the surface of the fibre would be of sufficient quality to guide the pump light efficiently. The preform was then pulled as for a normal fibre with low index coating to provide the protection and confinement of the pump light. Ten of these fibres were then taken and the end of the coating stripped off using dichloroethylene. They were then clamped together and glued in place using low index coating, as used to coat the original fibre. This method failed however, due to the difficulty in placing the fibres such that there was no gap between them. This meant that a significant quantity of pump power was not contained in the silica fibre, and caused the coating material to burn as it was absorbed.

In order to fabricate more fibre from a single preform, either the length of the preform must be increased or the cross-section of the preform needs to be increased. Increasing the length of the preform is difficult due to the problem with drilling very long distances into glass, as detailed in section 3.3.4. Increasing the cross-sectional dimensions of the preform requires a very large slab of high quality glass, which needs to be fabricated to order. The increasing of the preform size, should significantly increase the fibre yield, and also simplify the fabrication process.

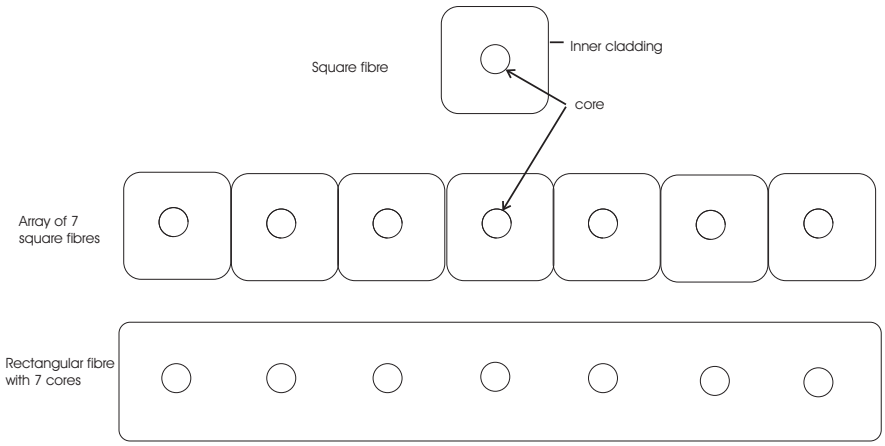

Figure 4.7: Square fibres, drawn from a machined preform can be placed together to simulate a ribbon fibre.

4.4.3 Large scale preform

The drawing tower used in the fabrication of standard optical fibres in the ORC, uses a graphite resistance element, with an internal diameter of $30mm$ as described in section 2.3.2. This limits the maximum width of a preform to $25mm$, constraining the maximum quantity of $250\mu m$ fibre attainable from a preform is $1m$ per $10mm$ of preform, or $10m$ for $100mm$, which is the longest length that can be drilled into such small preforms. A new furnace was installed which uses an RF induction element, which can accommodate preforms up to a diameter of $150mm$, as shown in figure 4.8. This required obtaining F300 grade glass with much larger dimensions, and therefore $10mm \times 100mm \times 1m$ glass slabs were acquired. The increase in cross-sectional dimension allows lengths of fibre up to $100m$ to be simply fabricated.

The largest difficulty in working with large glass slabs is the welding of slabs together, due to the large aspect ratio. Welding procedures for small tubes or rods (up to $30mm$ OD) are widely used on glass working lathes, which are also used to fabricate MCVD preforms. The process is different when using glass with a non-circular profile, since the variation in distance from the heating burner causes deformation. For any glass shape with a diameter of more than $40mm$, it is not possible for the object to fit over the burner used to heat standard tubes, which meant that for large ribbon preforms the current fabrication techniques were not suitable. The localised heating and rapid cooling of the glass means that there will be stresses within the glass. The stress within circular silica operates on all sides uniformly and thus there is no requirement for special treatment to increase the strength of the glass. For rectangular glass, the stress will not be uniform and so a slight knock, or heating elsewhere on the preform can cause the glass to fracture. After any welding or sealing procedure, the preform must be annealed, a process where it is uniformly heated and slowly cooled, to remove any stresses in the preform. The size of furnace required to anneal the proposed preform is greater than any within the ORC. The preform was therefore sent away to outside contractors for welding and annealing.

The preform is shown in figure 4.9. Holes were drilled into the length of the glass slab, extracted cores inserted, and then blocks were welded to the top and bottom of the preform to act as a support and drop respectively. Holes were then drilled into the side of each inserted core, to provide a route for the air to escape whilst being drawn into a fibre. The coating system was a copy of the original drawing tower, so there was no requirement for an adaption to the new tower to enable rectangular coating.

The increased size of the preforms meant that there was a larger gap between the drilled holes and the inserted preforms. The furnace calibration had been performed with rods of solid glass, which take up a large area inside the furnace, and require a large amount of heat to attain a certain temperature. The power required to heat the furnace to the right temperature will be lower than when a large volume of glass is inserted, and thus the power had to be reduced accordingly. The uncertainty in preform temperature, along with the increased air gaps, meant that the holes were not completely sealed, as was the case in early fibres fabricated on the standard drawing tower.

Figure 4.8: The large bore furnace used in the ORC. The preform shown has a diameter of $150mm$.

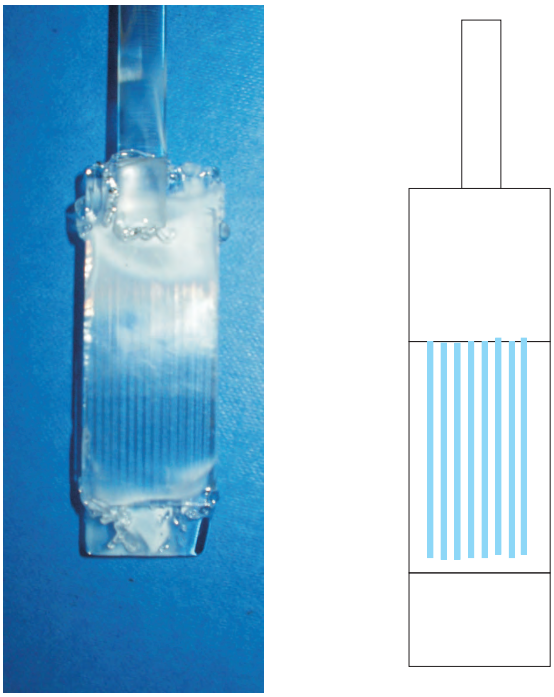

Figure 4.9: A handle is attached to the top of a block of machined silica, into which cores have been inserted. A drop is attached to the base to form the drop and to allow the fibre dimensions to stabilise to increase fibre yield.

4.4.4 Final design

In order to fabricate a preform with completely sealed cores, a new design was formed, as shown in figure 4.10. The preform has channels, which can be connected to a vacuum pump whilst pulling, to ensure that the air is completely evacuated from the preform. The fabrication of this design required the drilling of the holes to insert the cores into to a depth of $100mm$, and then connecting the top of these together by drilling one hole through the side of the preform. A single hole was then drilled down into the interconnecting hole from the upper end of the preform, to provide the route to the top of the preform where the vacuum pump would be attached. The point at which the interconnecting hole entered the side of the preform needed to be plugged, which was achieved by inserting a glass cone of the correct size, and then heating the area to weld it into position with an airtight seal. After this the preform was annealed, to relieve the stress formed by heating a small part of the structure and then being rapidly cooled.

The next stage was to attach a weight to the bottom of the preform to act as the "drop", which decreases the amount of preform wasted at the start of the

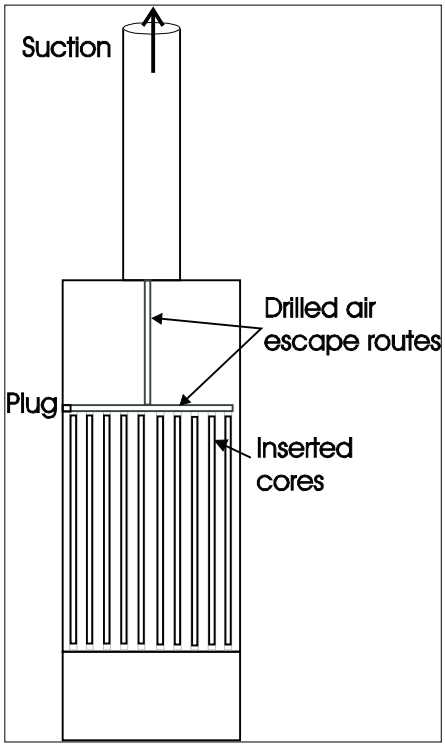

Figure 4.10: The final preform design for the fabrication of ribbon fibre lasers is shown. A system of air escape holes allows a vacuum to be applied for the complete sealing of air holes.

pulling process. By initialising the pull on the drop at the base of the preform (assuming that the drop is the identical shape to the preform), the fibre can be drawn down to the correct size and good stability attained before the actual perform itself is used up. The process of attaching two pieces of rectangular glass was learnt from the outside contractors used previously, who were visited to learn glass welding techniques for working on a large scale. The edges were chamfered on both sides for both blocks, and then held in specially made clamps that fit to the glass working lathe, as shown in figure 4.11. The edges were then moved together and welded together using a $2mm$ rod of silica as solder. There required a number of applications on both sides of the preform to ensure that the transition was smooth and that the weld would hold together during the drawing process. The smooth transition is needed in order for the fibre to be the right size and not fluctuate once the join is drawn. Once the welding had been done, another annealing process was needed, the annealing time was increased due to the large size of the join, and the amount of heat using during the welding process. This was performed using the large bore furnace, starting at 1600^oC where the glass is not yet malleable, and the temperature decreased slowly to 800^oC (the limit

of the pyrometer) over a 3 hour period.

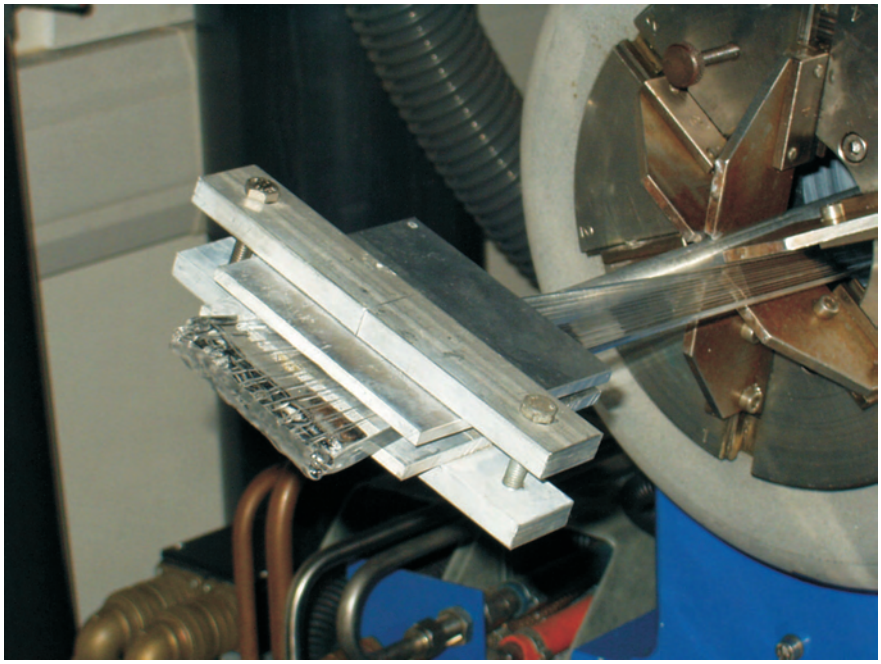

Figure 4.11: Clamps were designed and fabricated to allow rectangular glass to be firmly held whilst welding was performed. The devices were designed to connect to the existing glass working lathes allowing rotation of the preform to access all sides.

The final stage was the connection of a tube to the top of the preform to perform two functions; providing a handle which can be clamped to hold the preform, and allowing a vacuum pump to be attached to the holes in the preform. The tube was cut across the centre such that the slab would fit in the cut made, with glass on either side. This was then welded to the top of the preform using $1mm$ rods to seal all round the join to make it airtight. The finished preform is shown in figure 4.12, where the air extraction routes and drop can clearly be seen.

4.4.5 Drawing the ribbon fibre

The drawing of preforms in the large bore furnace requires a good control over temperature distribution within the furnace, which is complicated by the size of the furnace and the non-circular shape of the preform. The top of the furnace needs to be almost airtight, to reduce the heat lost due to convection. Fortunately, the length of the preform from the drop position, to the top of the rectangular section, is less than the distance from the hot zone of the furnace, therefore the

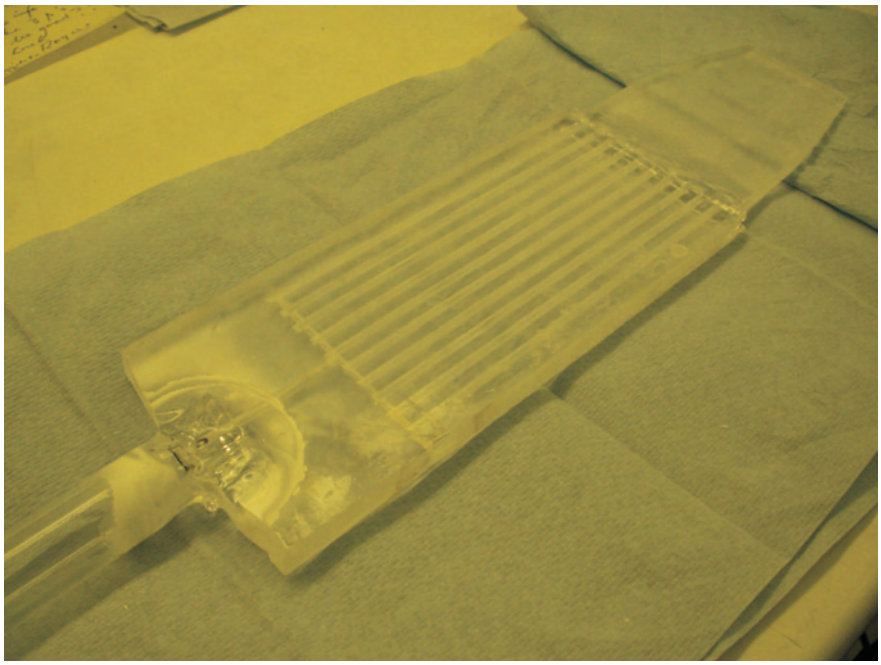

Figure 4.12: Photograph showing the finished final design of preform

top seal can be circular and is a constant size. In ordinary use the large bore furnace will have a preform of a uniform size all the way through the furnace, leaving only a small amount of area to be plugged to ensure that the system is air tight. With a rectangular preform, the hole at the top is $150mm$ in diameter, to allow the entrance of the preform, but the tube supporting the preform is only $20mm$ diameter, leaving a very large area to be plugged to ensure that the system is airtight. This puts a large strain on the material used for the top seal, which is a combination of graphite felt, graphite "card" and stainless steel. The graphite will oxidise in the presence of air, which is not a problem inside the furnace where nitrogen is used to purge the system, but the temperature at the top of the stack (as shown in figure 4.13) is high enough to cause oxidation and thus cause degradation of the top seal. Tests were performed using $20mm$ silica rods to simulate the temperature effects on the seal and, although the top two layers of graphite foam were significantly eroded the seal was still sufficient to have no adverse effects on the fibre draw and thus temperature distribution within the furnace.

The coating system, although the same as on the standard drawing tower, uses a curing unit without automatic control over the power output depending on the drawing speed. Whilst drawing test fibre to check the top furnace seal, coating

was applied and drawn at different speeds to ascertain the optimum speed for fibre coating using low index material.

The fibre was drawn at a temperature of 2060^oC, at a speed of $4m/min$, feeding into the furnace at $95mm/min$. This gave a fibre with dimensions of $240\mu m \times 1.9mm$, slightly less than was expected due to errors in the calibration of the machines used. The coating was cured correctly, but suffered from having large amounts on the flat surfaces with very little on the ends.

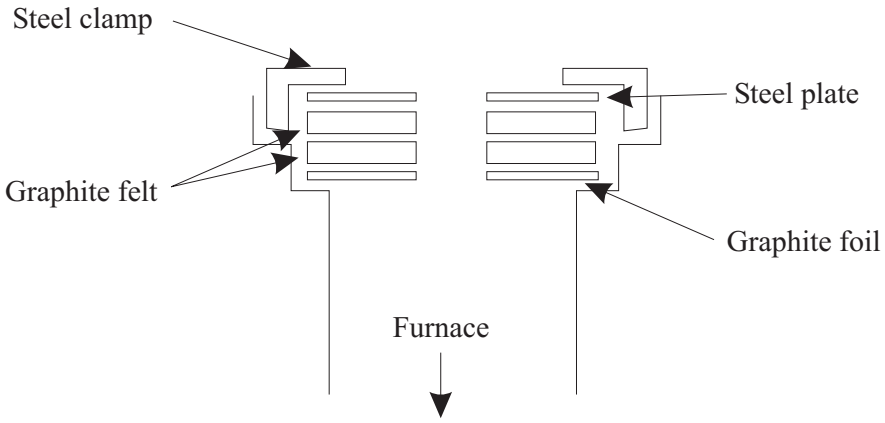

Figure 4.13: A system of insulation material is required to maintain temperature in the large bore furnace. A ring of graphite foil sits on the top of the furnace under two layers of graphite felt. Atop this is a stainless steel ring, which is then clamped down to the furnace top.

4.5 Ribbon fibre laser (RFL)

4.5.1 Ribbon fibre pumping

The setup used for the pumping of the ribbon fibre laser is shown in figure 4.14. The diode sources used were two twelve bar diode stacks with powers of up to 480W each. The outputs from the individual bars were collimated using fibre collimators for the fast axis, and a lens array for the slow axis. A slotted mirror system was then used to combine the outputs from the two arrays. The image the diode stack creates, once collimated, is less than half filled in the vertical direction and thus, by using a stack consisting of a mirror then a gap then another mirror continued down the stack, the outputs from two diode stacks can be simply

combined with no loss of beam quality.

After the multiplexing, the combined power was $850W$ and the beam had an M^2 in the x and y directions of 400 and 150 respectively. The smaller than planned dimensions made it difficult to couple all the pump light into the fibre, which could cause additional problems with burning very close to the actual fibre dimension of $240\mu m$, once NA and lens limitations are taken into account. In order to allow complete coupling of the pump light it was chopped and polarisation combined to reduce the M^2 in the y direction. The beam was $10mm \times 20mm$ so that once recombined, it would have the dimensions of $10 \times 10mm$. The mirror to chop the light was placed such that half the light passed over the mirror, and the other half reflected through a half wave plate then both parts recombined in the same plane using a thin film polariser. This yielded a beam with M^2 of 400 and 80 in the x and y directions respectively, although with a lower power of $640W$, due to losses from poor antireflection coating on the optical components.

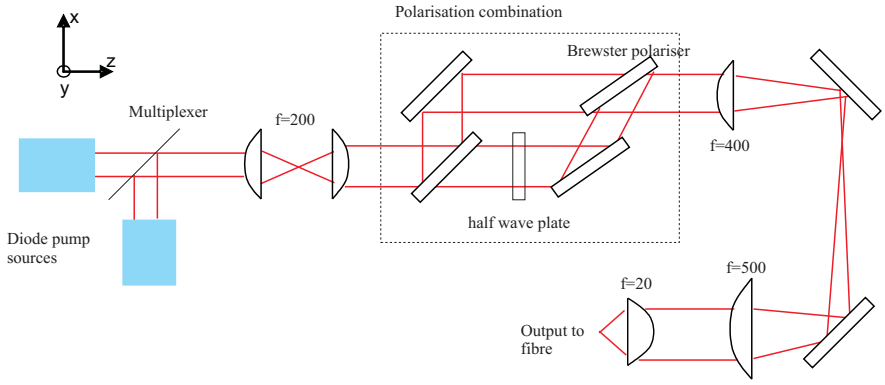

Figure 4.14: The pump sources used were two high power diode stacks. Due to the size of the fibre these needed to be multiplexed together using slotted mirrors, then the beam cut and polarisation combined to reduce the beam size to a dimension which could be launched into the fibre.

4.5.2 Ribbon fibre laser

A simple fibre laser setup was used to investigate fibre performance, as shown in figure 4.15. The laser cavity was formed through Fresnel reflection at the end facets of the fibre, with the pump light incident at one end of the fibre. Due to the high pump powers involved, and the non-uniform coating, most of the fibre was

held straight and sandwiched between two long blocks of metal with the input end of the fibre mounted in a metal clamp fixed to an adjustable stage, as shown in figure 4.16. The metal clamp at the input stage was constructed to be hollow, to allow cooling water to flow through, limiting any damage done to the coating at the high risk point.

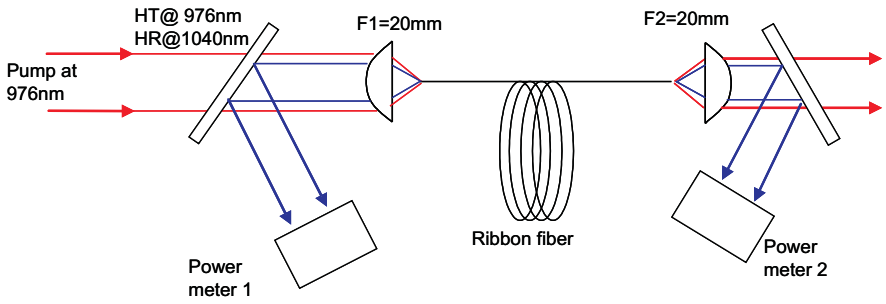

Figure 4.15: Schematic of the laser setup used to characterise the ribbon fibre laser. The output was measured from both ends of the fibre, and pumping from one end.

The laser output was measured at both ends of the fibre, and the pump through put was also measured. After the measurements with the fibre had been completed, the ribbon was cut back to measure the launch efficiency. The measured laser performance is shown in figure 4.17. With a fibre length of $2.2m$ the threshold was around $20W$ with a maximum output power of $250W$ for $430W$ of absorbed pump power [11]. The laser wavelength was $1042nm$, due to the short device length, with a slope efficiency of 65%, lower than is usually attainable with Yb doped fibre lasers.

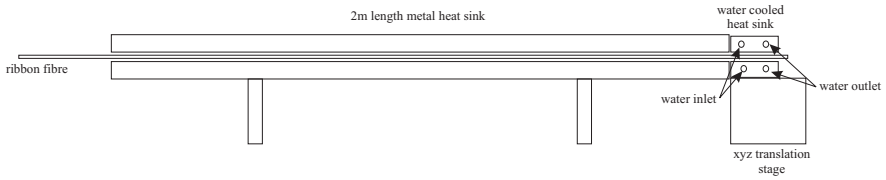

Figure 4.16: The ribbon fibre was held straight within a long heat sink to limit any potential thermal damage to the coating. The input end was mounted on a water cooled translation stage for accurate alignment, and the remaining fibre held between two $2m$ rectangular metal rods for heat sinking.

In order to maximise the output power of the laser, a single ended output laser was created, as shown in figure 4.18, which utilises the unabsorbed pump power after one pass. The reflection of one end of the laser is not routine however, since care must be taken to ensure that each core is imaged onto itself, and not the

mirror image as would be the case for a standard set up. The end of the fibre had to be re-imaged back onto itself using two lenses, rather than the one used in the standard setup. By measuring the efficiency of the set-up, it was possible to ensure that there were no extra losses due to misalignment in the external cavity. The results for the single ended output are shown in figure 4.19. The threshold was still $\sim 20W$ and the efficiency of the laser was 64%. The maximum attained power was $320W$ for $576W$ of launched pump power.

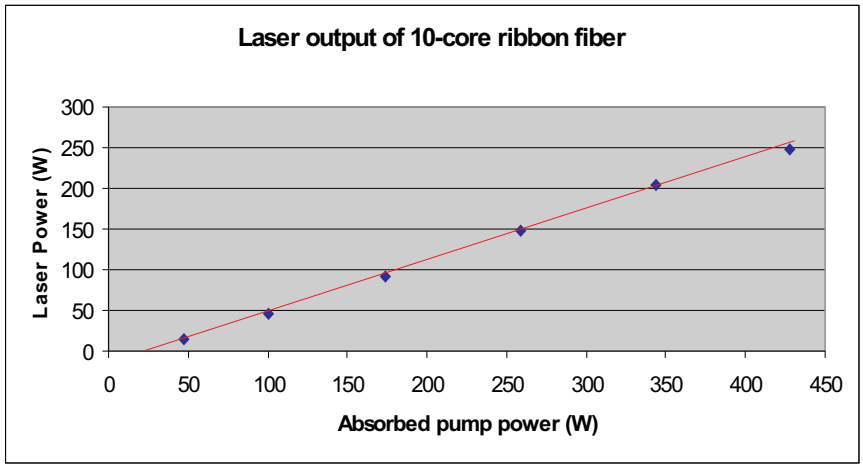

Figure 4.17: The laser power emitted from the ribbon fibre laser is shown, plotted against the absorbed pump power in the fibre.

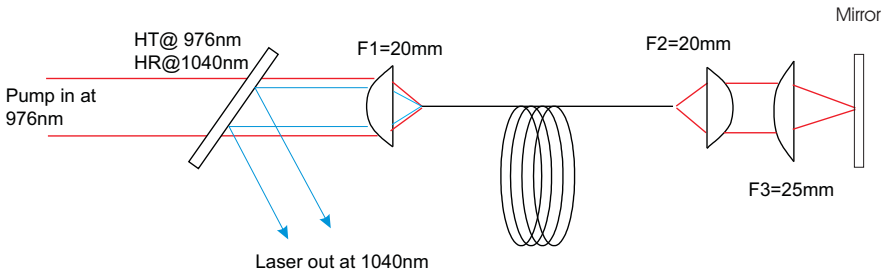

Figure 4.18: The experimental setup for gaining maximum power from the ribbon fibre laser is shown. The laser output has been changed to emit from a single end, using 100% at the other end.

4.5.3 Effect of core variation on RFLs

The process of making a large ribbon preform involves the use of a long length of core material. The core diameter in the ribbon preform was the same as that created in the MCVD process, so for the entire ribbon 1m of MCVD preform was required. A number of refractive index profiles along the length of a fabricated

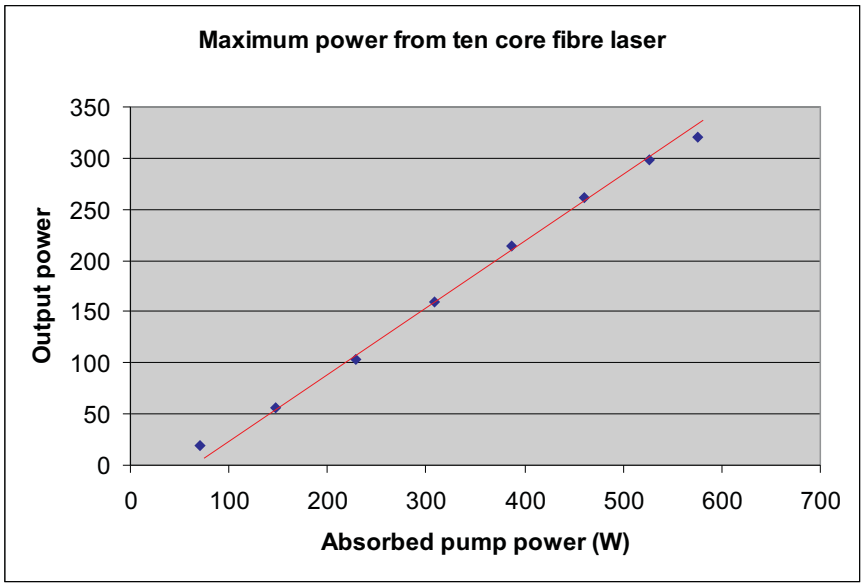

Figure 4.19: The laser power emitted from the single ended ribbon fibre laser setup is shown, plotted against the absorbed pump power in the fibre

preform of a length of $50cm$ were taken, which is a standard preform length fabricated through the MCVD process. There is a variation in the profile as one goes along the length of the preform, which will lead to differing properties depending on the position the fibre is fabricated from. The refractive index difference in the centre of the preform is only ≈ 0.0001, whilst at the ends the index changes by up to ≈ 0.0006. The refractive index of two preforms fabricated using identical parameters, will have slightly different profiles due to a very small variation in for instance initial diameter, wall thickness or another slight difference. Due to these variations, it is difficult to get a large number of identical preforms, which are essential in the fabrication of an ideal ribbon fibre laser.

The power from each core gives a good idea of the efficiency of the individual cores and possibly explain why the efficiency of the ribbon fibre is lower than standard Yb-doped fibre lasers. The percentage contribution of the total output power from each core is shown in figure 4.20, which indicates a very large variation in the efficiencies of the cores.

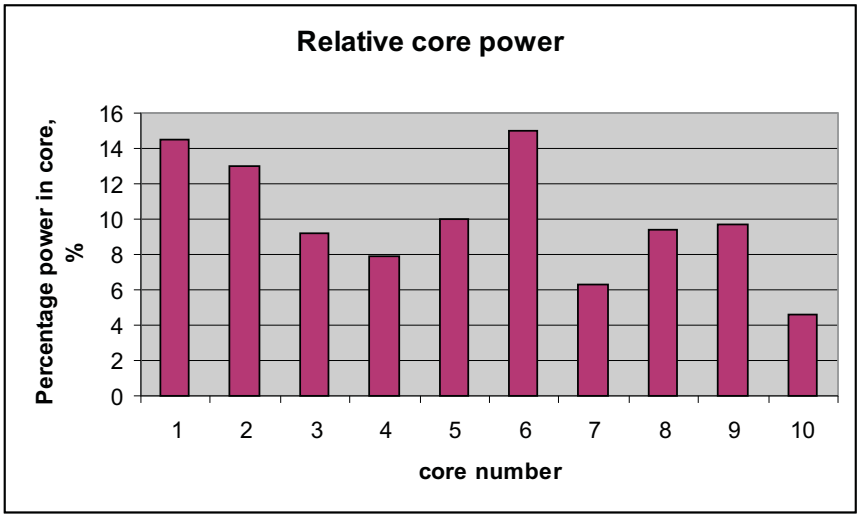

Figure 4.20: The percent of the total power emitted from individual cores is shown. The efficiency of the fibres is related to the power emitted, showing that for some cores the efficiency is less than half of that shown by adjacent cores. This is due to the variation of the fabricated preforms.

4.6 Spectrally combined RFL

4.6.1 Setup

The operational setup for a ribbon fibre laser in a spectrally beam combined configuration is shown in figure 4.21. The operation of spectral beam combination was described in detail in section 4.3.4. The initial set up is the same as shown in figure 4.19, for the single ended output fibre laser, with the output then used for spectral beam combination. The beam is collimated by the lens, and the grating defines a laser path and wavelength for each core, with the outcoupling mirror. Ideally for spectral beam combination each core would be individually collimated then directed to the appropriate point on the grating, thus eliminating any abberation due to the lenses used.

4.6.2 Issues

As shown in section 4.3.4, the alignment of the cores is critical for successful spectral beam combination. Figure 4.22 shows the end facet of the fabricated

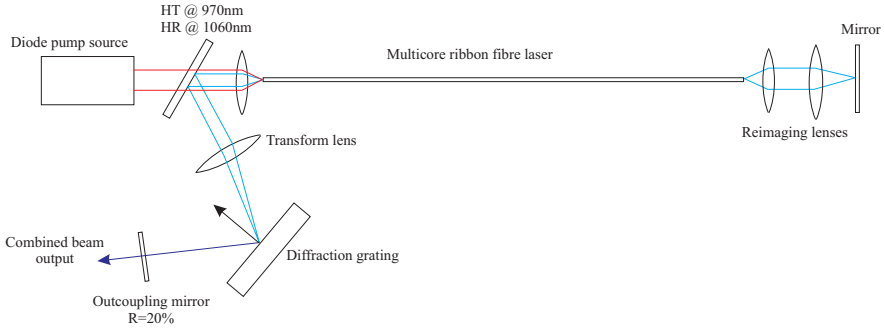

Figure 4.21: The setup for the spectral beam combination of a ribbon fibre is shown. A simple plano convex lens is used, along with a diffraction grating and outcoupling mirror, to determine each cores lasing wavelength.

ribbon fibre laser, with a line to show the offset of the cores. As can be seen, only 5 of the cores are in precisely a straight line, with the others slightly misaligned. Any misalignment causes a significant loss for the core and thus inhibits the onset of lasing. The problem with the different properties of the cores, as outlined in section 3.3.1, also hampers the possibility of creating a ribbon fibre laser. The point at which the cores will lase is dependent on the properties of the core and the position relative to the fibre axis, thus some will not lase until extremely high pump powers are reached.

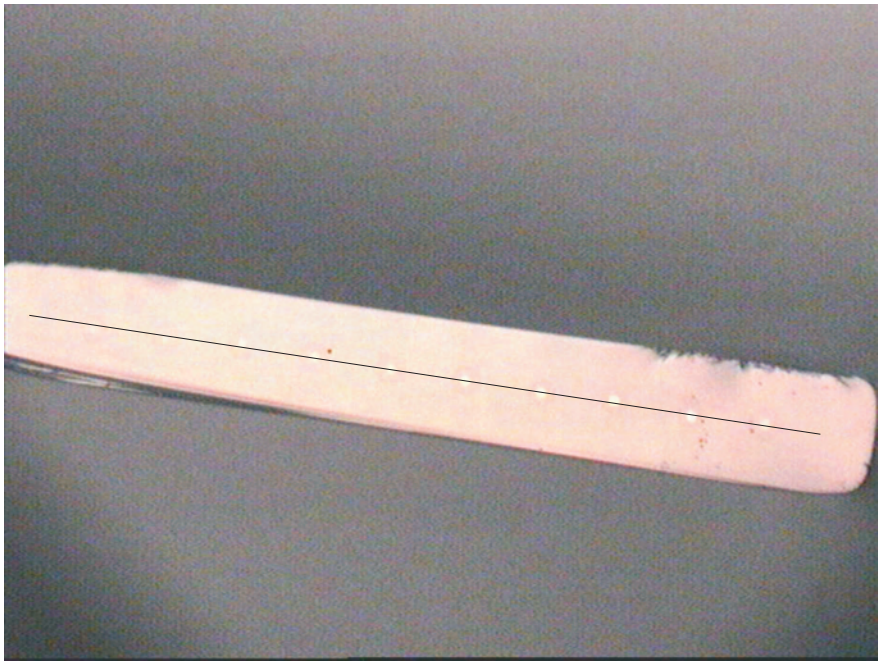

Figure 4.22: Photograph of the end face of the ribbon fibre laser. The cores are not in a perfectly straight line, which causes problems for the successful spectral beam combination of all the cores.

4.6.3 Spectral output

The results from the set up used are shown in figure 4.23 [12]. The ribbon laser was fine tuned in an attempt to spectrally combine the maximum number of cores, which was shown to be 5. This is due to the imperfect alignment of the cores, which increases the losses for the non-lasing cores to the extent where there is only ASE emission. The wavelength separation is $6.5nm$, which compares well with the predicted separation of $7nm$.

The output power is limited by the number of cores which are not lasing, due to the loss of half the lasing material which is absorbing pump power. The power is also limited by the lack of high pump powers due to damage to the end of the fibre where both pump coupling and core misalignment are significant energy loss contributors.

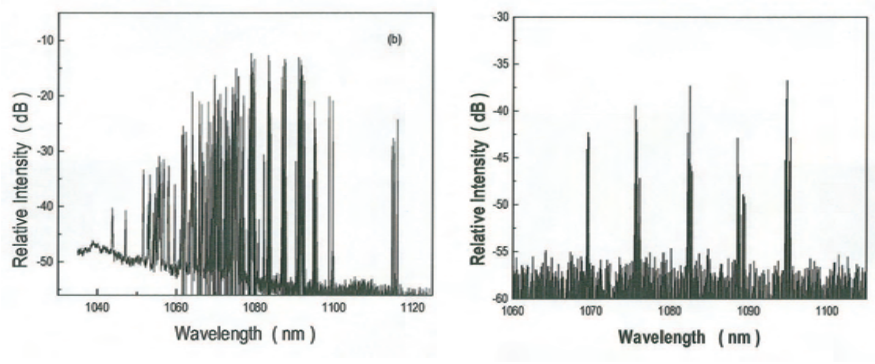

Figure 4.23: The alignment of the cores was insufficient to allow the spectral beam combination of all the cores. 5 cores were in sufficient alignment to allow successful beam combination.

4.7 Alternative multicore ribbon preform fabrication technique

4.7.1 Concept

The experiment using machined preforms and square fibres as detailed in section 4.4.2, lead to the concept of stacking the machined preforms and drawing

into a fibre. The sealing of the holes within the ribbon fibre indicated that the surfaces could fuse together due to the heat of the furnace. The rods would require a method for holding together the top ends of the preforms firmly, and the act of drawing the fibre could press the adjacent faces together with sufficient pressure for a ribbon to be produced. Previous experiments had been performed by colleagues [13] which used a drilled channel with canes inserted, which are then covered by a slab, as shown in figure 4.24. The fibre obtained from this method showed that all the spaces became sealed during fibre drawing, of particular interest the slab covering one side of the preform became fused into the fibre. This indicated that the method of placing square rods together in the furnace could yield a fused ribbon fibre.

4.7.2 Fabrication

Initial experiments were performed to determine whether the concept was feasible. Three rods with flats milled on either side were prepared, and fire polished to provide suitable fusing surfaces. These were then held using the clamps shown in figure 4.11, and the ends welded together using $1mm$ diameter silica rods as glass solder. Once firmly held together, a handle was welded to the fused end of the rods to allow the rods to be lowered into the furnace. The lower end of the rods were left unattached, with the assumption being they would attach together before dropping once in the furnace. The furnace temperature used was 2050^oC, higher than normal fibre drawing in order to ensure that the rods would indeed fuse together. The fibre drawn from this preform showed that the fibres did fuse together and the method of fusing rods in the furnace was a viable method for fabricating ribbon fibre.

The next stage was to fabricate a fibre with cores and a rectangular profile. The furnace used was on the standard drawing tower, and therefore the maximum preform diameter useable is $25mm$. The diameter of preforms is $\approx 12mm$ and, once milled into a square profile, the width is $\approx 8mm$. Due to the limitation in size four rods were used to test the ribbon fibre fabrication method with core material. The preform was fabricated in the manner of the three-rod preform mentioned above, although the lower portion of preform was welded to a short slab, as shown in figure 4.25. The short slab was intended to encourage the rods to

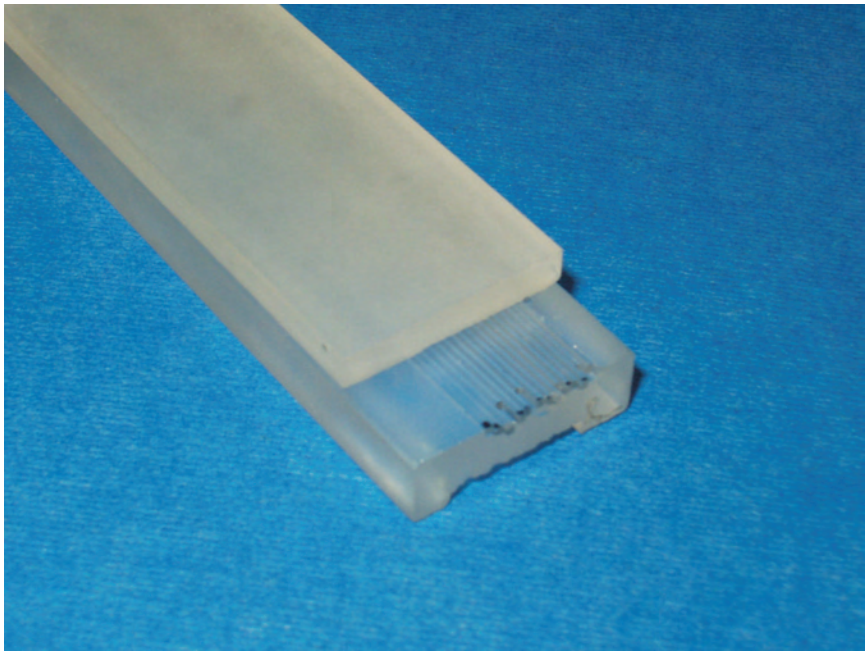

Figure 4.24: Demonstration of a method for fabrication of multiple core in a single fibre. A channel is cut into which caned preforms are inserted, and then covered with a slab of silica. When drawn the fibre is shown to be fused together indicating that two pieces of glass in contact within the furnace will fuse together.

weld together by performing the drop at this point, enabling a lower temperature to be used for the fibre drawing. The fibre was drawn at a temperature of 2030^oC, and sections examined to determine the success of the fusing method.

4.7.3 Results

The fibre fabricated with core material is shown in figure 4.26. The individual rods have clearly fused together, although even with the precaution of a lower drawing temperature the deformation of the fibre is severe. The cores have been squashed into ovals, with a ratio of 2:1, and the profile of the fibre has reduced from 4:1 to 2:1 with rounded corners. The alignment of the cores is good, and should be within the quarter of the core diameter required for spectral beam combination.

Figure 4.27 shows an attempt to fabricate a fibre with ten cores in a line. The problem with temperature has been solved, but the fibre shows large misalignment in the cores. The difficulty lies in working to the dimensions of the standard drawing tower furnace, which is $30mm$ in diameter. The accurate welding of canes together becomes increasingly difficult as their dimensions decrease, due to movement of the canes due to the force of the oxyhydrogen flame used in glass working. The hand torches used are designed for heating glass tubes or rods with cross sectional areas of $100mm^2$ and the flow rates are too high for more delicate work. The canes used to fabricate the 10 core preform were $2mm$ in diameter and $200mm$ in length. For a cane of these dimensions the loose end will be free to move to a large degree even when the other end is firmly held.

4.7.4 Future work

The method of fusing rods during the process of drawing has been shown to be a viable method for fabrication fibres. The scaling of the preform to 10 or more cores in a straight line makes the pre-drawing fusing difficult, and care will need to be taken to ensure that the alignment of the cores is not compromised. The use of the large bore furnace will simplify the process dramatically, but at the cost of using a large amount of preforms in the testing and refinement stage. The number

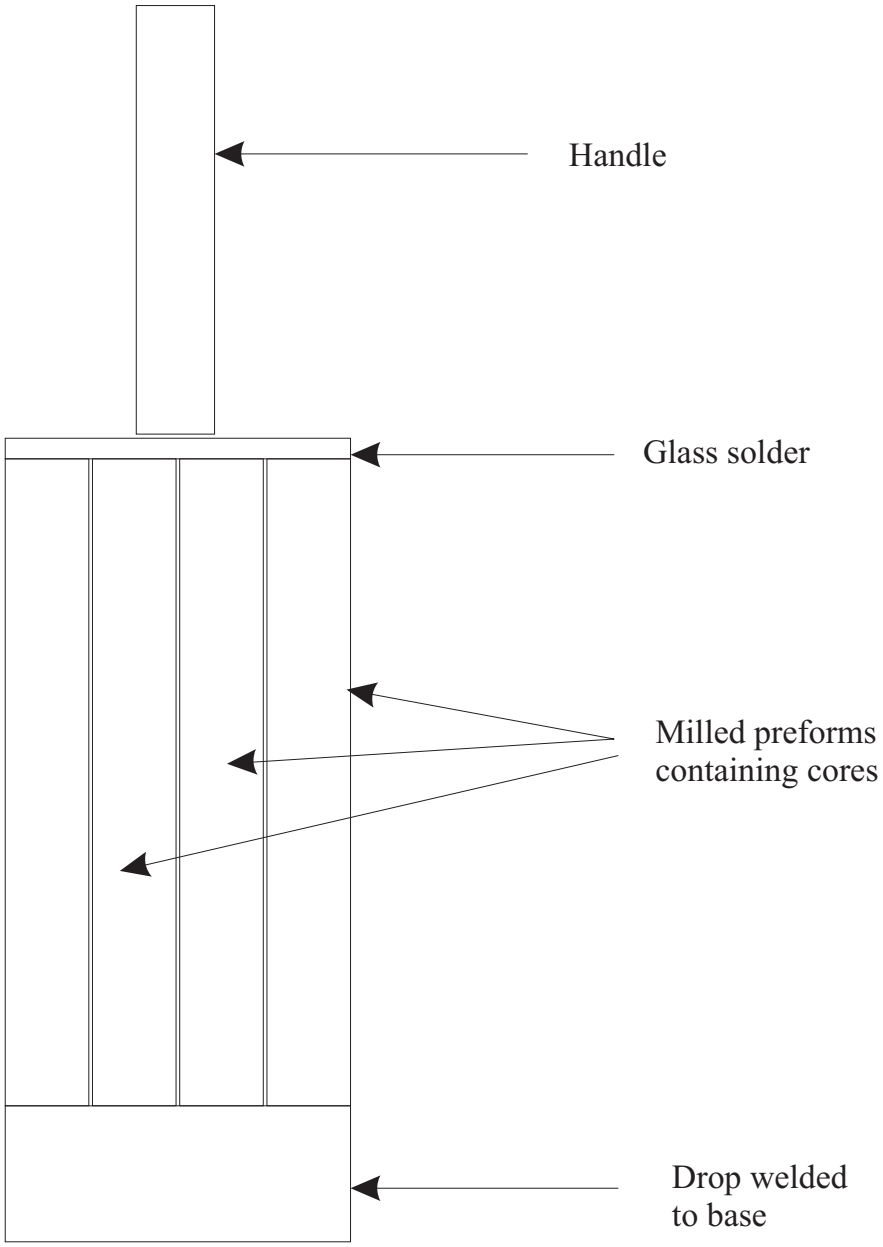

Figure 4.25: Diagram of the preform design for using the fusing effect of silica in contact with silica. The ends must be firmly held to ensure contact between the rods is maintained through the drawing process, which is most critical at the beginning of the fibre drawing.

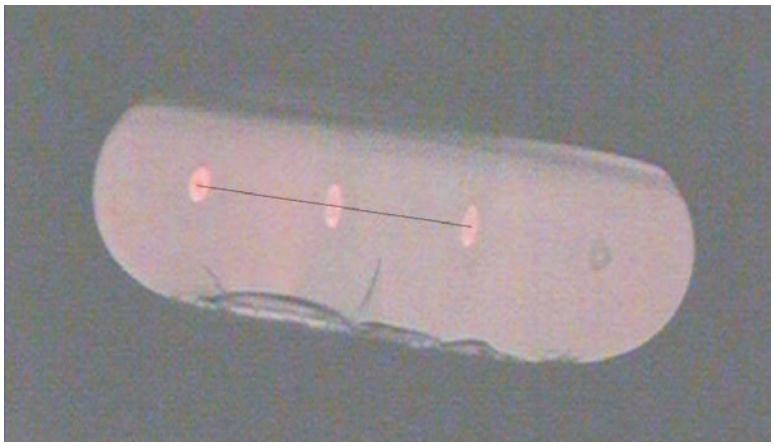

Figure 4.26: A photograph of the end face of the fibre fabricated using the fusing effect of silica in the furnace. The dimensions of the fibre are in a ratio of 3:1 whilst the preform had dimension in the ratio of 4:1. The cores bear evidence to the deformation of the fibre during drawing. The dimensions shown are $1mm \times 300\mu m$

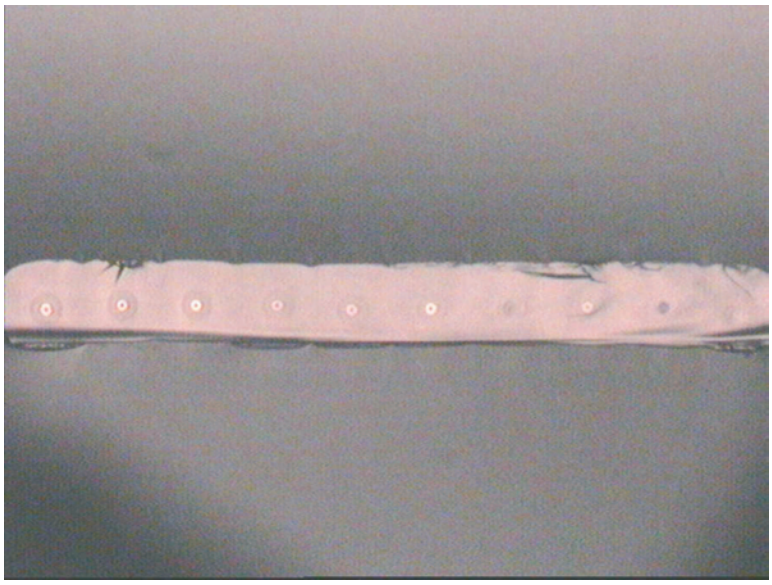

Figure 4.27: A photograph of the end face of a fabricated 10 core fibre. The alignment has suffered with the increase in number of cores, however the distortion due to over heating has been eradicated. The fibre has dimensions of $\approx 2mm \times 200\mu m$.

of preforms required will be as for the standard ribbon fibre fabrication technique (due to the constraint being the core material), and therefore the reproducibility of the preforms will again be an issue. There is also a high chance of impurities at the interface, due to the large quantity of processing required whilst exposed to the air. Even with the problems outlined this method will require far less processing and time, than the current method used.

4.8 Conclusion

The fabrication of a multicore ribbon fibre has been successfully demonstrated. The use of a ribbon fibre has been shown to provide excellent pump coupling properties as is expected due to the large area in which to focus the light. The spectral beam combination was not as successful as was hoped, due to problems with the fabrication, in particular the core alignment and the coating uniformity. A maximum output power of $320W$ from $576W$ of launched pump power was achieved, with a slope efficiency of 64%. 5 cores were combined together using the spectral beam combination technique

The largest problem is the adequate fire polishing of the internal surfaces of the holes drilled. This can not be performed using the equipment available at the ORC, and requires either a system where a large preform can be passed through the large bore furnace with no stretching or a method for heating large preforms on glass working lathes.To fire polish in the furnace requires a method of supporting the top and the bottom of the preform as it is moved slowly up and down through the hot zone. This would enable the high temperatures required to allow complete fire polishing of the surfaces to be achieved, whilst not deforming the shape of the preform itself. A system for doing this would need to be very rigid to ensure that there is no movement between top and bottom of the preform. The requirements to fire polish on a glass working lathe are new furnaces or heating elements, requiring a lot more work than to convert a furnace to this use.

The coating for rectangular fibre is currently a concern. Whilst it is possible to coat rectangular fibres the process is not accurate and, more often than not, leaves areas uncoated and thus the fibre very fragile. A method for coating fibres

with a very thin yet uniform coating could be the use of spray coating. A system could be constructed which uses highly viscous coating and sprays a very thin (a few tens of microns) coating on to the fibre. This would have the advantages of being uniform, capable of coating any shape required, and having no chance of bubbles at the glass coating interface.

The problems with non-uniform core materials can to a large extent be eradicated by using more preforms and avoiding the ends where large changes occur. This does not solve problems in repeatability, but any differences between the preforms will be very small in comparison to the changes in dopants at the start and finish of the fabricated preforms.

The process for fabricating multicore ribbon fibres is very time consuming and complicated, prohibiting the industrial applications of these fibres. With more research, it should be possible to fabricate ribbon fibres using square preforms fused within the furnace (as demonstrated in section 4.7) although whether it is possible to maintain the aspect ratio remains to be seen. For the current fabrication technique which is capable of making up to $100m$ of fibre, there are a number of processing steps that are difficult, but with a more robust drilling machine, would be routine.

4.9 References

[1] M. Jansen S. Wang, J. Z. Wilcox and J. J. Yang. In-phase locking in diffraction-coupled phased-array diode lasers. *Applied Physics letters*, 48(26):1770–72, 1986.

[2] A. Yariv M. Cronin-Golomb and I Ury. Coherent coupling of diode lasers by phase conjugation. *Allied Physics Letters*, 48:1240–43, 1986.

[3] E. J. Bochove. Theory of spectral beam combining of fibre lasers. *IEEE Journal of Quantum Electronics*, 38(5):432–445, 2002.

[4] W. A. Clarkson. Personal communication. *University of Southampton.*

[5] M. Wrage, P. Glas, M. Leitner, T. Sandrock, N. N. Elkin, A. P. Napartovich, and A. G. Sukharev. Experimental and numerical determination of coupling constant in a multicore fibre. *Optics Communications*, 175:97–102, 2000.

[6] R. G. Waarts D. Mehuys, W. Streifer and D. F. Welch. Modal analysis of linear Talbot-cavity semconductor lasers. *Optics Letters*, 16(11):823–825, 1991.

[7] J. Banerji, A. R. Davies, and R. M. Jenkins. Comparison of Talbot and 1-to-N-way phase-locked array resonators. *Applied Optics*, 36(7):1604–1609, 1997.

[8] W. A. Clarkson and D. C. Hanna. Two-mirror beam-shaping technique for high-power diode bars. *Optics Letters*, 21(6):375–377, 1996.

[9] C.C. Cook and T.Y. Fan. Spectral bean combining of Yb-doped fibre lasers in an external cavity. *Advanced Solid State lasers*, 26:163–166, 1999.

[10] W. A. Clarkson, L. J. Cooper, P. Wang, R. B. Williams, and J. K. Sahu. Power scaling concepts for fiber lasers. *Trends in Optics and Photonics*, 83(261-267), 2003.

[11] L. J.Cooper, P. Wang, R. B. Williams, J.K.Sahu, W. A. Clarkson, A. M. Scott, and D. Jones. Diode-stack-pumped Yb-doped multi-core ribbon fiber laser. *CLEO/IQEC*, San Francisco:16–21 May, 2004.

[12] P. Wang, L. J. Cooper, J. K. Sahu, W. A. Clarkson, A. M. Scott, and D. Jones. High-power Yb-doped multi-core ribbon fiber laser
. *Accepted by Optics letters*, manuscript 62661, 2005.

[13] A. Webb. Personal communication. *University of Southampton*.

Chapter 5

Multiple core circular fibre lasers

5.1 Introduction

5.1.1 Outline

High powers with single mode output have been demonstrated by large core fibres, with power levels over $1kW$ for a single fibre [1]. The fibre demonstrated by Jeong et al. uses bending loss to strip out higher order modes and reduce the M^2 to 1.05. This method has proved successful, but in dealing with large core fibres it has been noticed that the output is not completely stable, causing fluctuations which would not be acceptable for a number of high power applications. The fluctuations are caused by the high power storage capacity of the fibre due to the size of the active area. This allows the fibre laser to pulse even when operated in a laser configuration. This phenomenon is not seen in truly single mode fibres, since they have a much smaller area available for power storage. The problem can be avoided for large mode area fibres by using the laser as an amplifier in a MOPA setup.

A number of attempts have been made to use coherent combination to combine a circular structure of multiple cores. A multicore fibre with a ring of 40 cores was fabricated which showed a slope efficiency of 40% with a maximum output power of $450mW$ [2]. The first attempts using a ring of emitters in a fibre and a

talbot resonator [3, 4, 5] had power levels and slope efficiencies which were not disclosed. A seven core fibre with coherent output power of $5.2W$ and a slope efficiency of 65% [6] has been demonstrated, but beam quality has been noted to degrade as power levels increase [4].

As was discussed in section 2.4.2, there is a method of combining the output from a number of fibre cores in an incoherent manner, at the cost of the beam quality. For applications such as industrial welding, a beam with low M^2, of the order of 10, and a stable output would be attractive. By using a number of single mode fibres with a stable output, very high power levels could be attained.

5.2 Theory

A brief discussion of the method of incoherent beam combination was given in section 2.4.2 which is expanded in this section. The definition of M^2 is the factor difference between the beam divergence of a given fibre and the beam divergence of a Gaussian beam of the same beam waist, as quoted in section 2.4.2. Equation 2.21 was: $w_0 = \frac{M^2\lambda}{\pi\Theta_0}$. This definition can obviously be reversed such that the measure of M^2 is the ratio of the waist of a beam compared with the waist of a Gaussian beam with the same divergence.

$$\Theta_0 = \frac{M^2\lambda}{\pi w_0} \tag{5.1}$$

From this we are able to simply calculate the expected M^2 value from an array of independent cores. The divergence will be determined by the individual cores, the Gaussian waist is the diameter of the core, and the total beam waist is the diameter of the area the cores cover, as illustrated by figure 5.1.

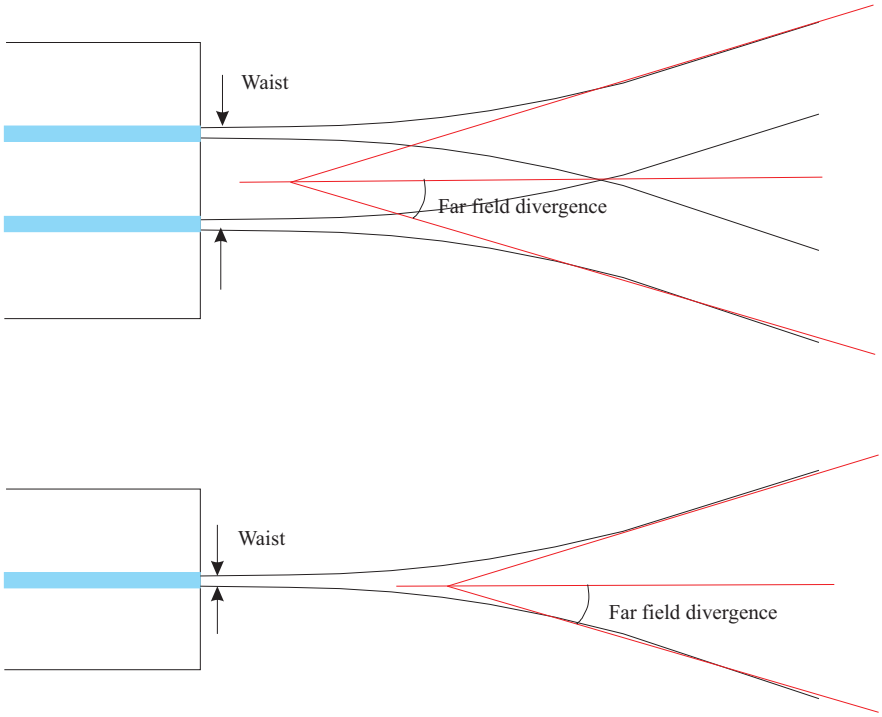

Figure 5.1: The beam emerging from emitters on the left. For the single emitter the beam waist is the width of the beam as it is emitted from the core, with the divergence being the far field angle. In the top case there are two emitters which make the effective beam waist the distance indicated, with the far field divergence being the same as for the single emitter.

5.3 Seven core fibre laser

5.3.1 Fabrication of 7-core fibre laser

The fabrication of a circular multicore fibre is similar to the technique used in chapter 4 for the rectangular multicore fibre. A large silica rod was drilled with seven regularly spaced holes, which were then filled with the extracted cores from a preform. The silica rod is F300 grade, which is the grade used for the deposition tube in MCVD preform fabrication. The cores were extracted from an ytterbium-doped preform, with an NA of 0.12 and an ytterbium concentration of $\approx 8000ppm$. The entire rod was then drawn on the drawing tower in to a fibre with seven cores arranged isometrically as illustrated in figure 5.2(a), with a picture of the end face in figure 5.2(b). The fibre was designed to be single mode at $1060nm$ wavelength with a $350\mu m$ outer cladding to allow high pumping powers to be used. The core to core separation was $90\mu m$, a core diameter of $8\mu m$ and core numerical aperture of 0.12.

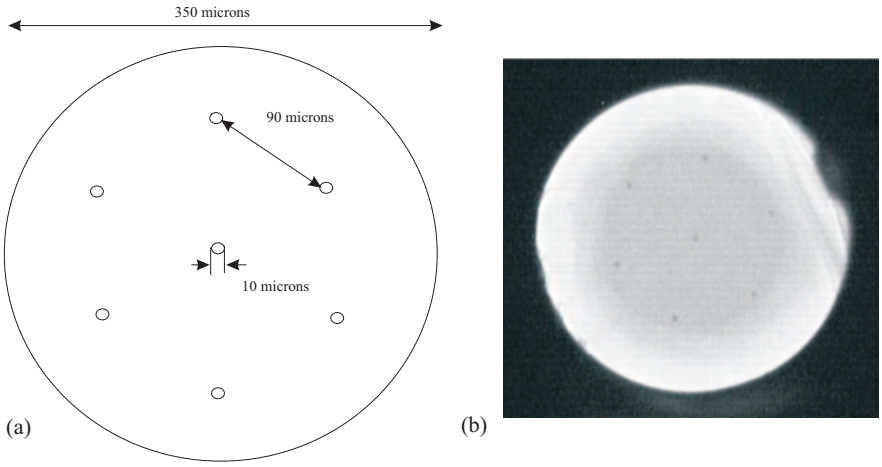

Figure 5.2: (a)Diagram of planned seven core fibre. (b)Photo of the end face of the fabricated seven core fibre

5.3.2 Results

The experimental setup is shown in figure 5.3. The 7-core fibre was pumped using a 500W Laserline source at $970nm$. Fresnel reflection from the cleaved ends of

the fibre form the laser cavity, and dichroic mirrors with high transmission at $976nm$ and high reflection at $1060nm$ are used to separate the pump light from the signal light.

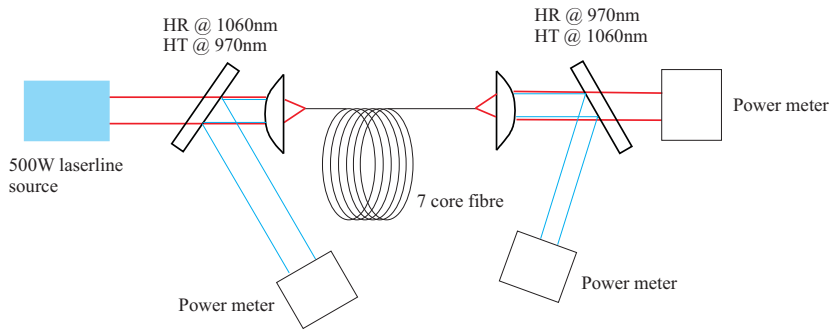

Figure 5.3: Experimental setup used to determine the performance of the seven core fibre. The spot size from the Laserline source is around $300\mu m$ which indicates that most of the pump was launched into the fibre.

The slope efficiency was measured to be 64% with a maximum output power of $270W$ as shown in figure 5.4. The M^2 of the individual cores was approximately 1, and the M^2 of the combined output of the fibre was 35. The high clad to core ratio leads to a long device length of $30m$. This length meant that losses from impurities in the cladding, due to the fabrication technique reduced the efficiency of the fibre. Planning the next fibre design with a lower ratio enabled the device length to be shorter, although at the cost of reducing the cladding area available for launching the pump light. Figure 5.5 shows the output spectra obtained from the 7-core fibre whilst operating at $270W$.

5.4 Three core fibre laser

5.4.1 Concept

The cores had a diameter of $8\mu m$ with an NA of 0.09. By using a Fibre CAD program the core separation could be determined by the fundamental mode profile. The cores were closely spaced to reduce the M^2 value to approximately 5. By the use of a length of multimode fibre spliced to one end of the fibre, the output could be combined to encourage lasing at one wavelength. The use of a

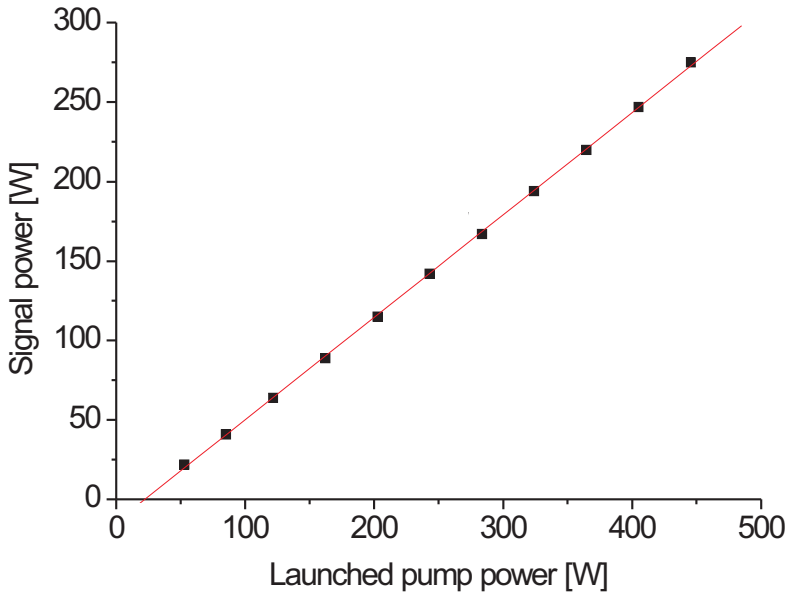

Figure 5.4: Graph showing the power achieved using the seven core fibre pumped with the Laserline source. The output power is plotted against the launched pump power, the slope efficiency is calculated using absorbed pump power.

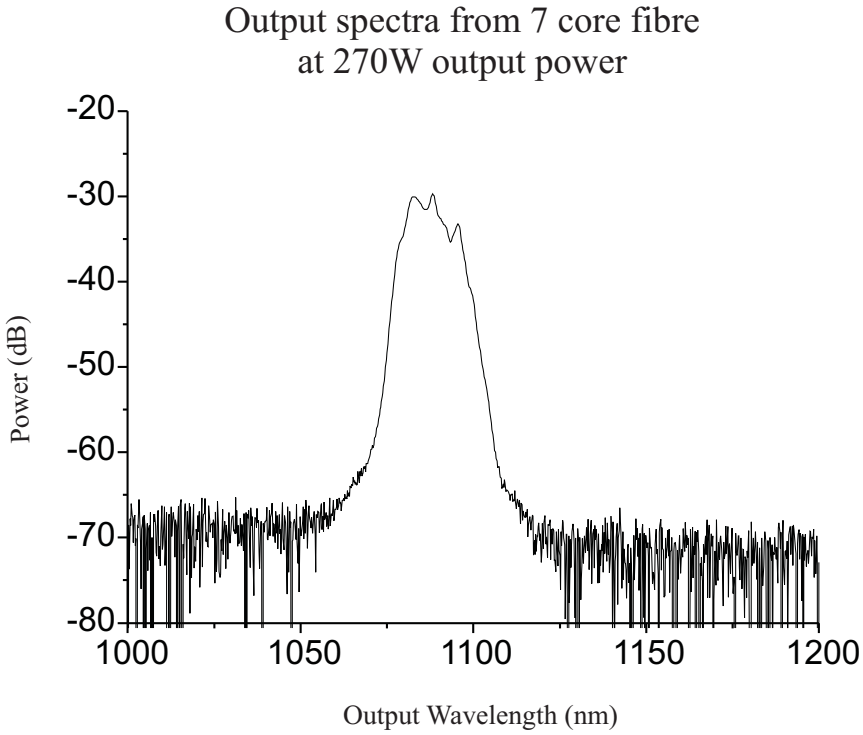

Figure 5.5: Measured spectra from the seven core fibre whilst operating at the maximum output power of $270W$, with a resolution of $2nm$.

multimode wave guide also allowed the possibility of an improved M^2 value due to mode mixing. Further improvements to M^2 value could also be attained by the use of tapering, with careful attention taken to maintaining the efficiency.

5.4.2 Fabrication

The fabrication technique was altered from the method used for the 7 core fibre to achieve more accurate separation control. The stacking technique was used, which although it has problems with contaminants, allows for the uniform arrangement of cores. The preform was created from three doped cores, with silica rods used to fill the spaces, as shown in figure 5.6(a). The rods and tube were cleaned using water, acetone and isopropanol, to remove the maximum quantity of contaminants. Once the rods were inserted into the tube, the preform was transferred to the lathe where with a purge of oxygen, the base of the tube was sealed, to trap the rods in place. A drop was welded to the sealed base and the entire assembly transferred to the drawing tower. The preform was then drawn and collapsed in the furnace into canes, with the assistance of an applied vacuum, which could then be over-clad to increase the fibre diameter, or drawn straight into a fibre.

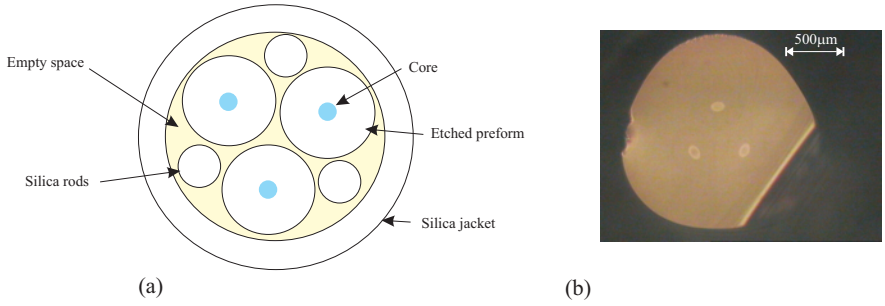

Figure 5.6: (a)Diagram of stacked three core fibre before collapse. (b)Photograph of end face of cane resulting from preform fabricated from (a)

The resultant fibre is shown in figure 5.6(b), it can be seen that the cores have become slightly elliptical. The filling rods helped to reduce the degree of deformity, but in order to completely eradicate any ellipticity would require numerous thin rods, increasing the chance of contaminants, as demonstrated in section 3.4.7. The fibre fabricated had an inner cladding diameter of $150\mu m$, core diameter of

$8\mu m$, with a core to core separation of $26\mu m$. This fibre should be single mode at $1060nm$, and there is little chance of any coherence between the cores since the cladding between cores has a thickness of $18\mu m$. This fibre has a calculated M^2 of 4.9.

5.4.3 Results for the 3 core fibre laser

The experimental set up for the measurement of the 3-core fibre is shown in figure 5.7. Due to the smaller cladding dimension compared with the seven core fibre, an $8W$ Puma source was used which has an operating wavelength of $972nm$. The Laserline source used to pump the 7-core fibre has a beam diameter of $300\mu m$, and thus is generally used for fibres with a diameter of $300 - 400\mu m$.

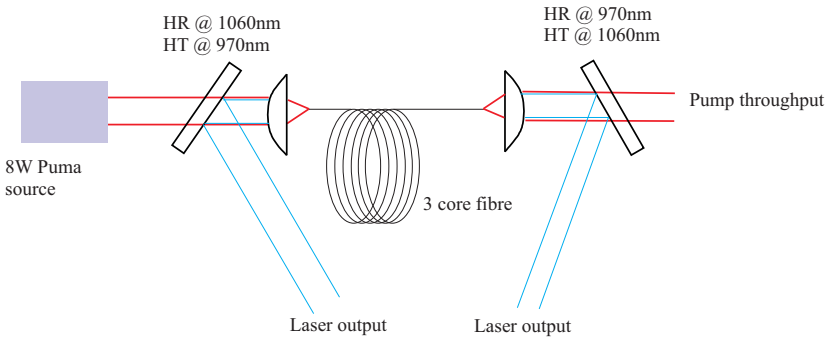

Figure 5.7: Experimental setup used to determine the performance of the seven core fibre.

The fibre showed a slope efficiency of 68% as shown in figure 5.8, an improvement on the result for the seven core fibre. The total power was limited to $3.9W$ due to the power of the source used. The output spectra of the fibre showed that the cores were lasing at slightly different wavelengths, $1036nm$, $1040nm$ and $1044nm$. The M^2 value of the individual cores were approximately unity, whilst the M^2 of the entire fibre was measured to be 5 in agreement with the predicted value by the theory. To encourage lasing at a common wavelength, multimode fibre was spliced to the output end of the fibre.

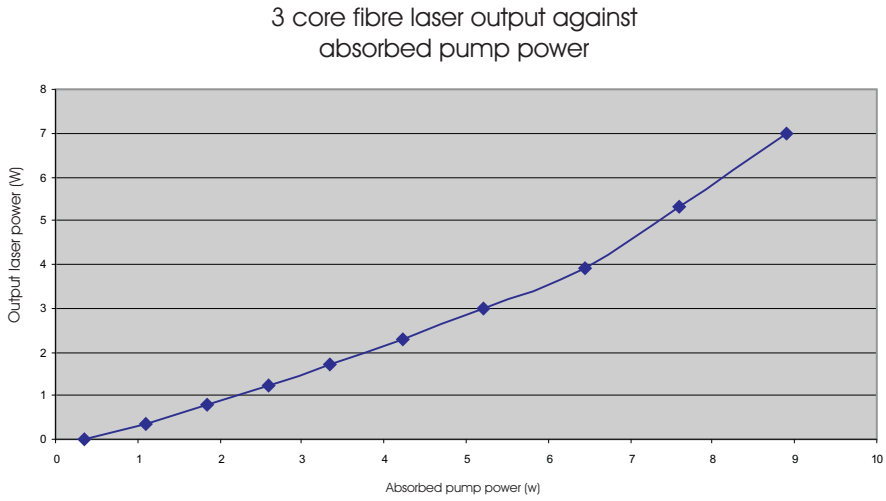

Figure 5.8: Graph showing output laser power against the absorbed pump power, with a slope efficiency of 68%.

5.4.4 Multimode fibre beam quality

The three core fibre was spliced to $300mm$ length of graded index multimode fibre. The multimode fibre was a commercially available fibre, with $125\mu m$ inner cladding diameter and $62.5\mu m$ core diameter. The cores of the three core fibre covered an area with a diameter of $32\mu m$, so the multimode fibre was tapered to a diameter of $80\mu m$ reducing the core size to $40\mu m$, more closely matching the area covered by the three cores. The slope efficiency achieved with the multimode fibre attached was only reduced to 63%, showing that the taper and splice introduced only a small loss. The M^2 value from the end of the multimode fibre was measured to be 3.5, a marked improvement over the previous three core fibre result. The mode excited in the multimode fibre will be that which most closely matches the distribution of the light coming from the 3 core fibre. The most closely matching mode, if it has a better M^2, will have a power loss associated with it, but as seen from the maximum power attained, the loss is small.

There is also the possibility of mode beating as the light passes through the multimode fibre, which would show up as periodic fluctuations of the beam quality as progressive cut backs are made. To investigate this possibility multimode fibre was again spliced to the three core fibre, however this time with no tapering of the multimode fibre. The results shown in figure 5.9 shows the M^2 measured at the output of the multimode fibre for a variety of different lengths. A number

of lengths of multimode fibre were used, ranging from $7mm$ to $120mm$ There is little change in the measured value as the multimode fibre is cut back, showing that there is little mode beating in the multimode fibre. The taper is then critical for the improvement of the beam quality, re-enforcing the belief that the excited mode in the multimode fibre can help improve the M^2 value.

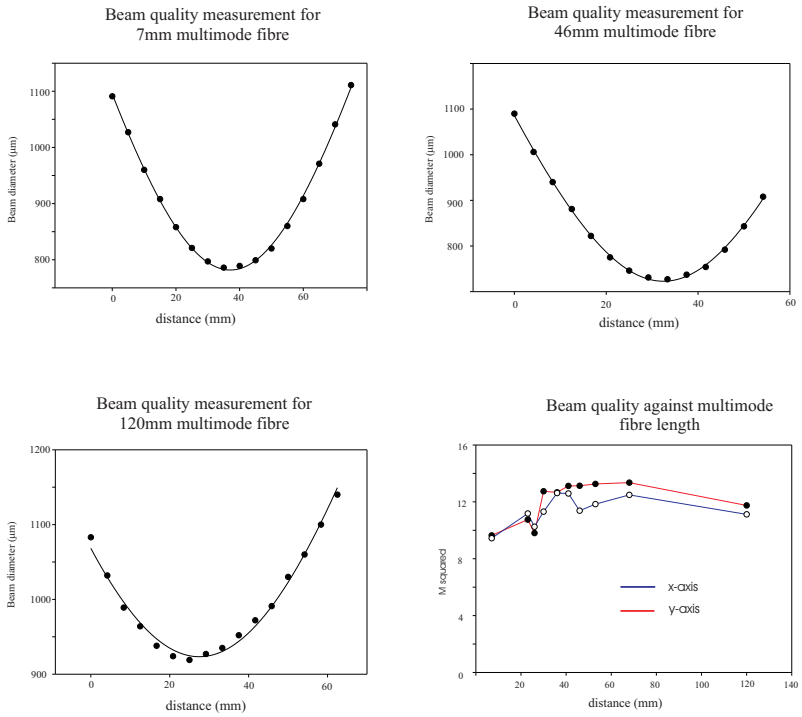

Figure 5.9: Figures showing beam diameter measurements performed, and the resulting best fit for a Gaussian beam with a variable M^2 value. The best fits have M^2 of 11.75, 12.6 and 9.8. The final graph shows the results for all the lengths of multimode fibre for both axes of the beam, indicating that there is little improvement of M^2 with the multimode fibre

5.4.5 Tapering of 3 core fibre laser

The beam quality of the 3 core fibre can be improved by tapering the fibre in a precise way, such that there is the minimum loss of efficiency. The size of core required for single mode operation is such that the V-value of the fibre is 2.4 [7]. Equation 2.13 in chapter 2 for determining the V-value for a fibre is $V = \frac{2\pi}{\lambda_0} a(n_1^2 - n_2^2)$. However, this applies for the fundamental mode, and the

onset of the next order mode will grow slowly as the V number is increased. In a laser system the loss associated with higher order modes will inhibit the amplification of all but the fundamental mode for a fibre with a low V number. The gradual onset of the higher order modes means that the size of the core can be increased to a point where it is no longer robustly single mode, but can still be single mode. In this case the core size can be scaled down without any loss since the mode will be reshaped, but there is no mode cutoff causing additional losses. This assumes that the change is done adiabatically, which can be achieved by having a long taper of a few centimetres. The decrease in the spacing of the cores will alter the effective core area, and therefore reduce the M^2 of the fibre.

Three tapers were fabricated, taking the diameter of the fibre from $150\mu m$ down to $80\mu m$, $100\mu m$ and 125μ. The beam quality is found to be 5.1, 3.5 and 4.3 for $80\mu m$, $100\mu m$ and $125\mu m$ tapered fibres respectively. The beam quality for the unaltered three core fibre was 5. The lack of improvement in beam quality for the $80\mu m$ fibre is thought to be due to the onset of coherent combination of the beams once the core diameter becomes smaller. The efficiency of the unaltered three core fibre was 69% and the efficiencies of the tapered fibres were 72%, 70% and 75% for the 80, 100 and $125\mu m$ tapered fibres respectively. The improvement in efficiency is due to the residual pump light escaping from the uncoated fibre at the taper and is thus difficult to measure. For this reason the pump throughput was assumed to be the same as for the unaltered fibre, which leads to an uncertainty in the measured efficiency.

Figure 5.10 shows the fundamental mode distribution for $1060nm$ wavelength light confined within a fibre with core diameter of $6\mu m$. The spacing between the edges of the cores was $20\mu m$ for the unaltered three core fibre, which is reduced to $10.7\mu m$ for the fibre tapered to $80\mu m$. The mode distribution for $6\mu m$ shows that at a distance of $11\mu m$ there is little energy left in the wing of the Gaussian distribution. At $5.5\mu m$ in the tapered fibre however, there is $\approx 5\%$ of the field which overlaps with the 5% of the adjacent core, making the cores loosely combined. This was shown by the beam fluctuating in beam diameter during the M^2 measurement since it was on the limit of coherent combination.

The expected improvement in M^2 is simply calculated, by adjusting the effective diameter of the area covered by the cores. With a fibre tapered to $125\mu m$, $100\mu m$

and $80\mu m$, the M^2 can be expected to become 4.1, 3.3 and 2.6 respectively. The degree of improvement will be affected by the size of the cores, since the original equation used the diameter of the original cores to calculate the beam quality. This becomes inapplicable once the core size approaches the diameter of the beam, as the beam size increases as it becomes less tightly confined with smaller core diameters. If the mode size remains constant, then the core size can be thought to be constant.

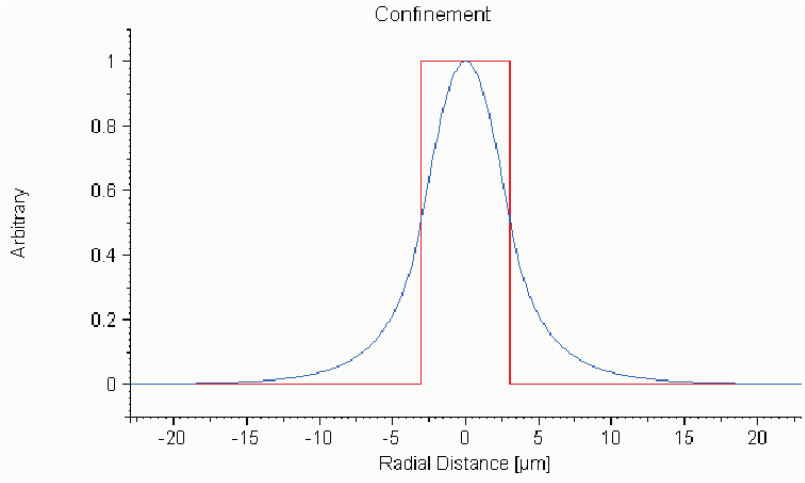

Figure 5.10: Graph showing the mode field overlaid on the refractive index profile. A large proportion of the power is not contained within the core area in the three core fibre tapered to $80\mu m$, and there will be overlap with the field from neighbouring cores.

5.5 Conclusion

The use of multiple cores for simple power scaling has been demonstrated. Fibres have been fabricated with seven and three cores, which display the predicted M^2 values according to the theory. Further work in increasing the number of cores with a minimum effective area is required, to verify the ability for further power scaling. By assuming that the maximum power attainable from a truly single mode core is $100W$ [8] then a fibre with 19 isometrically arranged cores will be capable of demonstrating greater than 1kW multicore fibre laser. A fibre with $10\mu m$ cores, and $20\mu m$ centre to centre spacing, will have an effective diameter of $80\mu m$ and hence an M^2 of 8.

A multimode fibre was used to wavelength lock the three cores together, and this displayed indications that there was an improvement in beam quality. When further investigated, the phenomenon was not repeatable, indicating that the improvement was due to coupling into a specific mode within the tapered multimode fibre, which is difficult to reproduce.

The tapering of the multicore fibres to smaller dimensions was shown to improve the beam quality, to a degree slightly less than predicted by assuming that the area covered by the cores was the only variable to be considered. To determine the exact improvement, further investigation is required, which can quantify the effect of the beam size within the fibre in relation to the beam quality. The efficiency was not decreased by the tapering, showing the taper was indeed adiabatic and there was little energy lost through altering the shape of the fundamental mode. This technique can be used to improve the beam quality by a small degree, possibly by a factor of 2 with no loss in efficiency. The usefulness of this technique is that the pump launch end of the fibre will be as large as possible, with the small end providing improved beam quality with no loss in power.

5.6 References

[1] Y. Jeong, J. K. Sahu, D. N. Payne, and J. Nilsson. Ytterbium-doped large-core fibre laser with 1.36kW continuous-wave output power. *Optics Express*, 12(25):6088–6092, 2004.

[2] P. Glas, M. Naumann, A. Schirrmacher, and T. Pertsch. The multicore fiber - a novel design for a diode pumped fiber laser. *Optics Communications*, 151:187–195, 1998.

[3] M. Wrage, P. Glas, D. Fischer, M. Leitner, D. V. Vystsky, and A. P. Napartovich. Phase locking in a multicore fiber laser by means of a Talbot resonator. *Optics Letters*, 25(19):1436–1438, 2000.

[4] M. Wrage, P. Glas, D. Fischer, M. Leitner, N. N. Elkin, D. V. Vysotsky, A. P. Napartovich, and V. N. Troshchieva. Phase-locking of a multicore fiber laser by wave propagation through an annular waveguide. *Optics Communications*, 205:367–375, 2002.

[5] M. Wrage, P. Glas, M. Leitner, D. V. Vysotsky, and A. P. Napartovich. Phase-locking and self-imaging properties of a Talbot resonator applied to circular structures. *Optics Communications*, 191:149–159, 2001.

[6] P. K. Cheo, A. Liu, and G. G. King. A high-brightness laser beam from a phase-locked multicore Yb-doped fiber laser array. *IEEE Photonics Technology Letters*, 13(5):439–441, 2001.

[7] *Melles griot product catalogue.* 2003.

[8] H. Zeller, U. Williamowski, A. Tunnermann, H. Welling, S. Unger, V. Reichel, H.R. Muller, J. Kirchof, and P. Albers. High-power cw neodymium doped fibre laser operating at 9.2W with high beam quality. *Optics Letters*, 20:578–560, 1995.

Chapter 6

Cladding pumped rod laser

6.1 Introduction

In the competitive field of high power lasers, there are four main competing techniques; CO_2 lasers, solid state lasers, diode lasers and the now emerging high power fibre lasers [1]. All the techniques are essentially limited by thermal effects, with the CO_2 laser current leading the field with commercial available multi-kW systems. Laser diode sources are approaching the kW level, but are limited to welding or pumping applications due to the imbalance of the beam qualities in the transverse dimensions of the output beam. Solid state lasers can be designed in such a way that the beam quality produced is high when pumped by diode lasers, however this must be balanced by thermal effects caused by the high pump and output powers. The fibre laser has the potential to circumvent many of the thermal effects found in other high power laser systems due to the long interaction length and high surface to volume ratio, although the small core area increases the potential of unwanted nonlinear effects at high powers.

The double clad fibre allows pump sources with low beam quality to be used to generate an output beam with far higher beam quality which is not dependent on power. By combining some advantages of the rod laser with the fibre laser, very high power lasers can be produced with good beam quality.

6.2 Concept

6.2.1 Large mode area fibre lasers

The highest achieved powers from fibre lasers, have been from double clad, large mode area, ytterbium-doped fibres [2]. The fibre used by Jeong et al. had $40\mu m$ core diameter, $600\mu m$ inner and $1mm$ outer cladding diameter. The aluminium-ytterbium doped silica core is surrounded by pure silica cladding, and this is all contained within an acrylate protective coating. The large outer cladding thickness reduces the efficiency with which the heat, generated through the large powers, can be dissipated. The thickness is a result of the fabrication process of the fibre, which in general will produce a cladding thickness of the magnitude of the core radius.

The coating quality of optical fibres depends partly on the 'centralising force' developed within the coating cup [3], which is determined by the taper angle within the coating die, and the fibre diameter as mentioned in section 2.3.2. The pressurised coating system, used within the ORC, is designed to enhance the centralising force, however for very large fibres this is not sufficient to keep the fibre centred. Trial runs with varying drawing speeds were required to ensure that the fibre would be coated completely, and great care was required to ensure perfect alignment when commencing fibre drawing. These factors lead to a necessarily large coating to ensure complete protection, and further limit the ability to bend the fibre.

The beam quality produced from large mode area fibres depends on the NA of the core and the bend used to strip higher order modes. Producing very low NA doped cores is difficult due to the dependence of the NA on the refractive index and the reduction in dopants which can be incorporated. Short fibre lengths are desirable in order to suppress the onset of non-linear effects, therefore the core diameter should increase with the inner cladding diameter to preserve the high core to clad ratio. The bending of very thick fibres is difficult, hence for fibres with thicknesses over a millimetre other methods of beam quality improvement will need to be used. Higher order modes have a larger divergence than the fundamental mode, as described in chapter 5, with approximately the same beam

radius as the modes leave the fibre. This means that higher order modes can be stripped to a small degree by placing a plane mirror a small distance from the fibre face. Lower order modes will diverge a small amount and couple back into the core, higher order modes will diverge to a larger degree and thus some of the power will be lost, reducing the efficiency of lasing in that mode.

6.2.2 Pump coupling

The coupling of multiple pump sources, as is currently required for extremely high output powers, requires the fibre to possess a large numerical aperture and large radius. The coating applied to double clad fibre currently gives a numerical aperture of 0.4 limiting the input angle to 30^o to the fibre axis. By reducing the refractive index of the coating, a significantly increased pump power can be coupled into the fibre. A silica fibre surrounded by air has a numerical aperture of 1.06 and can allow light with any input angle to couple into the cladding, limited only by the quantity of the beam which overlaps the core. An uncoated fibre would be susceptible to damage and dirt, but have the advantages of a very high numerical aperture and excellent heat dissipation.

A method of obtaining a very high refractive index difference between the inner and outer cladding is to use a jacketed fibre [4]. The fibre consisted of a $40\mu m$ core surrounded by an hexagonal inner cladding with the dimensions of $117\mu m$ (flat to flat) and $141\mu m$ (corner to corner). The inner cladding is surrounded by air holes to give a very high NA, which makes the inner cladding compatible with $400\mu m$ 0.22 NA pump delivery fibres. The NA of the core, compared with the inner cladding, is very low, so with careful control only the fundamental mode is excited. This technique can provide excellent beam quality, but is ultimately limited by the small core and cladding dimensions which will suffer from thermal effects at very high powers.

Water is extensively used for the cooling of high power laser diodes through the use of microchannels, within the structure of the diode. The water used must be ultra pure to ensure that the channels are not blocked, which would lead to over heating and can damage the diode. Water could be used both to cool and form confinement for a large fibre laser, since it has a refractive index of 1.33 and

hence give a numerical aperture of 0.6. This would give the fibre excellent heat dissipation properties and allow the power to be increased to a level far above that currently attainable by fibre lasers.

6.2.3 Design

To test the concept it was decided to have a fibre with a core diameter of $125\mu m$, which is a reduction by a factor of slightly less than 6 from the preform core diameter, giving a yield of 10 metres from a $400mm$ preform. The inner silica cladding dimension of $1mm$ was chosen such that the device length would be approximately 1m for a dopant concentration of $10000ppm$ of ytterbium in the core. There is no possibility for a fibre with an outer diameter of $1mm$ and core diameter of $125\mu m$ to be sufficiently bent such that the output would be single mode. The fibre symmetry must also be broken to increase the pump absorption, which will be achieved by milling flats on two opposing sides of the preform.

The fibre must be held at either end, both for support and also to allow the water to be within a sealed unit as shown in figure 6.1. The options available are to use silicone rubber or PTFE coating. The silicone rubber is an alternative to the acrylate coating used for low index coatings, which has the advantage of not being rigid when cured and therefore suitable for forming a watertight seal around the fibre. PTFE coating has been used as a method for grouping together fibres for the purposes of side pumping [5], and is commercially available in heat shrinking tubing which is ideal for the cladding of short lengths of fibre. The refractive index for PTFE is slightly lower than currently used optical coatings at 1.36, and can withstand temperatures of up to 400^oC. The drawback of using conventional fibre coatings, is that the numerical aperture for the coated section will be reduced where the coating is applied, potentially losing pump light.

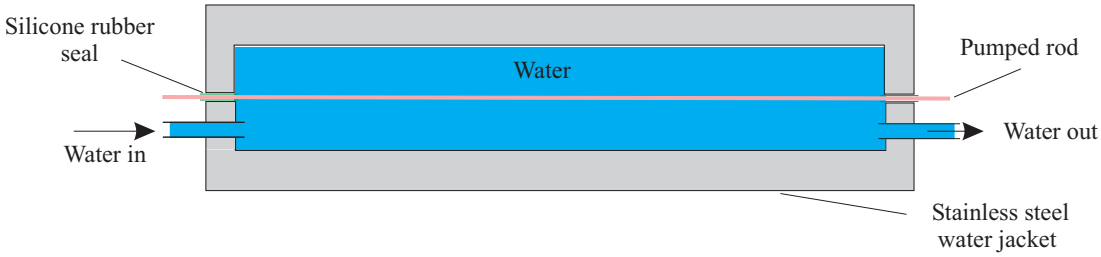

Figure 6.1: Diagram showing the water cooling system for the cladding pumped rod. The rod is supported at either end with a coating of silicone rubber clamped in a steel hole.

6.3 Preliminary testing

6.3.1 Method

The fabrication of very large core fibres requires a preform with a very uniform refractive index profile over both the core diameter and the length of the preform. For small core fibres the exact refractive index profile is less critical since the only mode supported is the fundamental mode. With large core fibres many modes will propagate and to maintain good beam quality the precise shape is critical. Chapter 2 details the problems with creating low index preforms, and explains that the core size is reduced to maintain the index profile. This is undesirable for the large core fibres since the yield decreases rapidly as the preform core size is decreased.

Small changes in preform fabrication, such as the point at which glass substrate tubes are joined together and temperature fluctuations, cause significant changes in the final properties of low index rare-earth doped fibres. To maximise the useable quantity of the preform the initial length should be as long as possible. The difficulties in fabricating long lengths of preform are in the handling, to ensure that soot is not dislodged during the solution doping stage, and in the collapsing, to ensure that the preform can support its own weight. The handling issues can be managed by enlisting assistance while moving the preform around, however for the preform to support its own weight limits the preform length to a maximum of 1m. The refractive index profile of the preform used to create the cladding pumped rod is shown in figure 6.2, which is a 0.08 NA Al/Yb-doped preform.

Once a suitable preform has been fabricated, the cladding diameter needs to be reduced to the correct ratio by etching. The core diameter within a rare-earth solution doped preform is approximately $0.7mm$ therefore the cladding should be $5.6mm$ in diameter to match the ratio required for the fibre. The etching of the preform must be achieved in a uniform manner, and thus care must be taken to ensure that the acid is mixed during the process. The hydrofluoric acid reacts with the silica and thus the reaction rate will decrease as the concentration decreases. The etch rate is approximately $100\mu m$ every hour at room temperature, so the preform will need to be immersed for 54 hours with regular mixing up of the acid. This is most easily achieved by removing the preform every four hours, which also gives an opportunity for measuring the etch rate.

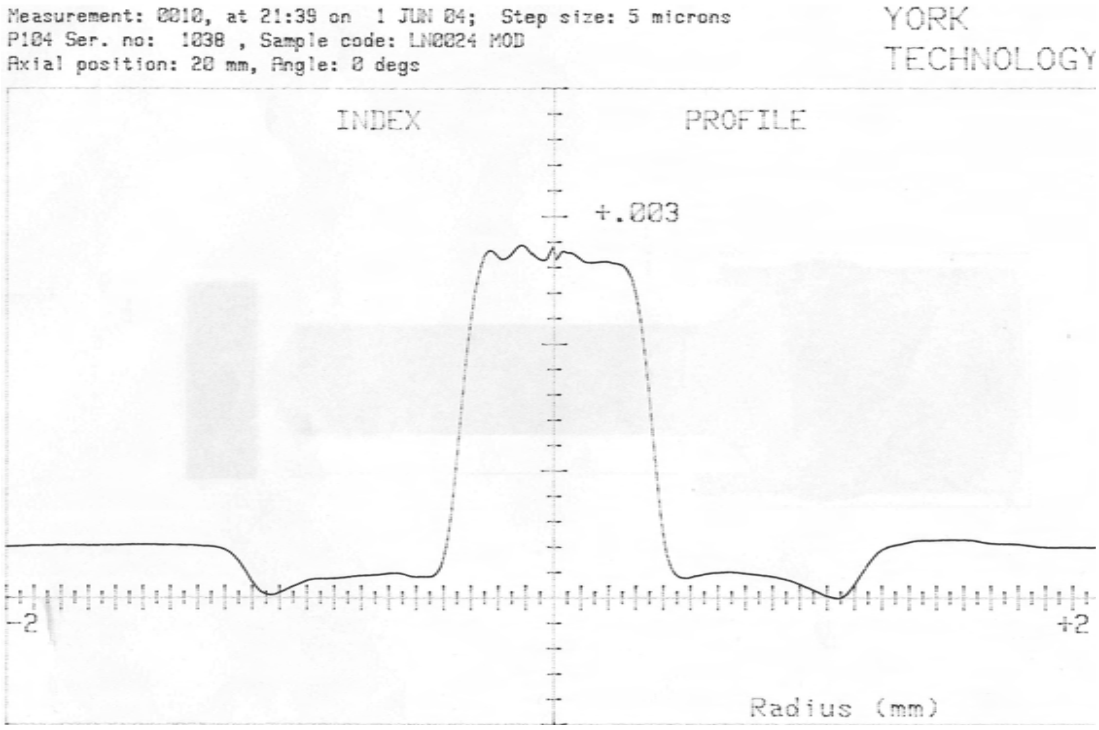

Figure 6.2: Diagram showing the refractive index profile of the preform used to create the cladding pumped rod. The index is quite flat topped, which is ideal for the cladding pumped rod scheme, which uses external methods to control beam quality.

Once the preform has been etched, the symmetry must be broken by milling flats. The rod is very delicate due to its small diameter, and therefore steps must be taken to ensure it is not damaged. The rod is waxed onto a metal block to provide support all along the length of the preform, and a number of passes are performed to mill down to the required depth. Once the rod has been rotated

and the process repeated on the opposite side, it is ready to be transferred to the furnace for fire polishing.

The rod is too thin for fire polishing on glass working lathes since it can be pushed out of shape by the force of the flame exiting the burner. For this reason the furnace is used for fire polishing, which is easily controlled and will not have a strong gas flow to move the preform about. The preform is mounted on the end of a $150mm$ rod with $5mm$ diameter to allow the entire preform to enter the hot zone of the furnace and pass through at a temperature of 1950^oC at $20mm/min$. This allows the rod to heat up and the surface to lose the roughness caused by the milling, which is illustrated in figure 6.3.

In order to obtain the maximum quantity of fibre from the preform, the loss at the beginning and end must be minimised. When drawing fibre at a standard speed of $10m/min$, approximately 10 metres of fibre are wasted at the beginning of the draw due to alignment and the stabilising of the fibre diameter. This can be reduced to a large degree by slowing the drawing rate, since it is merely waiting for the volume entering and leaving the furnace to match up, and reach a steady state. To further reduce the fibre lost, a matching rod can be welded to the bottom of the preform to act as the drop and to allow the diameter to stablise before the doped section is drawn. This method is not appropriate for drawing fibres which require coating since there is a widening of the drawn fibre as the interface between the drop and preform passes through the furnace, which can be large enough to become stuck in the preform dies. The widening of the fibre as the interface is drawn takes time to return to the steady state diameter, however the time taken to return to this diameter is far reduced and hence less fibre is lost.

The drawing of the fibre is performed slowly and the fibre is cut at regular intervals of $1m$ in length. This is limited by the distance between the traction unit and the capstan, which must be used for large diameter fibres or rods which cannot bend round the capstan. The amount of contact with the fibre should be kept to a minimum since in the uncoated state any scratch will cause the fibre to crack with any tension or to lose a large amount of the pump light.

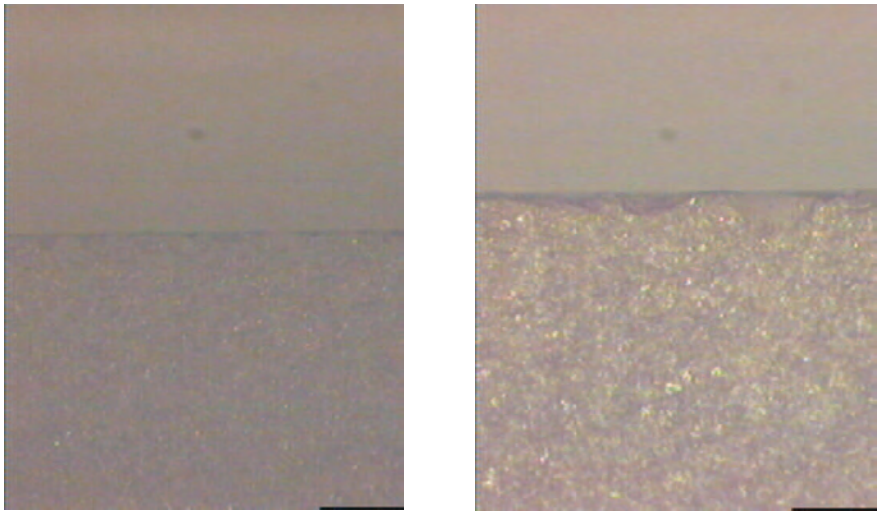

(a) (b)

Figure 6.3: A photograh showing the quality of the glass surface after machining, (a) at a magnification of 10 times, (b) at a magnification of 100 times.

6.3.2 Laser setup

Whilst the watercooled jacket was being made, tests were run with the fibre at low powers to measure the properties and provide a point for comparison with the water cooled system. The fibre was held using water cooled clamps, with a layer of silicone rubber to protect the points of contact. The fibre was pumped using a $500W$ Laserline source at $970nm$ in the setup shown in figure 6.4. The pump light was focused off centre on the fibre face to avoid the pump light coupling directly to the core and thus causing the fibre to overheat. The laser output was measured from both ends of the fibre, with the pump throughput also measured.

6.3.3 Results

The $1mm$ fibre had a number of imperfections on the milled surfaces which formed scattering centres for the pump light, hence reducing the transmission through the fibre. For a rod with a perfectly smooth surface, the transmission over $1m$ length for light at a wavelength of $808nm$ was approximately 90%. The corresponding transmission measured for the fabricated fibre with milled flats was only 30%.

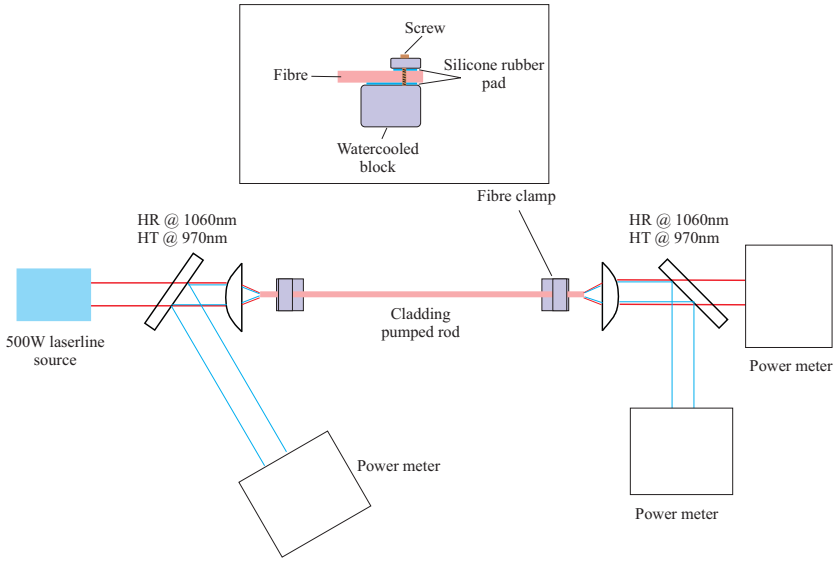

Figure 6.4: Diagram showing the setup for test cladding pumped rod. Inset is a diagram of the water cooled clamp used to hold either end of the fibre, with silicone rubber to protect the surfaces.

An attempt was made to improve the surface quality of the fibre through the use of etching and fire polishing. Figure 6.5(a) shows a magnified image of the flat surface of the fibre. The fire polishing was not sufficient to completely remove the small scratches left from the milling, and these remained during the drawing process. As the fibre was drawn in the furnace the fast preform feed speed meant that further fire polishing during drawing was not as effective as expected. This meant that the scratches were stretched and glass covered the indentations causing the formation of highly elongated bubbles just below the surface of the fibre. To improve the surface, the top layer of glass was etched away by immersing the fibre in hydrofluoric acid for a short time. Once the imperfections were exposed, fire polishing was again employed to smooth the fibre surface.

The fire polishing of long rods is made difficult due to the weight of fibre hanging under the furnace as it is passed through. A number of silica rods with a diameter of $800\mu m$ were tested to find the highest temperature at which fire polishing could be performed with no deformation of the fibre through stretching, the result of which is shown in figure 6.5(b). This was determined to be at 1970^oC with a feed speed of $20mm/min$. The fibre however has a large core doped with aluminium which softens at a lower temperature than pure silica, and during drawing the fibre began to stretch near the end of the process.

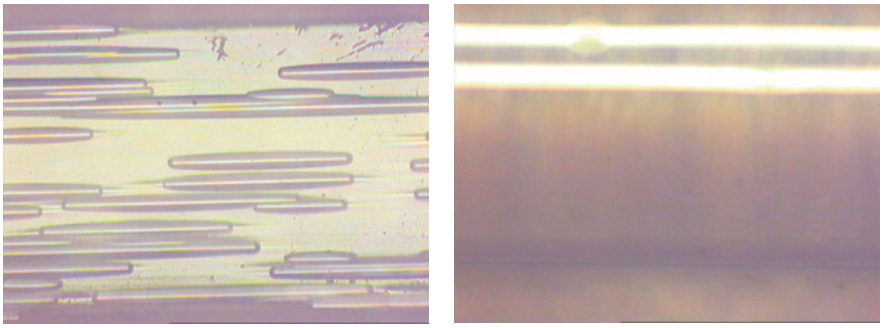

(a) (b)

Figure 6.5: (a)A photograh showing the bubbles under the surface of the milled side of the cladding pumped rod. (b) A photo of the same rod after etching and fire polishing at 1970^oC, showing no bubbles or imperfections.

This fibre was then tested using the $500W$ Laserline source, in the setup shown in section 6.3.2. Figure 6.6 shows the fibre whilst being pumped, with the pump light scattering from the fibre being particularly intense two third of the way down the fibre. The results attained from the fibre was a maximum power output of $13.4W$ from $113.4W$ absorbed power. The slope efficiency was only 20% due to the loss from the scattering. The fire polishing was still insufficient to perfectly polish the fibre, however further polishing was not possible due to the stretching of the fibre.

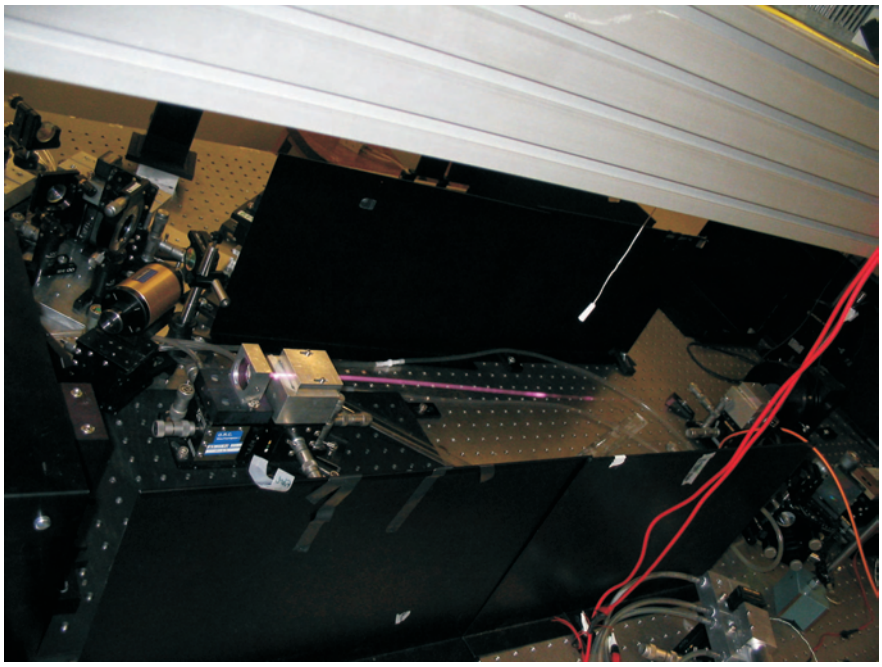

Figure 6.6: A photograph showing the loss in the cladding from the test cladding pumped rod. The light is intense at certain points along the fibre where the surface is particularly rough.

6.4 Cladding pumped rod

6.4.1 Revised fabrication method

The fabrication of the cladding pumped rod initially followed the technique given in section 6.3.1. The area for improvement was the polishing of the milled flats, and it was decided that fire polishing alone would not be sufficient to remove all surface imperfections. Fibre facets are routinely prepared for laser devices using mechanical polishing, where graded rough papers are used to ensure a flawless plane surface. The papers start with $50\mu m$ embedded grains of mono-crystalline diamond, to remove large scale scratches in the face. The size of the embedded grains is reduced steadily to a diameter of $0.3\mu m$, with the surface checked before each change in grain size to ensure that the larger scale imperfections have been removed. The use of polishing paper would enable the larger flaws in the milled surface to be removed, and the small imperfections left could then be smoothed by fire polishing.

The polishing was performed immediately after the milling, whilst the preform was still attached to the metal block. The preform had a diameter of only $5.6mm$ so care was taken to ensure that little pressure was applied for a long period to avoid breakage. The polishing process was repeated again once the fibre had been rotated and milled, resulting in a rod with good surface quality which could then be fire polished to almost perfect smoothness.The fire polishing was performed at 1950^oC, which for the $400mm$ of preform would ensure that there was no deformation. During the drawing process, a higher furnace temperature was used, 2000^oC as opposed to 1950^oC to ensure that the fire polishing was completed.

6.4.2 Setup

A silica rod was used to test the water cooling system, with the input light being at a wavelength of $808nm$. A diode source was used in place of the Laserline source, since multiple diode sources is the ultimate aim for the cladding pumped rod. The results showed that there was a very large loss in the cladding due to either the water cooling or the method for sealing and holding the fibre ends.

The watercooling of the bare rod causes too many losses due to a combination of; particles on the rod surface or in the cooling water, and the silicone rubber used in sealing the water jacket. The maintaining of the beam quality is the next important factor and therefore experiments were implemented to test the beam obtained from the fibre.

The fibre was loosely held on a fibre mount, using external mirrors to form the laser cavity, as shown in 6.7. The source used was a $500W$ laser diode source shaped using external optics and focused onto the face of the fibre. As stated previously, the beam is directed off centre of the core, which allows for the potential of using a second pump beam directed to the opposite side of the fibre, thus doubling the pump power. The high pump powers cannot be used however, due to the lack of cooling which is an issue for the length of fibre used. The plane mirrors used to form the laser cavity have a reflectivity of 100% for the input coupler and 50% for the output coupler, and are mounted on translation stages for alignment. The output beam quality is measured primarily by measuring the spot size of the resultant beam, with the entire beam parameters are measured periodically to ensure that the spot size is indicative of the beam quality. The beam is improved by varying the distances of the mirrors to the end facet of the fibre to select modes with high beam quality.

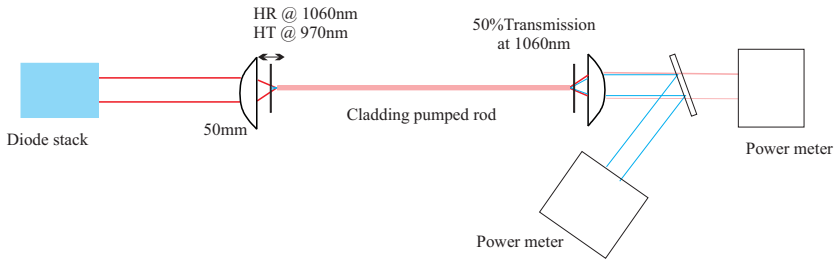

Figure 6.7: Pumping configuration for the cladding pumped rod. The fibre is supported at either end by translation stages, with the fibre in contact with the metal. Mirrors placed close to the fibre faces form the laser cavity.

6.5 Results

The surface quality of the rod was again tested using $808nm$ light to measure the transmission of the fibre, with the optimum input NA tested using the same

source as shown in figure 6.8. The transmission through the fibre was over 90% until the input NA reached 0.5 at which point the transmission dropped to about 80%. Transmission of 95% indicates that the surface quality of the fibre is very good, but losses due to contact with the fibre mounts cause significant losses for larger NAs.

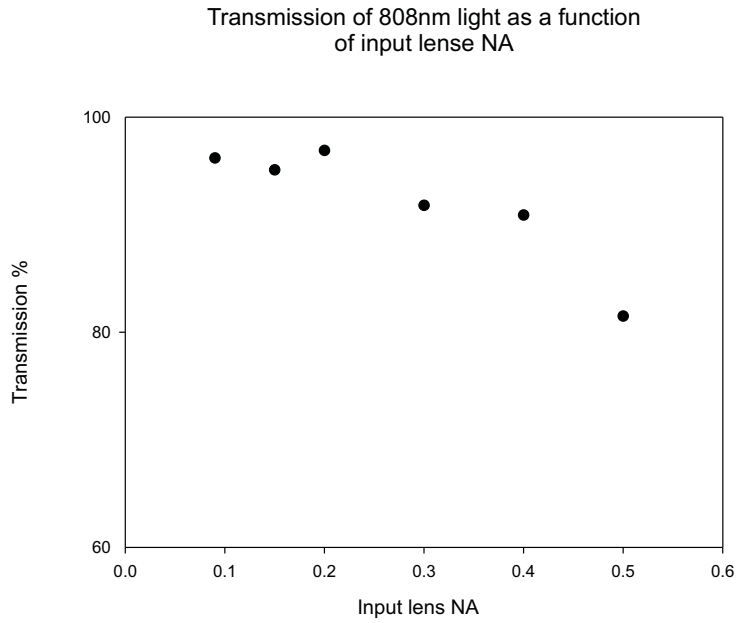

Figure 6.8: Graph showing the transmission losses for the cladding pumped rod with a number of different launching lenses. 808nm light was used to measure the value due to the availability of the source and lack of absorption in Yb fibres.

The rod was pumped by a maximum power of $39.3W$ and had an output power of $19.55W$, the slope efficiency was 69% as shown in figure 6.9. The beam quality, M^2 is approximately half the V-value of a fibre [6], which for the cladding pumped rod is 33, giving an expected M^2 of 16.5. The initial experimental beam quality was measured to be 14 with mirrors placed at the fibre faces to obtain the maximum output power. By adjusting the distance of the input mirror to the fibre face, the beam was improved to an M^2 of 12.9 at a mirror distance of $250\mu m$ and to 11 at a mirror distance of $1mm$. The fibre suffered during the course of the experiments due to dust particles alighting on the surfaces, causing losses due to scattering. The fibre therefore required cleaning at least once a week to reduce pump losses, after which the entire system required realigning.

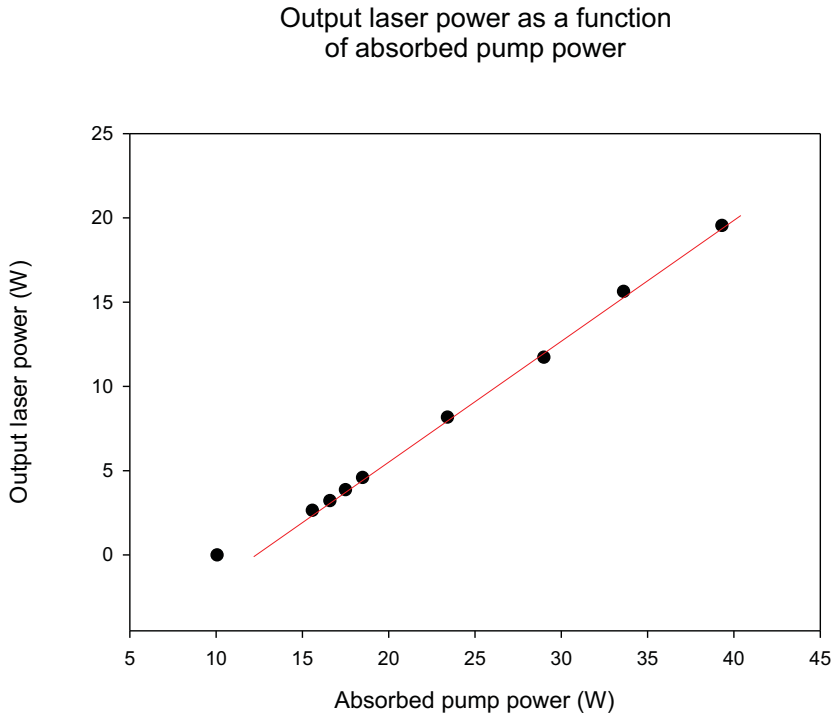

Figure 6.9: Graph showing the power output as a function of absorbed pump power. The slope efficiency was found to be 69%.

6.6 Conclusion

The results obtained from the cladding pumped rod shows that the scheme could be a very good method for creating high power lasers with M^2 around 10. The output power attained was $13.4W$ for $113W$ of input pump power, this was recorded for the fibre with a low slope efficiency of 20%. For the improved fibre, with a slope efficiency of 69%, the maximum output power was $19.55W$ for $39.3W$ incident power.

The beam quality was measured at 14 with plane mirrors placed directly at the fibre ends, compared with 16.5 as calculated from the fibre V-value. The beam quality was improved to an M^2 of 12.9 when the input mirror was moved $250\mu m$ from the fibre face, and then to 11 when the mirror was moved $1mm$ from the face. This modest improvement could be enhanced through the use of convex mirrors, or by using the cladding pumped rod as an amplifier in a MOPA setup.

The failure of the water cooling system was a setback for the high power results expected from the cladding pumped rod. The primary problem is in contami-

nation of the surface of the fibre, through handling or environmental particles. The obvious solution to this is to coat the fibre in a coating to protect the fibre from dirt, yet ensure that it is thin so that the thermal cooling is not compromised. This solution eliminates the numerical aperture improvement for the pump launching, decreasing the potential power improvement for the cladding pumped rod. The difficulty in creating thin uniform coatings on large fibres can easily be solved due to the comparatively short lengths of fibre involved. $1.5m$ lengths of PTFE shrink wrap tubing are commercially available, which can be applied to the cladding pumped rod using a heat gun mounted on the glass lathe. This allows the fibre to be rotated and the heat gun to traverse smoothly along its length, creating a uniform thin coating with no trapped air. Tests performed with the PTFE tubing have shown that the losses are less than $0.01dB/m$ for $808nm$ light.

6.7 References

[1] R. Poprawe and W. Schultz. Development and application of new high-power laser beam sources. *RIKEN Review focused on Laser Precision Microfabrication*, 50:3–9, 2003.

[2] Y. Jeong, J. K. Sahu, D. N. Payne, and J. Nilsson. Ytterbium-doped large-core fibre laser with 1.36kW continuous-wave output power. *Optics Express*, 12(25):6088–6092, 2004.

[3] P. W. France, P. L. Dunn, and M. H. Reeve. Plastic coating of glass fibres and its influence on strength. *Fibre and Integrated Optics*, 2(3-4):267–286, 1979.

[4] J. Limpert, N. Deguil-Robin, I. Manek-Honnonger, F. Salin, F. Roser, A. Liem, T. Schreiber, S. Nolte, H. Zellmer, A. Tunnermann, J. Broeng, A. Petersson, and C. Jakobsen. High-power rod-type photonic crystal fiber laser. *Optics Express*, 13(4):1055–1058, 2005.

[5] P. Polynkin, V. Temyanko, M. Mansuripur, and N. Peyghambarian. Efficient and scalable side pumping scheme for short high-power optical fiber lasers and amplifiers. *IEEE Photonics Technology Letters*, 16(9):2024–2026, 2004.

[6] V. Shcheslavskiy. Personal communication. *University of Southampton*, 2004.

Chapter 7

Conclusions and future work

The work presented in this thesis is reviewed, and the results achieved by the author are outlined. Future directions for all the projects worked on are also proposed.

Chapter 2 - Fibre lasers

Recent progress towards multi-kW power levels from optical fibre lasers have been researched and the techniques used to achieve these levels examined. The operation of a laser is outlined, and the equations governing its action derived. The fabrication of preforms through the three main techniques; Outside Vapour Deposition, Vapour Axial Deposition, and modified chemical vapour deposition were described. The use of MCVD, was described in detail, since it is implemented within the University of Southampton for the fabrication of silica based preforms. The ease with which the MCVD technique can be adapted to incorporate solution doping of rare-earths is a distinct advantage of this system. The processing of preforms, for the purpose of either breaking the cladding symmetry or inducing birefringence in the fibre, is important for the work carried out in this project. The final stage of fibre fabrication, the drawing of the preform into a fibre is discussed, drawing attention to the coating of the fibre. Finally, methods for increasing of output powers by the use of beam combination is examined, looking at various methods for this and describing the theory behind them.

Chapter 3 - Helical core fibre laser

The helical core fibre is introduced and the equations governing the passage of

polarised light along the core derived. A number of equations for the loss in the core due to the path of helical core have been presented, and through experiment the accuracy of these different techniques was determined. A method of fabrication was proposed and implemented for helical core fibre lasers. The fabrication of the helical core fibre required the improvement in both low NA preform fabrication and the development of new fabrication methods for off-centred preforms. The improvement in low NA preforms was achieved through the discovery of the effect of thin soot deposition, and then experimental tests to improve the results further. The drilling technique for preform fabrication has been developed to a stage where off-centred preforms can routinely be fabricated, with no imperfections at the inserted core/cladding interface and hence no additional losses in the cladding. The successful demonstration of the first core pumped helical core fibre with an output power of $350mW$ and M^2 value of less than 1.1 was performed, in collaboration. The results from the core pumped fibre were severely limited by the loss due to the bending in the helical core and by the difficulty in coupling the pump light. Bend loss theory has been applied, which showed to be approximately correct for longer pitch lengths, to determine the optimum bend radii, and hence helix parameters, to allow the propagation of only the fundamental mode. The fabrication and demonstration of a helical core cladding pumped fibre laser, which was shown in collaboration to improve the beam quality of a $30\mu m$ core from an M^2 of 3.3 to near diffraction limited, with a maximum output power of 180W and slope efficiency of 84%. The loss in the cladding has been reduced to a level where there is little adverse effect on the efficiency of the fibre laser, and the loss is due to scattering from the helical core. The helical core fibre has shown that it can create single mode output from a multimode core, although the power levels are not near the kW devices created through large mode area fibre laser with bending. An improved coating technique is required to allow the device integrity to be increased and large pump powers used. The efficiency of the fibres show that this would enable to helical core fibres to challenge the highest achieved fibre laser output powers. The spectrum emitted from the helical core fibre laser is shifted towards shorter wavelengths, due to the lower loss predicted through the bend loss theory. This could enable helical core fibres to be used in wavelength suppression, for example in Yb or Nd to gain lasing in the 900nm region.

Chapter 4 - Multicore ribbon fibre laser

By examining the pump geometry the ribbon fibre has been shown, with its large aspect ratio, to more closely match the beam shape produced by diode stacks. The ribbon fibre geometry also lends itself to the inclusion of a linear array of laser cores. The spectral beam combination method has been investigated as a potential method for gaining very high powers from a single fibre laser. A method has been developed for the fabrication of a ribbon fibre with a number of cores, firstly on a small scale ($2mm \times 20mm$) and then on a larger scale ($20mm \times 200mm$). The fabrication on a small scale yielded very little fibre for the time consumed in fabricating the preform, hence a larger solution was required. The step to the large preform required the solving of new fabrication issues, and the reemergence of issues which were previously controlled when performed on a small scale. The successful fabrication of multicore ribbon fibres has been shown, on both a small and a large scale. The ribbon fibre fabricated from a small preform was tested in collaboration and achieved $\sim 440mW$ from a seven core ribbon fibre. By fabricating a large preform, the successful creation of a multicore ribbon fibre laser has been demonstrated. This fibre was used in collaboration to achieve an output laser power of $250W$, with a slope efficiency of 65%. This fibre was then used for spectral beam combination at low pump powers to combine the output of the cores into a single beam. The results from this indicated that the alignment of the cores was not sufficiently straight leading to the combination of only five out of the ten cores. The ribbon fibre was shown to provide excellent pump coupling properties as is expected due to the large area and optimised shape into which to focus the light. An alternative preform fabrication technique was proposed, which has been demonstrated with four and ten cores. The four core attempt used large rods and hence the alignment was good, but the temperature control was insufficient. The seven core attempt used small rods, and although the temperature was correct, the alignment was poor. The fabrication of a multicore fibre by this technique is simpler than the previous method and far less time consuming. The multicore fibre has a power level well below that of current high power fibre lasers, due to the low efficiency and poor coating. The fabrication technique is currently not precise enough to ensure complete spectral beam combination of all the cores, and new techniques will need to be implemented to correct this.

Chapter 5 - Multicore circular fibre lasers

A multicore fibre with no beam combination, to provide a beam of reasonable

quality (M^2 around 10), very high power and excellent stability, was proposed. The multicore fibre lasers were fabricated using drilling and stacking techniques, and measured the beam quality attained. For the first fibre with seven widely spaced cores, an M^2 value of 30 was obtained, comparing well with the theoretical expectation of 35. The power achieved with this fibre was over $270W$. For the next fibre with three closely spaced cores, the expected M^2 was 4.9 and the measured value was ≈ 5. A tapered multimode fibre was spliced to the three core fibre to wavelength lock the three cores together, and this displayed indications that there was an improvement in beam quality to an M^2 of $\approx$ 2.4. When investigated in detail, the phenomenon was not repeatable, indicating that the improvement was due to coupling into a specific mode within the multimode fibre, which requires precise dimension matching and excellent splice quality to reproduce. Tapering of the three core fibre was then used, in order to improve the beam quality from the cluster of cores. The measurements showed that the tapering of the fibre to $125\mu m$, $100\mu m$ and $80\mu m$ altered the M^2 to 4.3, 3.5 and 5.1. The result of the $80\mu m$ taper is due to a combination of the very poor beam confinement, and the loose coupling between adjacent cores due to the reduced separation. The fibre has a good efficiency which is not compromised by slight tapering of the fibre. The power levels used were low, but can easily be scaled up to the kW level to challenge current high power fibre lasers.

Chapter 6 - Cladding pumped rod

The high powers achieved using large core fibres led to the design of very large core ($> 100\mu m$) fibres which could deliver extremely high output powers. An Yb-doped preform was fabricated, and processed such that it had an outer diameter of $5.6mm$ and two flats to break the circular symmetry. From this a fibre was drawn of a thickness of $1mm$, in lengths of $\approx 1m$. This fibre showed large cladding losses due to scattering from bubbles formed due to machining and drawing the fibre. The power attained was $13.4W$ with a slope efficiency of 20%. A water cooled fibre holder was bought, but this method proved unsuccessful due to contaminants in the water and problems with supporting the fibre. The fabrication method was revised to completely remove the rough surface produced by milling the preform, and drew a second fibre. This fibre had few surface defects, and had a transmission of over 90% at $800nm$, showing that the fabrication process was significantly improved. The fibre was tested by a colleague and showed results of $19.55W$ for $39.3W$ absorbed pump power, limited by the danger of over heating

the fibre due to the lack of cooling once the water cooling was abandoned. The beam quality measured, was 14 with plane mirrors placed directly at the fibre ends, compared with 16.5 as calculated from the fibre V-value. The beam quality was improved to an M^2 of 12.9 when the input mirror was moved $250\mu m$ from the fibre face, and then to 11 when the mirror was moved $1mm$ from the face. The power attained from the fibre must be increased by making the fibre more robust before it can find any commercial use.

Future work

Fibre coating

The poor coating on the helical core fibre is a serious problem, and coating of larger fibres will also be a problem. An ideal solution to this would be a system whereby the coating can be applied in an aerosol fashion. A proposed system for this is shown in figure 7.1. Low index coating material is supplied with a thickening agent since the addition of fluorine decreases the viscosity making it difficult to use in a coating cup setup, due to coating flowing on the fibre once it leaves the coating cup. This could be possible to pass through a number of nebulisers, to spray a thin coating on the outside of the fibre. The thin coating would be homogeneous around the fibre, and the heat dissipation would also be improved. This would also be ideal for the coating of irregularly shaped preforms, such as the ribbon fibre.

Large core preform fabrication

As the core size is scaled up, the length of fibre achievable from a preform decreases, therefore a method for producing larger core preforms is essential. One such system under development is the use of a heated vessel containing rare-earth chlorides inside the deposition tube, as shown in figure 7.2. This can deposit multiple layers of rare-earth doped silica, however the process is not uniform currently, so further work is required.

Off-centre preform fabrication

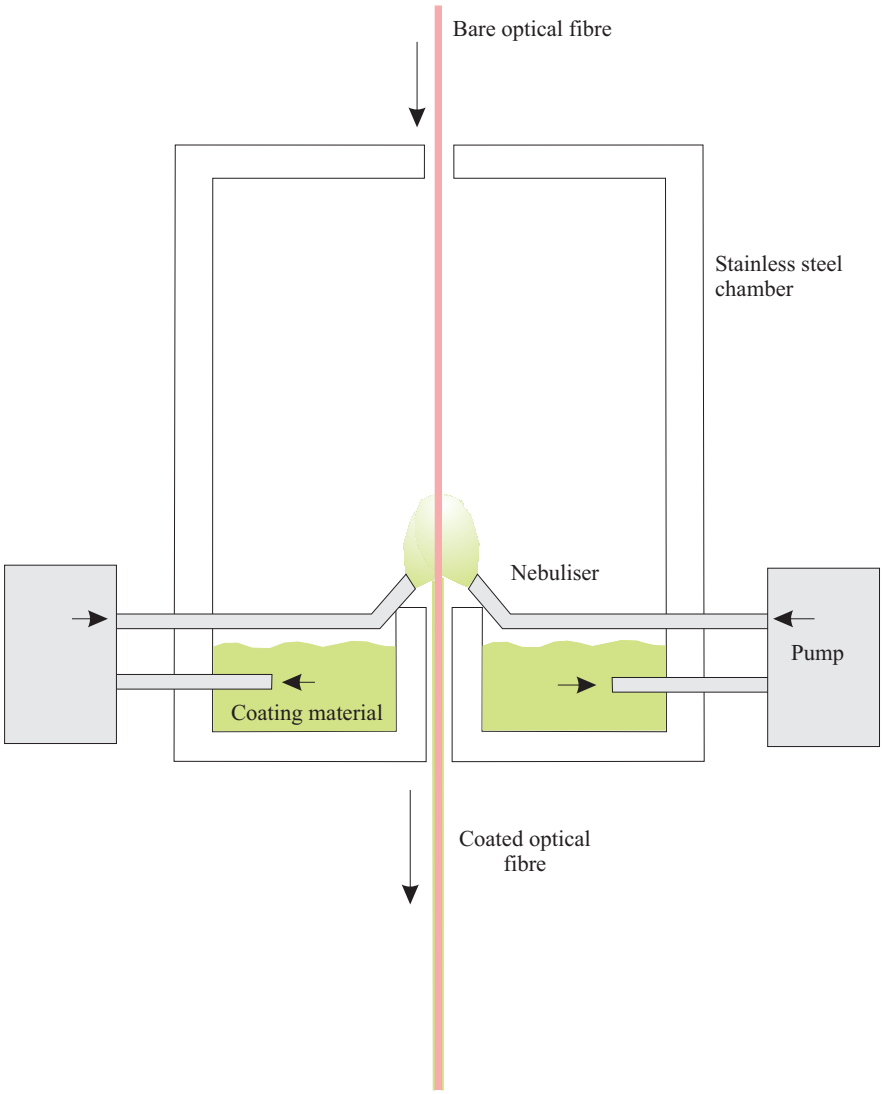

Figure 7.1: A proposed coating system using diffusers to spray a coating onto the fibre. The coating would be very thin giving excellent heat dissipation properties and homogeneous around the fibre. The unused coating would be collected at the base of the chamber and recirculated.

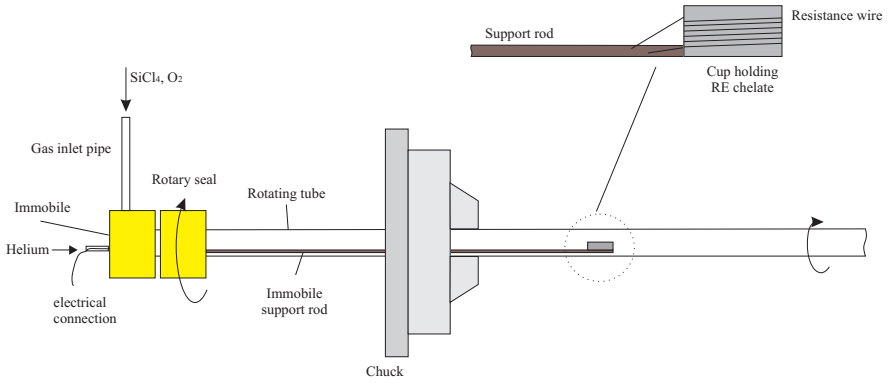

Figure 7.2: A heated container is placed a short distance upstream in the gas flow, which is filled with RE-chelate. Chelates are used since they require a temperature of only $200 - 250^oC$ to produce adequate vapour.The heater is turned on when REs are required, eliminating the need for solution doping.

The current technique for fabrication of offcenter preforms has difficulties in both drilling small long holes, and etching preforms to uniform sizes. An alternative fabrication method has been suggested using over clad preforms and drilling out the entire offcentre preform. This process would have less opportunity for contaminants, and be far easier to fabricate. A standard preform is over-clad with a silica tube with a thickness of $20mm$. The resultant preform can now be drilled out with a drill with an internal diameter of $14mm$, as illustrated in figure 7.3. This technique requires the purchase of suitable drill bits, although it can offer significant time savings over the current technique and is easier to ensure the elimination of contaminants.

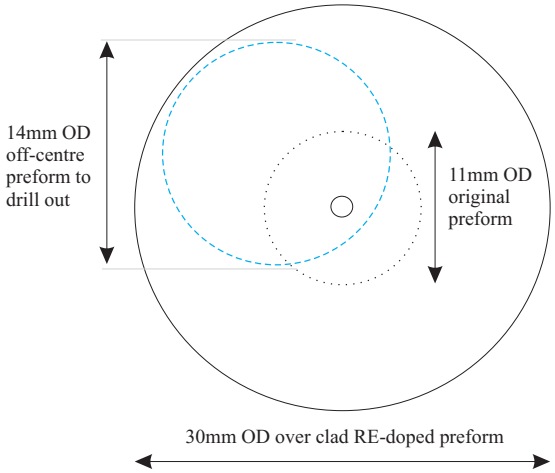

Figure 7.3: Over-cladding a standard preform with a thick silica tube. The offcentre preform can then be drilled out with far less work than is currently required.

Multiple core M^2 combination

Further work in increasing the number of cores with a minimum effective area is required, to verify the ability for further power scaling. By assuming that the maximum power attainable from a truly single mode core is 100W then a fibre with 19 cores will be capable of demonstrating output powers greater than 1kW, and produce an isometric uniform effective core area. A fibre with $10\mu m$ cores, and $20\mu m$ centre to centre spacing, will have an effective diameter of $80\mu m$ and hence an M^2 of 8. The beam can then be improved using the tapering of the output end of the fibre. To determine the exact improvement, further investigation is required, which can quantify the effect of the beam size within the fibre in relation to the beam quality. The usefulness of this technique is that the pump launch end of the fibre will be as large as possible, with the small end providing improved beam quality with no loss in power.

Cladding pumped rod

The failure of the water cooling system was a setback for the high power results expected from the cladding pumped rod. The primary problem is in contamination of the surface of the fibre, through handling or environmental particles. The obvious solution to this is to coat the fibre in a coating to protect the fibre from dirt, yet ensure that it is thin so that the thermal cooling is not compromised. This solution eliminates the numerical aperture improvement for the pump launching, decreasing the potential power improvement for the cladding pumped rod. The difficulty in creating thin uniform coatings on large fibres can easily be solved due to the comparatively short lengths of fibre involved. $1.5m$ lengths of PTFE shrink wrap tubing are commercially available, which can be applied to the cladding pumped rod using a heat gun mounted on the glass lathe. This allows the fibre to be rotated and the heat gun to traverse smoothly along its length, creating a uniformly thin coating with no trapped air. Tests performed with the PTFE tubing have shown that the losses are less than $0.01dB/m$ for $808nm$ light. Experiments using this technique are ongoing in the University of Southampton.

Appendix

Publications from work contained in this thesis

L.J.Cooper, P. Wang, J.K.Sahu, W.A.Clarkson, A.M.Scott, D.Jones
High-power Yb-doped multi-core ribbon fiber laser
Optics Letters 2005 Vol. 30 pp.2906-2908

P.Wang, L.J.Cooper, V.Shcheslavskiy, J.K.Sahu, W.A.Clarkson
Cladding-pumped Yb-doped helical-core fibre lasers and amplifiers
CLEO/Europe-IQEC Munich 12-17 Jun 2005

P.Wang, L.J.Cooper, V.Shcheslavskiy, J.K.Sahu, W.A.Clarkson
Cladding-pumped ytterbium-doped helical-core fiber laser
ASSP 2005 Vienna 6-9 Feb 2005

P.Wang, L.J.Cooper, R.B.Williams, J.K.Sahu, W.A.Clarkson, A.M.Scott, D.Jones
High-power Yb-doped multi-core ribbon fibre laser
EPS-QEOD Europhoton Lausanne 29 Aug - 3 Sep 2004

P.Wang, L.J.Cooper, R.B.Williams, J.K.Sahu, W.A.Clarkson
Helical-core ytterbium-doped fibre laser
Electronics Letters 2004 Vol.40(21) pp.1325-1326

L.J.Cooper, P.Wang, R.B.Williams, J.K.Sahu, W.A.Clarkson, A.M.Scott, D.Jones
Diode-stack-pumped Yb-doped multi-core ribbon fiber laser
CLEO/IQEC 2004 San Francisco 16-21 May 2004

D.B.S.Soh, J.Nilsson, J.K.Sahu, L.J.Cooper
Geometrical factor modification of helical-core fiber radiation loss formula

Optics Communications 2003 Vol.222 pp.235-42

Other publications

D.Y.Shen, W.A.Clarkson, L.J.Cooper, R.B.Williams
3.7-Watt single-frequency cw Ho:YAG ring laser end-pumped by cladding-pumped Tm-doped silica fibre laser
ASSP 2004 New Mexico 1-4 Feb 2004

D.Y.Shen, W.A.Clarkson, L.J.Cooper, R.B.Williams
Efficient single-axial-mode operation of a Ho:YAG ring laser pumped by a Tm-doped silica fiber laser
Optics Letters 2004 Vol.29(20) pp.2396-2398

D.Y.Shen, A.Abdolvand, L.J.Cooper, W.A.Clarkson
Efficient Ho:YAG laser pumped by a cladding-pumped tunable Tm:silica-fibre laser
Applied Physics B 2004 Vol.79(5) pp.559-61

D.Y.Shen, L.J.Cooper, W.A.Clarkson
Highly efficient Ho:YLF and Ho:YAG lasers pumped by Tm-doped silica fibre laser
EPS -QEOD Europhoton Lausanne 29 Aug - 3 Sep 2004

J.K.Sahu, Y.Jeong, C.Alegria, C.Codemard, D.B.S.Soh, S.Baek, V.Philippov, L.J.Cooper, J.Nilsson, R.B.Williams, M.Ibsen, W.A.Clarkson, D.J.Richardson, D.N.Payne
Recent advances in high power fiber lasers
ASSP 2004 New Mexico 1-4 Feb 2004 (Invited)

D.B.S.Soh, S.W.Yoo, J.Nilsson, J.K.Sahu, S.Baek, Y.Jeong, L.J.Cooper, C.Codemard, P.Dupriez, C.Alegria, V.Philippov, K.Oh
Cladding pumped Nd-doped fiber laser tunable from 908 to 938 nm
CLEO/IQEC 2004 San Francisco 16-21 May 2004

D.Y.Shen, W.A.Clarkson, L.J.Cooper, R.B.Wlliams
Efficient Tm:silica fiber laser pumped Ho:YAG lasers

CLEO/IQEC 2004 San Francisco 16-21 May 2004

D.B.S.Soh, S.W.Yoo, J.K.Sahu, L.J.Cooper, S.Baek, K.Oh
A cladding pumped neodymium-doped fiber laser tunable from 932 nm to 953 nm
ASSP 2004 New Mexico 1-4 Feb 2004

A.Abdolvand, D.Y.Shen, L.J.Cooper, R.B.Williams, W.A.Clarkson
Highly efficient Ho:YAG laser pumped by a Tm-doped silica fiber laser
CLEO/QELS 2003 Baltimore 3-5 Jun 2003

W.A.Clarkson, L.J.Cooper, P.Wang, R.B.Williams, J.K.Sahu
Power scaling concepts for fiber lasers
Trends in Optics and Photonics 2003 Vol.83 pp.261-267

A.Abdolvand, D.Y.Shen, L.J.Cooper, R.B.Williams, W.A.Clarkson
Ultra-efficient Ho:YAG laser end-pumped by a cladding-pumped Tm-doped silica fibre laser
ASSP 2003 San Antonio 2-6 Feb 2003

W.A.Clarkson, A.Abdolvand, D.Y.Shen, R.A.Hayward, L.J.Cooper, R.B.Williams, J.Nilsson
High power two-micron fibre lasers
SPIE Proceedings on Gas and Chemical Lasers - High Power Lasers Conference 2002 (Invited)